Rheo-NMR Studies of Macromolecules

A thesis presented in partial fulfillment of the requirements for the degree of

Master of Science in Physics

at Massey University, Palmerston North, New Zealand.

Motoko Kakubayashi

2008

Abstract

In this thesis, the effects of simple shear flow on macromolecular structure and interactions are investigated in detail via a combination of Nuclear Magnetic Resonance (NMR) spectroscopy and rheology, namely Rheo-NMR. A specially designed NMR couette shear cell and benchtop shear cell, developed in-house, demonstrated that the direct measurement of the above phenomena is possible.

First, to determine whether the shear cells were creating simple shear flow, results were reproduced from literature studies of liquid crystal systems which report shear effects on: Cetyl Trimethyl Ammonium Bromide (CTAB) in deuterium oxide, and Poly(gamma-benzyl-L-glutamate) (PBLG) in m-cresol.

Next, the possible conformational changes to protein structure brought about by shear were investigated by applying shear to Bovine β-lactogobulin (β-Lg). As the protein was sheared, a small, irreversible conformational change was observed by means of one-dimensional and two-dimensional ^{1}H NMR with reasonable reproducibility. However, no observable change was detected by means of light scattering. A large conformational change was observed after shearing a destabilized β-Lg sample containing 10% Trifluoroethanol (TFE) (v/v). From an NMR point of view, the sheared state was similar to the structure of β-Lg containing large amounts of α-helices and, interestingly, similar to the structure of β-Lg containing β-sheet amyloid fibrils. Gel electrophoresis tests suggested that the changes were caused by hydrophobic interactions. Unfortunately, this proved to be difficult to reproduce.

The effect of shear on an inter-macromolecular interaction was investigated by applying shear during an enzyme reaction of pectin methylesterase (PME) on pectin. Experimental method and analysis developments are described in detail. It was

observed that under the conditions studied, shear does not interfere with the de-esterification of pectin with two types of PME, which have different action mechanisms at average shear rates up to 1570 s^{-1}.

Acknowledgements

I would like to thank the following people who have helped me throughout this project:

My supervisors, Dr. Bill (M.A.K.) Williams, Dr. Pat Edwards, and Dr. Robin Dykstra, for their support, enthusiasm, and constantly encouraging me to do better work.

Terry Southern, Rinni Singh, and the mechanical workshop staff for developing, improving, and constant maintenance of the rheo-device and shear cell.

Grant Platt for cutting all of my glassware.

My fellow graduate students in physics and chemistry for all of their quality advice and support.

Biomaterials group members, especially Aurelie Cucheval for teaching me everything about pectin and PME.

All the staff at the Physics department for keeping me focussed and happy during my studies.

Raymond Raman for support and technical advice during my thesis write up.

My family and friends for putting up with me, and helping to create a comforting work environment during my thesis write up.

Contents

Title page ..... **i**

Abstract ..... **ii**

Acknowledgements ..... **iv**

Contents ..... **v**

List of Figures ..... **viii**

List of Tables ..... **xii**

1 Introduction **1**

1.1 Introduction 1

1.2 Rheo-NMR 4

1.3 Rheology of Macromolecules 6

1.3.1 Bovine β-lactoglobulin 6

1.3.2 Pectin 7

1.4 Shear 8

1.4.1 Shear in a Couette cell 9

1.5 Nuclear Magnetic Resonance (NMR) 10

1.5.1 Basic Principles of NMR 11

1.5.1.1 NMR 11

1.5.1.2 Chemical Shift 13

1.5.1.3 Bulk Magnetization 14

1.5.1.4 Pulses 15

1.5.1.5 Relaxation 15

1.5.1.6 Water Suppression 16

2 Experimental Method **18**

2.1 Shear Cell 18
2.1.1 NMR Couette Shear Cell 18
2.1.2 Benchtop Shear Cell 24
2.2 Cetyl Trimethyl Ammonium Bromide (CTAB) in D_2O 25
2.2.1 Introduction 25
2.2.2 Experimental Method 26
2.2.3 Results and Discussion 27
2.2.4 Conclusion 30
2.3 Poly(gamma-benzyl-L-glutamate) (PBLG) in m-cresol 30
2.3.1 Introduction 30
2.3.2 Experimental Setup 31
2.3.3 Results and Discussion 32
2.3.4 Conclusion 36
3 Bovine β-lactoglobulin 37
3.1 Introduction 37
3.2 Experimental Method 37
3.3 Results and Discussion 39
3.3.1 Initial NMR Spectra 39
3.3.2 Effect of Shear on Bovine β-lactoglobulin 41
3.3.2.1 1D ^{1}H NMR 41
3.3.2.2 2D NMR Experiments 45
3.3.2.3 Light Scattering Tests 48
3.3.3 Effect of Shear on Destabilized β-Lg – Addition of Trifluoroethanol 49
3.3.3.1 Gel Electrophoresis Test 54
3.4 Conclusions 55

4 Enzyme Activity in Pectin 56

4.1 Introduction 56

4.1.1 Pectin 56

4.1.2 Pectin Methylesterase (PME) 57

4.1.2.1 Plant Pectin Methylesterase (pPME) 59

4.1.2.2 Fungal Pectin Methylesterase (fPME) 59

4.2 Experimental Method 60

4.3 Results and Discussion 67

4.3.1 Initial NMR spectra 67

4.3.2 Control Experiments 68

4.3.2.1 Michaelis-Menten Model 71

4.3.2.2 Simultaneous Control Experiments 73

4.3.3 The Effect of Shear on the Enzyme Activity of Plant PME (pPME) on Pectin 76

4.3.3.1 Shearing Experiments using the NMR Couette Shear Cell 76

4.3.3.2 Shearing Experiments using the Benchtop Couette Shear Cell 78

4.3.3.2.1 Shearing Experiments at Higher Concentrations 81

4.3.4 The Effect of Shear on the Enzyme Activity of Fungal PME (fPME) on Pectin 82

4.4 Conclusions 84

5 Conclusions 85

5.1 Summary 85

5.2 Future Directions 87

Appendix A 89

Bibliography 92

List of Figures

Figure 1.1: Shear flow in a couette cell with the inner cylinder rotating with angular velocity ω, creating a velocity gradient across the annular gap. 9

Figure 1.2: Energy levels for nucleus with spin quantum number ½ and positive γ. 12

Figure 1.3: Hydrogen atom in a magnetic field B_0, causing the electron to circulate and generate an extra field B'. 13

Figure 1.4: Example of the bulk magnetization vector acting along the +z-axis at equilibrium, in a Cartesian reference frame. 15

Figure 1.5: Example of a bulk magnetization vector precessing about the +z-axis..... 15

Figure 2.1(a): Scale diagram of the NMR couette shear cell used in this project..... 19

Figure 2.1(b): NMR couette shear cell set inside 500 MHz NMR spectrometer..... 19

Figure 2.2: Cross-sectional view of NMR tube setups: (a) thin-walled 5mm tube and thin-walled 3mm inner tube, (b) medium-walled 5mm tube and thin-walled 3mm inner tube. 20

Figure 2.3: Example of the shear rate calculator: shows average and maximum shear rates, as well as the shear rate across the annular gap. 22

Figure 2.4: Collars used in shearing tests: bottom collar in (a) simple ring design and (b) cup-ring design, and (c) top collar. 23

Figure 2.5: (a) The benchtop couette shear cell setup, and (b) a cross-sectional view. .. 24

Figure 2.6: Control experiment of CTAB system under no shear in (a) isotropic, (b) - (d) isotropic and nematic, and (e) nematic phase. 28

Figure 2.7: Shearing experiment for CTAB system at $T_{I\text{-}N}$ + 1 K: (a) reference spectrum under no shear, (b) under 120 s^{-1} shear, and (c) 10 min after shear cessation..... 29

Figure 2.8: PBLG sample in NMR spectrometer, the PBLG director is in same direction

as magnetic field B 32

Figure 2.9: PBLG 14.02% shearing test: sample (a) under no shear, (b) under shear, and (c) after shear stopped for a few minutes. 33

Figure 2.10: Theoretical plot of $\left|\left(3\cos^2\theta - 1\right)\right|$ vs. angle made between PBLG director and magnetic field in the NMR spectrometer. 34

Figure 2.11: PBLG 12.54% shearing test: sample (a) under no shear, (b) under shear, and (c) after shear stopped for a few minutes. 35

Figure 3.1: The β-Lg backbone structure, and a standard spectrum of β-Lg under no shear, recorded in a 500 MHz NMR spectrometer showing backbone amide protons, backbone α protons, and side chain protons $H_{side\ chain}$ 40

Figure 3.2(a): Shearing experiment carried out on a β-Lg sample subjected to an average shear rates of 120 s^{-1} overnight, and compared with a spectrum of the sample prior to shear application. 41

Figure 3.2(b): Shearing experiment carried out on a β-Lg sample subjected to an average shear rate of 120 s^{-1} over 2 days, and compared with a spectrum of the sample prior to shear application..... 42

Figure 3.2(c): Shearing experiment carried out on a β-Lg sample subjected to an average shear rate of 120 s^{-1} over 4 days, and compared with a spectrum of the sample prior to shear application..... 43

Figure 3.3: Rate of conformational change in a β-Lg shearing experiment. 44

Figure 3.4(a): 2D TOCSY spectrum of 6 mM/g β-Lg. 46

Figure 3.4(b): TOCSY β-Lg structure assignment established by Uhrinova et al. [1]... 47

Figure 3.5: Fingerprint region overlay of 2D TOCSY spectra before and after shear application. 48

Figure 3.6: β-Lg containing various amounts of TFE (v/v), under no shear, at 298 K... 50

Figure 3.7: Shearing experiment on a β-Lg sample containing 10% TFE (v/v) under an average shear rate of 1570 s^{-1} over 2 days. 51

Figure 3.8(a): Comparison of the sheared β-Lg sample (containing 10% TFE (v/v) and sheared at 1570 s^{-1} for 2 days) with a control sample (containing 10% TFE (v/v)), and a reference β-Lg sample containing 20% TFE. 52

Figure 3.8(b): Comparison of the sheared β-Lg sample (containing 10% TFE (v/v) and sheared at 1570 s^{-1} for 2 days) with a β-Lg sample known to contain amyloid fibrils..... 53

Figure 4.1: Linear chain of the smooth homogalacturonan region in pectin 57

Figure 4.2: The de-esterification of pectin, catalyzed by pectin methylesterase. 58

Figure 4.3: An example of pPME acting on a pectin chain over time. 59

Figure 4.4: An example of fPME acting on a pectin chain over time. 60

Figure 4.5: Setup of sample preparation: syringe used to de-gas NMR sample, and a sonicator used on a low sonicating setting for 1 min to remove air bubbles. 64

Figure 4.6: NMR tube set up of control sample. 65

Figure 4.7: NMR spectrum showing peaks from the methyl ester group $COOCH_3$, methanol CH_3OH, and DSS, before and after pPME was added. 68

Figure 4.8(a): Control experiment showing the rate of methanol liberated over time....70

Figure 4.8(b): Rate of de-esterification (DM) over time corresponding to figure 4.8 (a).....70

Figure 4.9(a): $1/V$ vs. $1/[S]$ plot of experimental data of pPME acting on pectin. 72

Figure 4.9(b): Theoretical Michaelis-Menten model derived using K_m and V_{max} from figure 4.9 (a), compared with experimental data for pPME acting on pectin..... 73

Figure 4.10: Amount of methanol liberated over time, with experiments conducted on different days. 74

Figure 4.11: Control experiments showing the rate of methanol liberated over time,

carried out at different temperatures: 303.2 K and 305.3 K.....75

Figure 4.12(a): Control experiment of pPME and pectin under optimized protocol, with a control sample, and a sample in the NMR couette shear cell with no shear applied. 77

Figure 4.12(b): Shearing experiment with pectin and pPME sample sheared at 240 s^{-1}, and compared with a control sample that showed no change in kinetics.....78

Figure 4.13: (a) Benchtop couette shear cell setup, and (b) close up of the sample waterbath being heated by water from a variable temperature waterbath. 79

Figure 4.14: Shearing experiment with pectin and pPME sample sheared at 1570 s^{-1}, and compared with a control sample that showed no change in kinetics. 81

Figure 4.15: Shearing experiment on a 5% pectin sample (5 times usual concentration) with an average shear rate of 1540 s^{-1}, compared with control sample that showed no change in kinetics. 82

Figure 4.16: Shearing experiment with an average shear rate of 240 s^{-1} applied to a pectin and fPME sample, and compared with control sample that showed no change in kinetics. 83

Figure A.1: Diagram of sample loaded in the annular gap between two cylinders, with the inner cylinder rotating with angular velocity ω..... 89

List of Tables

Table 2.1: Summary of possible NMR tube setups and shear rates using couette shear cell..... 22

Chapter 1

1 Introduction

1.1 Introduction

Effects of shear can be seen all around us; it deforms fluids and generates flow. The effects of shear on polymer systems are of great importance in order to understand how nature uses it as a tool to trigger biological functions. For example, shear mechanisms are important modulators of cellular function in many body tissues, and especially in the cardiovascular system [2]. Here, shear forces are known to alter the blood flow, which stimulates the release of vasoactive substances, changing gene expressions and cell metabolism [2]. It is equally important to understand the effects of shear on polymers in order to improve modern material processing in laboratories or industrial factories. An example of this is easily observed in commercial factories where food production of natural polymers such as proteins takes place. Because of the numerous procedures carried out to extract and refine food products such as milk, reliable and accurate rheological data are required. This helps to find potential improvements or problems in the design of flow processes during different engineering operations [3].

Although these examples highlight how important shear processes are biologically and industrially, most previous studies of the effects of shear on macromolecules have been carried out with high concentrations of polymers, focusing on measurements of non-Newtonian rheology, such as the effects of shear on altering rheological properties

of biopolymer gels [4]. It is difficult to find work on dilute solutions of polymers under shear flow that might reveal the behaviour of single chains. Considerable theoretical studies provide evidence that shear flow affects ideal polymer chains. For example, one way of studying macromolecular dynamics under shear flow, carried out by Khare et al. [5], used molecular dynamics simulations to study shear flow effects on a particular model of polymer molecules (long polymer bead-spring chains that interact via purely repulsive potentials). They found that compared to equilibrium (no shear), long polymer chains stretched and aligned in the flow direction under shear [5]. A different study by Xu et al. used on-lattice Monte Carlo methods to simulate the effects of simple shear flow on self-avoiding walk (SAW) macromolecular chains and investigate consequential chain dynamics [6]. Here too, it was found that long polymer chains were elongated under shear flow as a result of the purely elongational flow, while chain tumbling was a result of rotational flow [6]. These results are consistent with the experimental work by Smith et al., who studied configurations of fluorescently labeled lambda bacteriophage DNA (λ-DNA) molecules under uniform shear flow using single-molecule imaging techniques [7]. Their data showed that there were large fluctuations in the extension of the flexible molecule, consistent with end-over-end tumbling of the nucleotide [7].

Experimental data on proteins under shear, however, have not produced clear answers, and some studies have had contradictory results. Protein volume interactions complicate the theoretical problem, and in addition to this it is well known that proteins are extremely sensitive to conditions such as temperature, pH, concentration, etc. Two recent studies in literature provide interesting insights. Firstly, a study about von Willebrand factor (VWF), an extremely large protein present in our circulatory system that helps to stop bleeding, was carried out by Schneider et al. in

2007 [8]. A previous study carried out by Minstry et al. in 2000 had already demonstrated that pre-treating the human platelet glycoprotein (GP) Ib/V/IX complex with inhibitors such as cytochalasin D enhanced the extent of platelet aggregation induced by VWF and high shear stress [9]. In addition to this, Schneider et al. identified individual VWF fibres as hydrodynamically activated biopolymers, being active only under high shear rates. After conducting experiments, they found that by applying unusually high shear rates ($> 10^3$ s^{-1}) above a certain critical shear rate, VWF fibres abruptly elongated from a compact coiled structure to a stretched chain [8]. Computer simulations gave consistent results, and indicated that the mechanical stress response was due to its large repeating unit size [8]. Another study, by Jaspe et al. in 2006 [10], investigated protein destabilization of a small globular protein (horse cytochrome C, 104 amino acids) by applying high shear rates. By subjecting the protein to shear rates as large as 10^5 s^{-1} experimentally, the protein did not destabilize significantly over short periods [10]. By using model calculations they made further suggestions that shear rates of at least 10^7 s^{-1} would be needed to denature a small globular protein [10]. However, shear rates of this magnitude may create extremely large tensions in the chemical bonds, and cause protein chain breaking.

The first aim of this project was to refine the development of a shear cell that could generate shear flow, while inside a Nuclear Magnetic Resonance (NMR) spectrometer, which would be tested by reproducing results from various literature studies with well established shear effects that were observed using NMR. After developing the Rheo-NMR device, we sought to investigate the possible conformational changes on proteins brought about by shear using the resolving power of high resolution NMR spectroscopy. One-dimensional (1D) ^{1}H NMR spectra could be run to monitor any conformational consequences of shear flow, then two-dimensional (2D) spectra used

to identify precise locations (or frequencies) of changes to the protein spectra, and hopefully isolate the amino acids affected.

Two systems were selected: the first involved investigating β-lactoglobulin (β-Lg), a small globular protein (162 amino acids) with some studies suggesting that shear flow leads to protein aggregation, which implies that conformational changes must have occurred to expose interacting groups. However, the details of such unfolding events are unclear. Secondly, we also used an enzyme reaction (the demethylesterification of pectin with pectin methylesterase) to study the effects of shear flow on this interaction. This interaction was chosen because NMR could monitor any changes to the rate of inter-macromolecular interactions during enzymatic processing, and previous studies from the 1970's suggested that shear modifies enzyme kinetics [11, 12]. This was a contrast from studying macromolecular structure conformations directly under shear flow.

1.2 Rheo-NMR

Rheology is, traditionally, the study of mechanical properties of complex fluids. The name itself derives from the Greek word 'rheo' which means "to flow", and was introduced by Bingham in 1929 [13]. Recently, there has been growing attention towards investigating the mechanical properties of fluids at a molecular scale, especially polymers, which are constantly submitted to some form of shear stress or flow during natural or industrial processes. In order to study the conformations of macromolecules, several techniques have been developed over the years, such as neutron scattering [14, 15], x-ray and optical methods [16-19], or bifringence and

dichroism techniques [20, 21], all of which can involve the addition of a shear producing device [22]. Over the past two decades, an alliance between rheology and NMR has become another powerful tool to investigate polymer behaviour at both microscopic and macroscopic scales, creating Rheo-NMR [23]. The advantage that Rheo-NMR has over the other techniques is the range of operations that can be applied. For example, Rheo-NMR offers the ability to study optically opaque samples, and can combine velocimetry with localized spectroscopy, and thereby study molecular dynamics, orientation, and organization.

The first study that investigated the rheological properties of polymer systems using NMR was by Martins et al. in 1986. They found that by suddenly (yet carefully) rotating a sample tube containing a nematic liquid crystal, poly(4,4'-dioxy-2,2'-dimethyl azoxybenzenedodecanediyl), in an NMR magnet, the director (a vector that describes the preferred orientation of the liquid crystal molecules) would re-align itself with the NMR magnetic field, indicated by a slow change in the ^{1}H NMR spectra [24]. In Rheo-NMR today, the sample is sheared by means of a shearing device in a cone and plate, or couette cell geometry located inside a NMR spectrometer, and the NMR signals recorded in real time [25]. One of the first notable Rheo-NMR experiments using a shearing device was described by Nakatani et al. in 1990 [26], who acquired the NMR signal of poly(vinyl methyl ether)-water, and applied a shear rate of 4 s^{-1} to study shear flow effects on the polymer. The results found that by means of ^{1}H NMR, the NMR spectrum broadened under shear and slowly relaxed back after shear cessation [26], indicating a shear induced phase transformation from a clear transparent phase to an opaque melt, usually obtained by heating the sample. The following year, Xia and Callaghan showed that NMR microscopy could be used to measure velocity profiles to study

shear-thinning effects in semi-dilute solutions of high molecular weight polymers, where they found that shear thinning is associated with significant enhancement of the polymer Brownian motion along the axis of shear [27]. These examples show the useful ability of Rheo-NMR to provide unique information, leading to its favourable use as a probe for investigating the effects of shear flow on macromolecular structures and inter-macromolecular interactions in this thesis.

1.3 Rheology of Macromolecules

Macromolecules, also known as polymers, are built up of a large number of molecular units that are linked together by covalent bonds [28].

1.3.1 Bovine β-lactoglobulin

Bovine β-lactoglobulin (β-Lg) is the major protein found in the whey fraction of milk from mammals such as cows, sheep, and pigs [29]. Industrially, β-Lg is found in milk and milk products such as ice-cream, whipped creams, coffee cream, etc. There are eight identified genetic variants of β-Lg, however, variants A and B are the most common and exist at almost the same frequency [30], only differing by Asp64Gly and Val118Ala substitutions [31]. With a molecular weight of 18.3 kDa, β-Lg contains two internal disulfide bonds and a single free thiol group, which is of great importance to milk denaturation [30].

Considerable research into the effects of rheological processes on β-Lg have and are still being carried out by food industries, since milk is subjected to a range of

processing conditions that can change its structure. For example, during commercial milk production, β-Lg denaturation by heating and shear flow can produce a number of undesired effects such as fouling [32], but it can also be useful to obtain desired modifications and improvements in products (e.g. yoghurt texture). By studying the individual proteins, it leads to a better understanding of how to improve these industrial operation conditions. A study by Hill et al. suggested that shear induces β-Lg aggregation, implying that shear induces conformational changes to the β-Lg structure, exposing interacting residues [33]. However, like most of the other available shear studies that have found similar results, these experiments have been performed at high temperatures where protein denaturation occurs naturally due to heating, and it is difficult to distinguish sole shear flow effects. The aim of this study was to investigate the sole effects of shear flow on β-Lg protein structure.

1.3.2 Pectin

Pectin is the major component of plant cell walls, and industrially it is used in jams, fruit juices, bakery-fillings, and various confectionary as a gelling agent [34]. Its abundance means 4 – 5 g of pectin is consumed daily in a normal western diet [35], amounting to a 45,000 tonne annual worldwide consumption, worth over 400 million euros on the global market [36]. The name is derived from the Greek word 'pektikos' which means "congeal" or "solidify" [37]. Pectin's structural 'backbone' is largely homogalacturonan, a linear polymer containing large amounts of Galacturonic acid (GalA), which can be methyl-esterified by enzymes. The degree of methyl-esterification (DM) within the pectin structure has large effects on its functional properties. This has fuelled interest into understanding the sensitive relationship between pectin structure and its function, which would have direct implications in industrial processes to produce, modify, or manipulate fruits and

vegetables to a desirable form [34].

The relationship between gelling properties and DM has been investigated in several studies. For example, Rosenbohm et al. studied a natural citrus pectin (DM 64%), and changed it to various DM values by using anhydrous methanol acidified with acetyl chloride (increasing DM) or treating pectin with aqueous base (lowering DM) [38]. The results showed that pectin DM could be controlled to create pectin with novel gelling abilities compared to raw citrus pectin [38], therefore, showing that pectin with desirable properties could be produced. Another study by Denès et al. focused on the action mechanism of pectin methylesterase (PME) enzymes acting on the de-esterification process in pectin (75% DM) [39]. Their results found that apple PME action mechanism was pH-dependent. At pH 7 (optimal enzyme conditions), single-chain mechanism was observed, where binding of the enzyme was followed by a conversion of all contiguous substrate sites on the polymer chain. However, at pH 4.5 a multiple-chain mechanism was observed, where PME catalysed the de-esterification of the carboxyl groups randomly [39]. By using our Rheo-NMR device, we aimed to study the effects of shear on the inter-macromolecular interactions of pectin and PME under optimal conditions.

1.4 Shear

An important characteristic of a fluid is that it deforms continuously whilst acted upon by a *shear force* acting tangential to a fluid area [40]. The ratio of the shear force acting to the area is called *shear stress*. The study of macromolecular systems under shear has been important because it provides an insight into how systems behave in

the real world, where they are constantly exposed to various shear forces created by nature or by industrial processes.

1.4.1 Shear in a Couette cell

Shear flow measurements in this study were carried out using a custom built NMR couette shear cell and benchtop couette shear cell, both of which were developed in-house, and consisted of two concentric glass cylinders consisting of NMR tubes of different diameters, with the sample placed inside the annular gap (figure 1.1, 2.1).

The outer cylinder remained stationary while the inner cylinder was connected to a programmable stepper motor (figure 2.1), which rotated the inner cylinder at an angular velocity ω, to create a velocity gradient across the liquid sample placed in the annulus, as seen in figure 1.1.

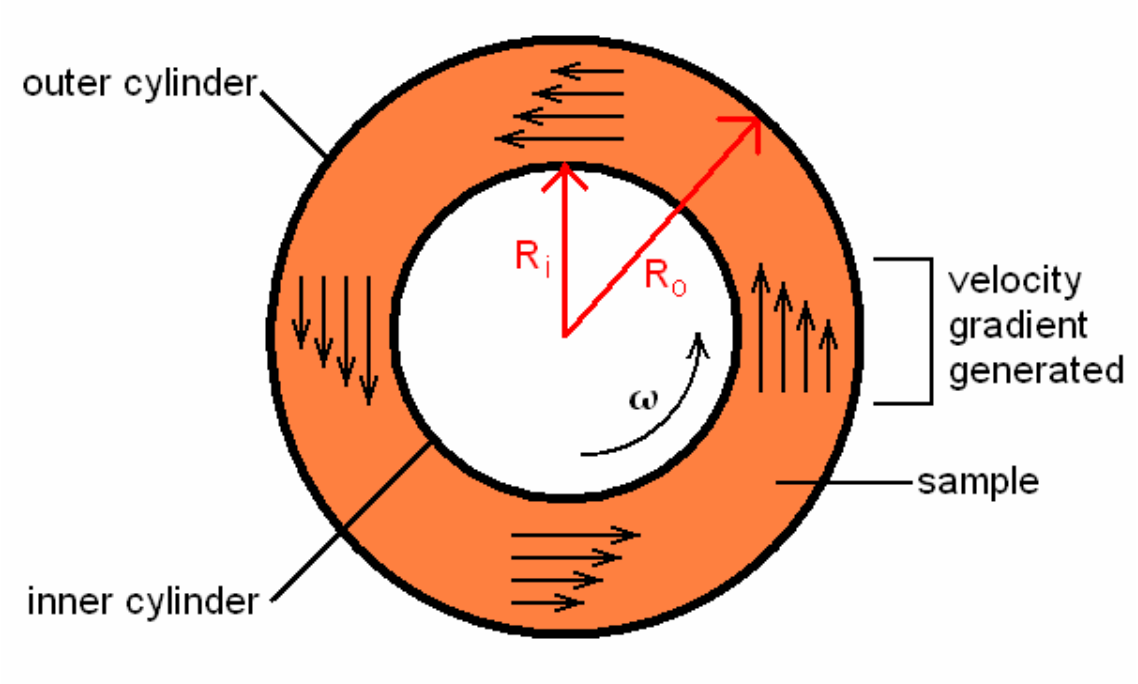

Figure 1.1: Shear flow in a couette cell with the inner cylinder rotating with angular velocity ω, creating a velocity gradient across the annular gap.

The shear rate $\dot{\gamma}$ applied to the sample in the annular gap of the cylinders was calculated using:

$$\dot{\gamma} = -\frac{2\omega}{1-\left(\frac{R_i}{R_o}\right)^2} \tag{1.1}$$

where ω is the angular velocity of the rotating inner tube, while R_i and R_o correspond to the inner radius of the gap (outer radius of the inner NMR tube) and outer radius of the gap (inner radius of the outer NMR tube) respectively [41]. A detailed derivation of the shear rate equation is discussed in Appendix A.

1.5 Nuclear Magnetic Resonance (NMR)

Nuclear Magnetic Resonance (NMR) spectroscopy is based on the fact that certain atomic nuclei absorb radio frequency (RF) electromagnetic radiation in the presence of an external magnetic field at characteristic frequencies [42]. This enables the observation of individual atoms within a macromolecule, and may be used to determine its molecular structure, conformation and dynamics [43].

The most common nucleus within a biological macromolecule is typically hydrogen, which is most sensitive to detection by NMR [43]. The first published NMR spectrum of a biological macromolecule was in 1957, which showed a 40 MHz ^{1}H spectrum of pancreatic ribonuclease, whose poorly resolved NMR spectrum was nonetheless consistent with the protein's amino acid composition, highlighting the technique's potential to study macromolecular systems with high accuracy [43].

Since then, NMR has undergone tremendous developments in both instrumentation and methodology, and is widely used in a diverse range of research fields such as chemistry, medicine, and physics. Studies of its conformations and interactions of biological macromolecules (typically using multi-dimensional NMR, where the resonance intensities are recorded as a function of two, three, or even four frequency variables) have now become routine [43].

1.5.1 Basic Principles of NMR

1.5.1.1 NMR

The fundamental property of the atomic nucleus involved in NMR is the nuclear spin, denoted by quantum number I, which has values of 0, ½, 1, etc. The value of the nuclear spin depends on both the mass number and the atomic number of the atomic nucleus. NMR experiments cannot be conducted on nuclei with $I = 0$, such as ^{12}C, ^{16}O and ^{32}S, since they have no spin angular momentum, and therefore, no magnetic moment to interact with the external magnetic field. Examples of normal nuclei with roughly 100% natural abundance, that have $I = ½$, are nuclei such as ^{1}H, ^{19}F and ^{31}P, while other less abundant nuclei include ^{13}C, ^{15}N and ^{29}Si [42].

The spinning action of the nucleus and its positive charge generates a small magnetic field. This means that it has a nuclear magnetic moment, $\vec{\mu}$, given by:

$$\vec{\mu} = \frac{\gamma \vec{I} h}{2\pi} \tag{1.2}$$

where h is Planck's constant, $\vec{I}$ is the spin angular momentum, and γ is the gyromagnetic ratio (a constant characteristic of a particular nuclide).

When a uniform magnetic field of magnitude B_0 is applied, the nuclear magnetic

moments within the atoms orient themselves. The number of possible orientations is determined by I and quantum mechanics, which tells us that a nucleus with spin I has $(2I + 1)$ possible orientations. The nuclei commonly observed in NMR spectroscopy, ^{1}H and ^{13}C, have spin $I = ½$, and therefore two orientations $(2(½) + 1)$. In the absence of a magnetic field, these orientations have equal energy. In a magnetic field, the energy levels become non-degenerate, as seen in figure 1.2, characterized by a magnetic quantum number $m = ½, -½$ (in general, $m = +I, I\text{-}1, I\text{-}2,..., -I$).

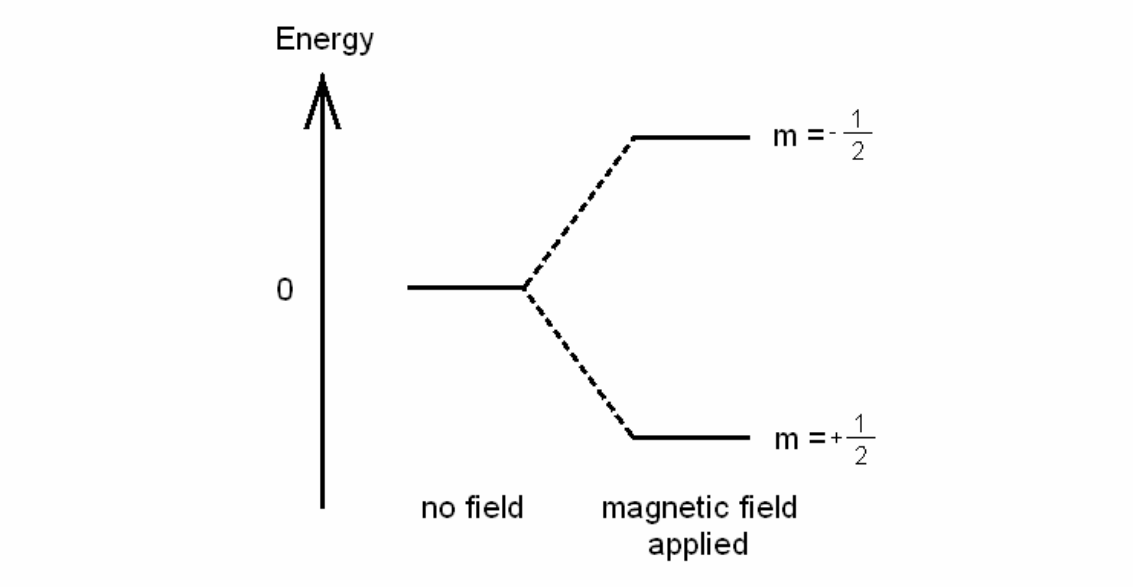

Figure 1.2: Energy levels for a nucleus with spin quantum number ½ and positive γ.

Now, the energy of each spin state is proportional to $\vec{\mu}$ and the magnetic field strength B_0, and is written as [44]:

$$E = -\frac{\gamma\hbar m B_0}{2\pi} \tag{1.3}$$

The selection rule for NMR transition is that the magnetic quantum number m can only change by one unit, so $\Delta m = \pm 1$. Thus, the difference between energy levels, or transition energy can be rewritten as [44]:

$$\Delta E = \frac{\gamma\hbar B_0}{2\pi} \tag{1.4}$$

If we substitute for ΔE using the Bohr frequency condition: $\Delta E = h\upsilon$, then the

resonance frequency can be written as:

$$\nu = \frac{\gamma B_0}{2\pi} \tag{1.5}$$

1.5.1.2 Chemical Shift

In a real sample, nuclei will be shielded to a small extent by the surrounding electrons. The motion of the electrons circulating around the nuclei is equivalent to an electric current flowing in a closed loop, creating its own magnetic field that opposes B_0 (figure 1.3). This means that the total field experienced by the nuclei is slightly less than B_0, and thus the resonant frequency must also shift [42] compared to that expected for a hypothetical bare nucleus.

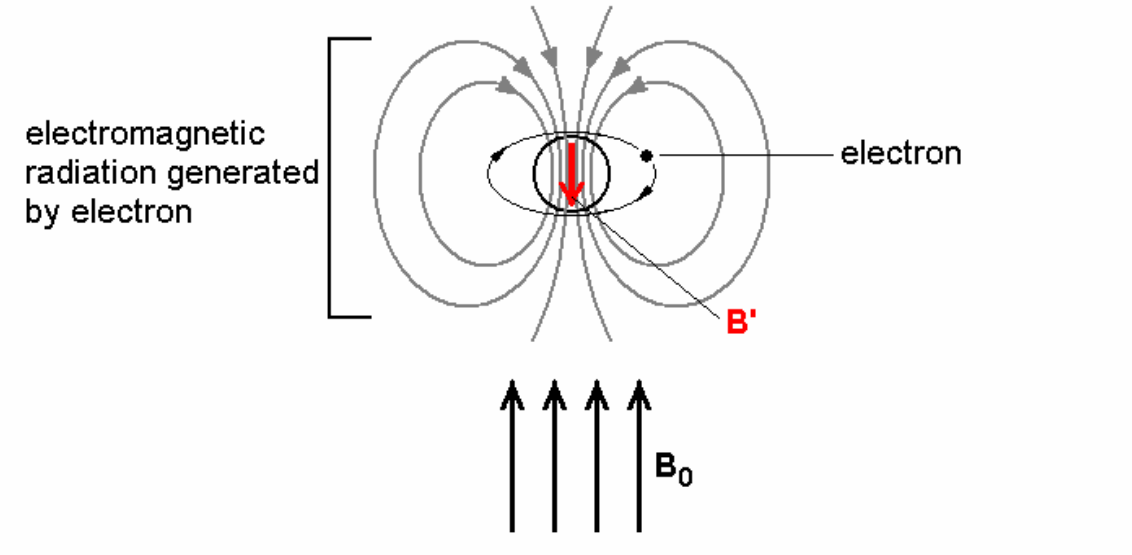

Figure 1.3: Hydrogen atom in a magnetic field B_0, causing the electron to circulate and generate an extra field B'.

As a result of the nuclear shielding, the resonance condition (equation 1.5) becomes:

$$\nu = \frac{\gamma B_0 (1-\sigma)}{2\pi} \tag{1.6}$$

where σ is the proportionality constant between B' (the magnetic field generated by the nucleus) and B_0 (the external field generated by the spectrometer's magnet) [45]. σ will often differ for nuclei of different atoms with a molecule according to the local

electron density, giving rise to multiple peaks in the NMR spectrum. This phenomenon of nuclear shielding by the surrounding electrons is called the *chemical shift*.

Chemical shifts are usually reported using the δ scale:

$$\delta[ppm] = \frac{(\nu - \nu_{ref})[Hz]}{\nu(spectrometer)[MHz]} \tag{1.7}$$

where ν-ν_{ref} is the frequency difference between the nucleus of interest and a reference nucleus, all divided by the spectrometer frequency, and quoted in *parts per million*, or ppm.

1.5.1.3 Bulk Magnetization

As explained in 1.5.1.1, a nuclear spin interacts with an external magnetic field of magnitude B_0, resulting in energy levels and ultimately an NMR spectrum. However, a typical NMR sample contains a large number of (^{1}H) nuclei. These are distributed between energy levels according to the Boltzmann distribution.

If we consider an ensemble of spins with a particular chemical shift, then at equilibrium, their magnetic moments are aligned in a way that their contributions are added up. This creates a net magnetic field from the nuclei along the direction of the external field $\vec{B}_0$, coincident with the z-axis of a Cartesian reference frame (figure 1.4) (assuming a positive gyromagnetic ratio, which is the case for ^{1}H). This is called the *bulk magnetization vector* $\vec{M}$.

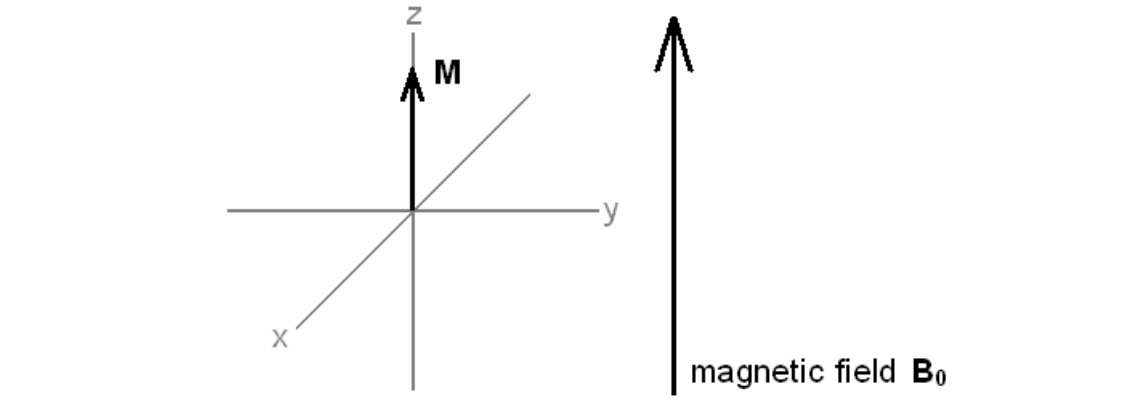

Figure 1.4: Example of the bulk magnetization vector aligned along the +z-axis at equilibrium, in a Cartesian reference frame.

1.5.1.4 Pulses

The bulk magnetization vector $\vec{M}$ can be tilted away from the +z-axis by applying an RF pulse, such that a small magnetic field is generated along the x-axis of the reference frame. This rotates $\vec{M}$ away into the xy-plane. Once tilted away from the z-axis, $\vec{M}$ rotates about the direction of the magnetic field $\vec{B}_0$, sweeping out a cone (figure 1.5). Here, $\vec{M}$ is said to precess about the magnetic field, generating a signal detected by the spectrometer.

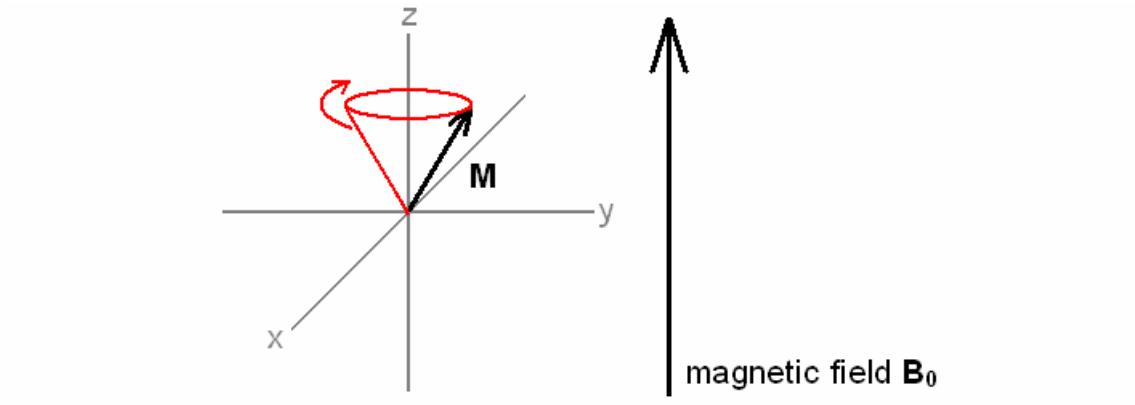

Figure 1.5: Example of a bulk magnetization vector precessing about the +z-axis.

1.5.1.5 Relaxation

After $\vec{M}$ has been tipped into the xy-plane by the RF pulse, it will relax back to its

equilibrium position along the +z-axis. This relaxation involves two processes: the first involves the exchange of energy between the excited spins and the surrounding medium (the lattice). The time constant for this process is called T_1, the spin-lattice relaxation time. T_1 characterizes the time for re-establishment of the equilibrium Boltzmann populations. From a practical point of view, T_1 determines how quickly we can repeat the NMR experiment.

The other relaxation process involves the exchange of energy between spins rotating in the xy-plane. The result of such a process is that some spins will rotate faster and others will rotate slower. The divergence of the precession rates of the spins leads to the loss of the x and y component of the bulk magnetization vector and decay of the time domain NMR signal. This process is characterized by T_2, the spin-spin relaxation time. T_2 is related to the line widths in the NMR spectrum. It tends to decrease with increasing molecular size, leading to broader lines in the NMR spectrum for large molecules.

1.5.1.6 Water Suppression

In an aqueous NMR sample, water is ~50 M, but the solute is ~1 mM. Therefore, the sizes of the signals are very different. In fact, water has a very intense signal that exceeds the dynamic range of the spectrometer's analog-to-digital converter [46], meaning that water and solute signals differ so much that they can not be accurately digitized simultaneously (i.e. if the water signals are scaled so that its maximum intensity is the biggest number the analog-to-digital converter can handle, the solute peaks will be so small that they will be less than the smallest number that can be stored in the analog-to-digital converter – their signals disappear). Therefore, water suppression schemes such as presaturation are used to reduce water proton signals, so

that a high signal to noise ratio can be achieved to produce clean spectra. Presaturation follows a simple procedure where a long (several seconds) low power pulse is applied to the solution, exactly at the frequency of the water solvent to be suppressed [47]. This selective pulse equalizes the Boltzmann populations of the spins in the vicinity of the water chemical shift so that when a high power pulse is applied to all the spins, there is no z-magnetization at the water frequency, meaning that no xy-magnetization can be created for these spins, and thus removing the water peak. However, presaturation is never perfect, largely due to the imperfections in the magnetic field homogeneity, so there is often a small residual water peak, but this is typically of the order of the height of the solute peaks.

Chapter 2

2 Experimental Method

2.1 Shear Cell

Shear is generated when two parallel plates or walls containing a liquid between them move relative to one another, creating a velocity gradient across the liquid (figure 1.1) [48]. In this project, two shear cells were used to generate shear: an NMR couette shear cell, and a Benchtop couette shear cell.

2.1.1 NMR Couette Shear Cell

A custom-built couette shear cell developed in-house was used for these studies. The cell consisted of two cylindrical NMR glass tubes of varying diameters, one inside another. The outer cylinder remained stationary in a modified NMR tube sample holder (spinner) while the inner cylinder was rotated by a drive shaft located inside a long cylindrical cell shaft, connected to a programmable stepper motor (figure 2.1 (a)). The shear rates obtainable with this setup are summarized in Table 2.1. The NMR couette shear cell setup was designed to be fitted into a NMR spectrometer (figure 2.1 (b)) to enable real-time NMR observations of shear flow on macromolecular systems.

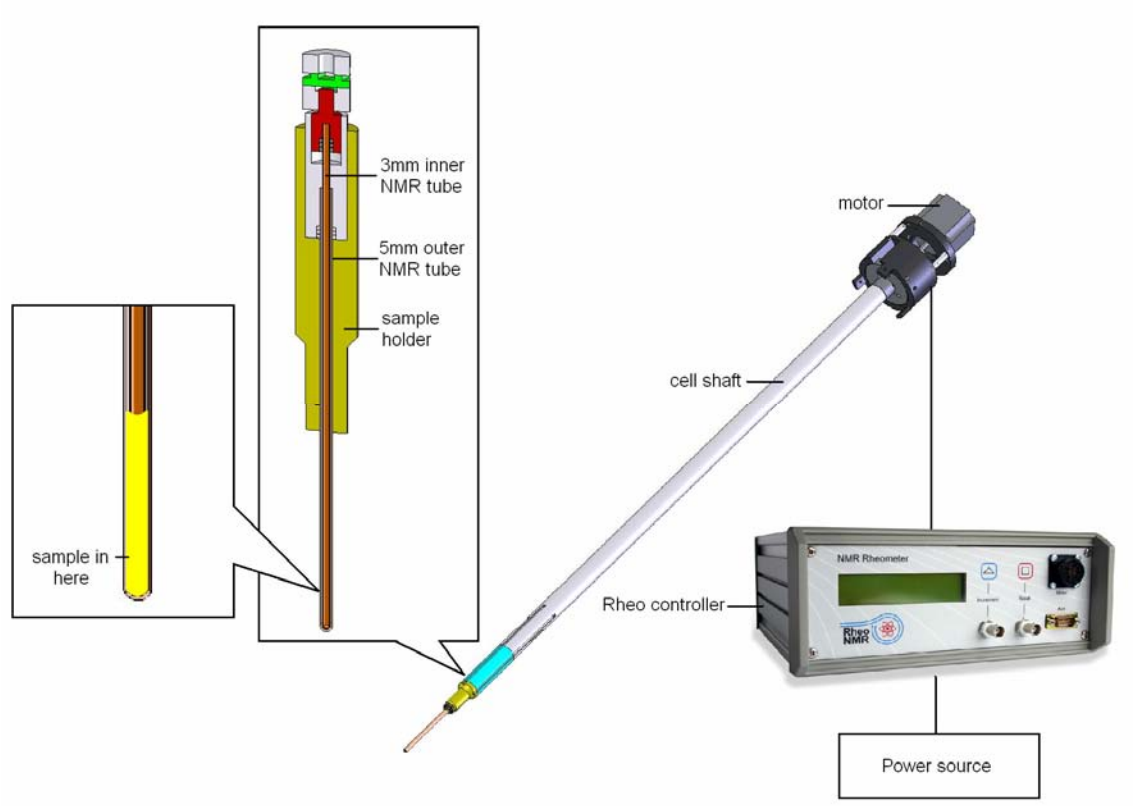

Figure 2.1 (a): Scale diagram of the NMR couette shear cell used in this project.

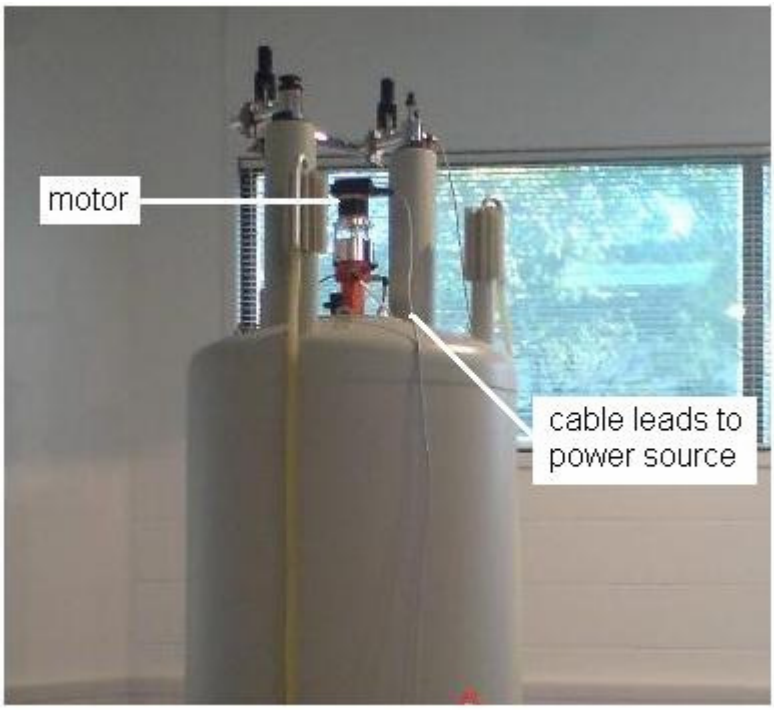

Figure 2.1 (b): NMR couette shear cell set inside 500 MHz NMR spectrometer.

Two sets of NMR tubes were used: a thin-walled 3 mm NMR tube (type 307-PP, Wilmad Glass Co.) and either a thin-walled 5 mm NMR tube (type 507-PP, Wilmad Glass Co.), or a medium-walled 5 mm NMR tube (type 504-PP, Wilmad Glass Co.) (figure 2.2 (a), (b)). The shear rate of the cell was controlled using a 24V programmable stepper motor, capable of rotating the inner tube up to 14 Hz. Table 2.1 summarizes the obtainable shear rates for both NMR tube sets, where higher shear rates could be reached by having a smaller annular gap at the expense of a smaller sample volume.

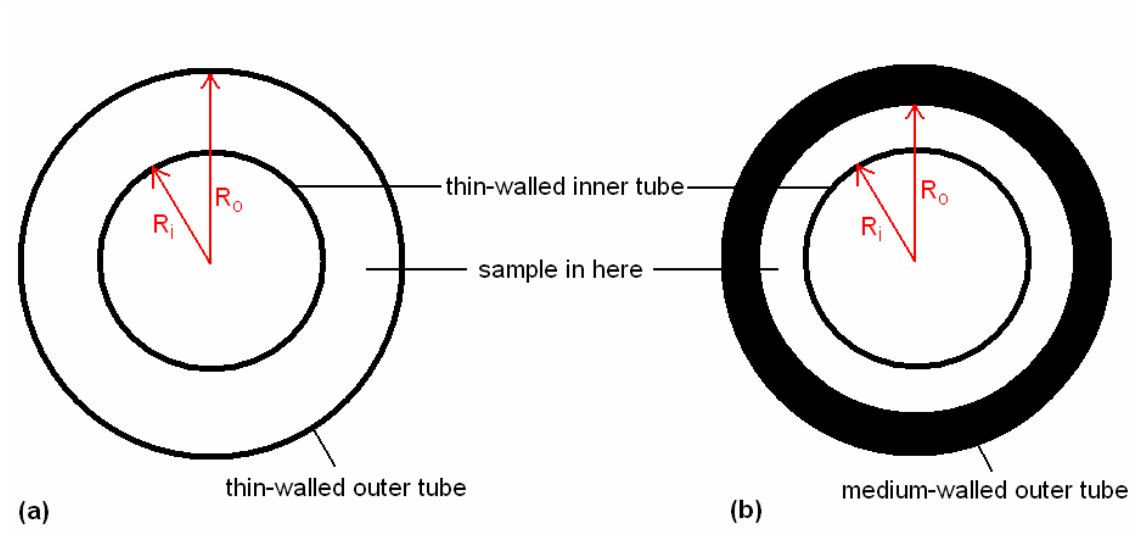

Figure 2.2: Cross-sectional view of NMR tube setups: (a) thin-walled 5mm tube and thin-walled 3mm inner tube, (b) medium-walled 5mm tube and thin-walled 3mm inner tube.

NMR tube setup	Thin-walled 3 mm / Thin-walled 5 mm tubes	Thin-walled 3 mm / Medium-walled 5 mm tubes
Outer radius of inner tube, R_i / inner radius of outer tube, R_o (mm / mm)	1.5 / 2.12	1.5 / 1.73
Gap (mm)	0.62	0.23
Possible (average) shear rate range using NMR couette shear cell (s^{-1})	0 – 240	0 – 710
Possible (average) shear rate range using Benchtop couette shear cell (s^{-1})	0 - 1570	n/a

Table 2.1: Summary of possible NMR tube setups and shear rates.

The shear rate applied across the annular gap, where the sample sits, was calculated using equation 1.1 (refer to Appendix A for detailed derivation). The equations in Appendix A were implemented into a simple Delphi computer program (figure 2.3), in which inputting data about the angular velocity, R_i, and R_o, would result in an output providing information about the average and maximum shear rates across the annular gap.

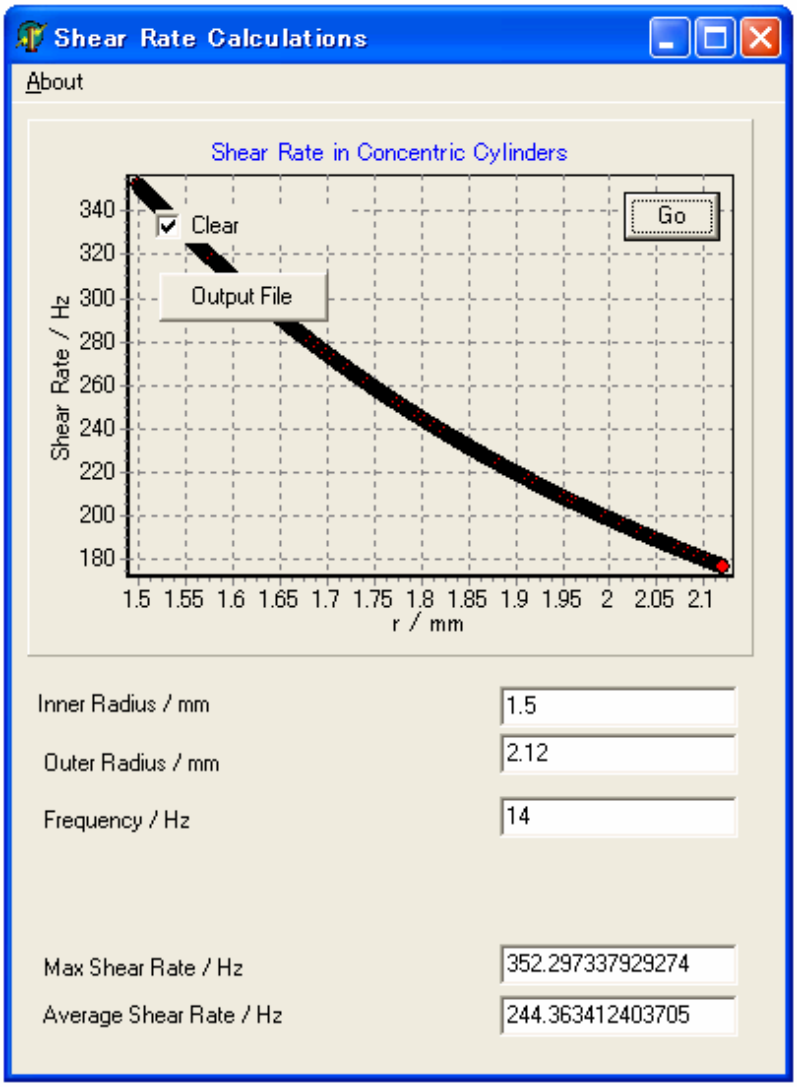

Figure 2.3: Example of the shear rate calculator: shows average and maximum shear rates, as well as the shear rate across the annular gap.

Collars were placed at the bottom of the 5 mm outer tubes (figure 2.4). Preliminary tests showed that without a collar, there were problems with the inner tube scratching against the outer tube walls, and so a collar was placed inside the setup to prevent any damage to NMR tubes and to keep the inner tube rotating concentrically. The collars were made using PEEK plastic, chosen for its thermal stability, chemical resistance, and low NMR signal, ensuring that it would have minimal interference with experiments.

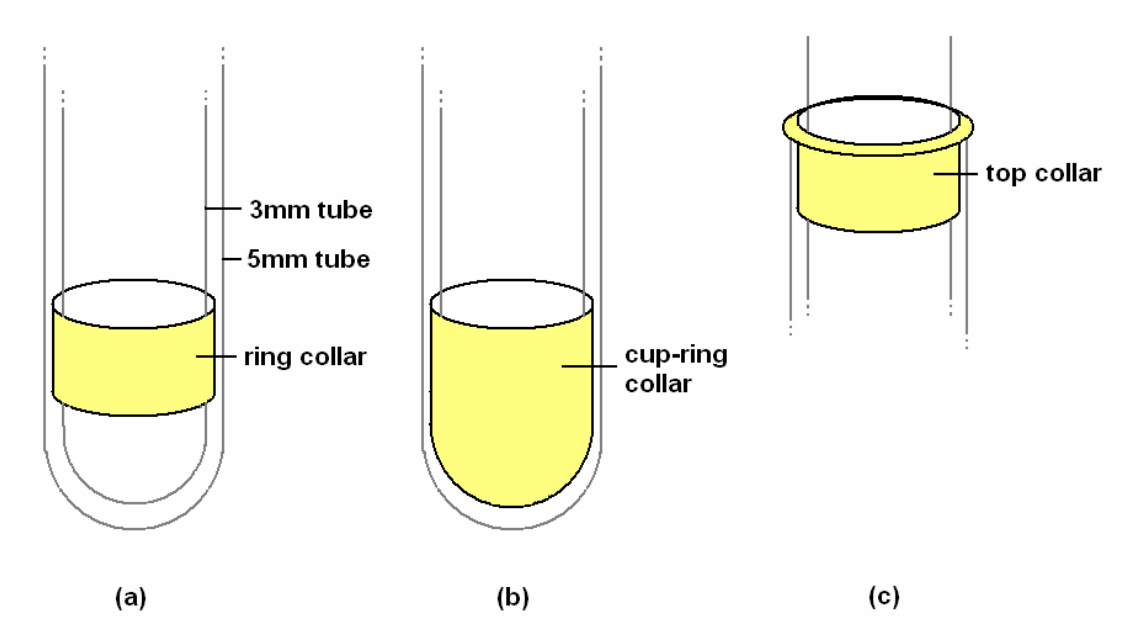

Figure 2.4: Collars used in shearing tests: bottom collar in (a) simple ring design and (b) cup-ring design, and (c) top collar.

The cup-ring design (figure 2.4 (b)) was selected after further shearing tests revealed that at high shear rates, above 170 s^{-1}, simple ring collars (figure 2.4 (a)) would move up the sample and remain in place at the sample/air interface. This was a problem as the moving collar would interfere with some of the NMR signals during an experiment, and would allow the inner tube to scratch against the 5 mm outer NMR tube. To overcome this problem, the cup-ring model was adopted to enable the collar to remain in place at the bottom of the 5 mm tube, where it would not interfere with many NMR signals and keep the inner tube rotating concentrically.

During preliminary experiments, high temperatures would cause the sample to evaporate off, observed via NMR as a drop in signal intensity of the evaporating substance. Therefore, a top collar was developed to be placed at the top of the 5 mm outer tube (figure 2.4 (c)). This collar solved problems by acting as a lid to prevent significant sample evaporation. In addition to this, the collar also helped to keep the 3 mm inner tube rotating concentrically.

2.1.2 Benchtop Shear Cell

After small changes in macromolecular structures were observed under low shear rates (refer to chapter 3, 4), it became apparent that higher shear rates were desirable in order to investigate the behaviour of macromolecules under high shear rates, and therefore a benchtop shear cell was developed (figure 2.5). The setup was identical to the NMR couette shear cell (figure 2.1), except that the NMR tube sample holder had been modified, and the cylindrical cell shaft had been eliminated. Because of the shorter distance between the shear motor and the rotating inner tube, the 24 V programmable stepper motor could rotate the drive shaft up to 90 Hz with the inner tube still rotating concentrically. Shear rates that are obtainable with this set up are summarized in Table 2.1.

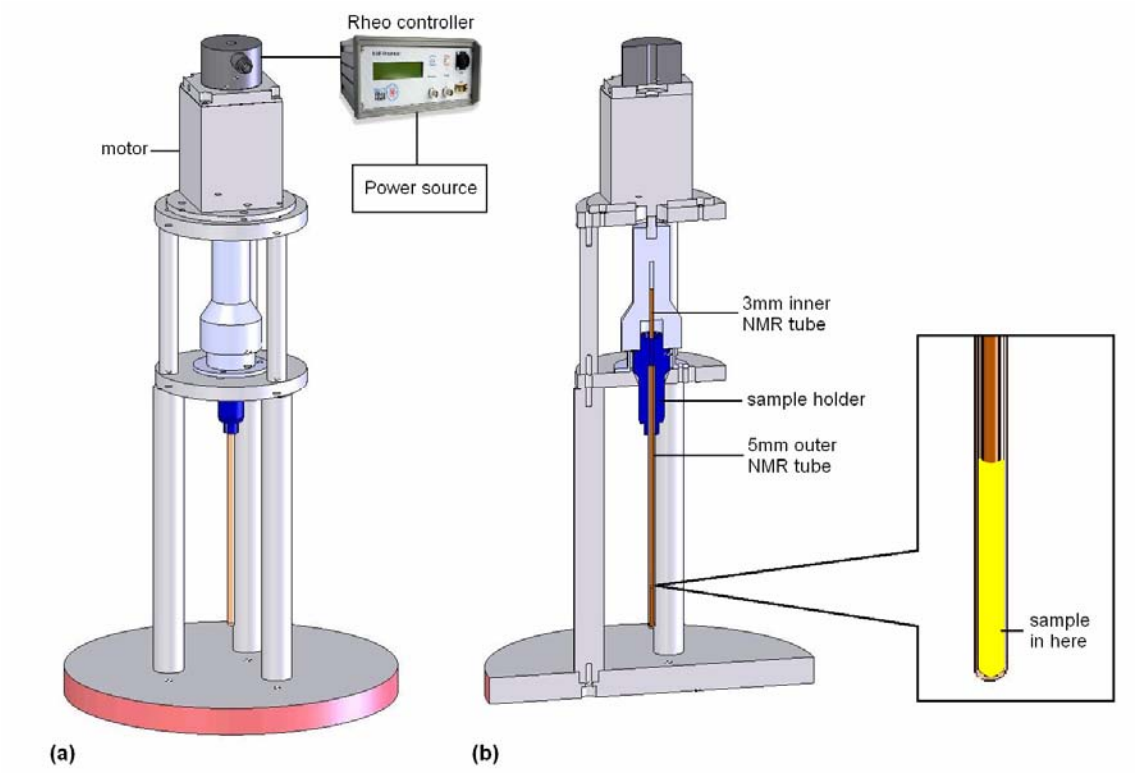

Figure 2.5: (a) The benchtop couette shear cell setup, and (b) a cross-sectional view.

Collars were also used in this setup, although a top collar was not needed as the top of the 5 mm tube was sealed up by a wall at the top of the shear cell.

In order to test if the shear cells were producing a shear profile across the annular gap, two liquid crystal systems were studied that have well-established effects under shear: Cetyl Trimethyl Ammonium Bromide (CTAB) in deuterium oxide (D_2O) and Poly(gamma-benzyl-L-glutamate) (PBLG) in m-cresol.

2.2 Cetyl Trimethyl Ammonium Bromide (CTAB) in D_2O

2.2.1 Introduction

CTAB is an amphiphile, characterized by having one end of the molecule being polar and attracted to water while the other end is non-polar and attracted to hydrocarbons. At sufficiently high concentrations in aqueous solutions, CTAB self assembles into wormlike micelles. As these micelles grow (e.g. by increasing the CTAB concentration or lowering temperature) they may reach a point where they spontaneously self-organize into a liquid crystal phase (characterized by having orientational but not translational order) such as a nematic phase. Although concentration or temperature alteration are the usual ways liquid crystalline ordering is induced, Fischer and Callaghan demonstrated by means of deuterium (^2H) NMR that close to the isotropic-nematic phase transition, orientational ordering of CTAB micelles can also be induced by the application of shear [49]. These results have been reproduced in this experiment under similar conditions. ^2H NMR spectroscopy is a powerful technique that can be used to investigate the director distribution of nematic liquid crystals [50], where the director simply refers to the direction in which

the majority of CTAB molecules are pointing. In isotropic solutions of amphiphiles in D_2O, the quadrupolar interaction of ^2H is averaged to zero, giving a NMR spectrum containing a single peak. On forming a liquid crystal phase, the averaging is incomplete, resulting in a NMR spectrum containing a doublet peak, whose peak-to-peak separation is affected by the angle made between the director and the magnetic field vector within the NMR spectrometer. Therefore, any preferred orientation obtained as a consequence of applying shear can be detected by the observation of this doublet in the ^2H NMR spectrum [50, 51].

2.2.2 Experimental Method

Samples of CTAB (Sigma-Aldrich) in D_2O (99.9% deuteration degree for NMR spectroscopy, Merck) were made up with a weight fraction of 0.20, and left to incubate in a waterbath at 318 K for 1 hour.

All NMR work reported here was carried out on a Bruker 400 MHz NMR spectrometer, operating at 60 MHz, with a spectral width of 5.0 kHz. Each of the FIDs used 1 scan, with a recycle delay of 1.0 s.

A control experiment involved preparing the CTAB sample in the NMR couette shear cell using thin-walled inner and outer tubes with 3 mm and 5 mm outer diameters respectively. NMR spectra of the sample were recorded at various temperatures above and below the isotropic-nematic phase transition under no shear. By doing this, we were able to establish the temperature of the isotropic to nematic and nematic to isotropic phase changes.

The sample used in the CTAB shearing test was prepared identically to the control

experiment sample. The test started with obtaining an NMR spectrum of the solution in the isotropic phase, then applying an average shear rate of 120 s^{-1} before another spectrum was recorded, and a final spectrum after shear cessation. Then, the temperature was lowered by 1.0 K, and the process repeated again until spectra showed nematic ordering under shear. Each time the temperature was lowered, the sample was left to adjust at that temperature for 10 min before another spectrum was taken to ensure that the liquid crystal structure had enough time to equilibrate at the new temperature.

2.2.3 Results and Discussion

The results of the control experiment are shown in figure 2.6.

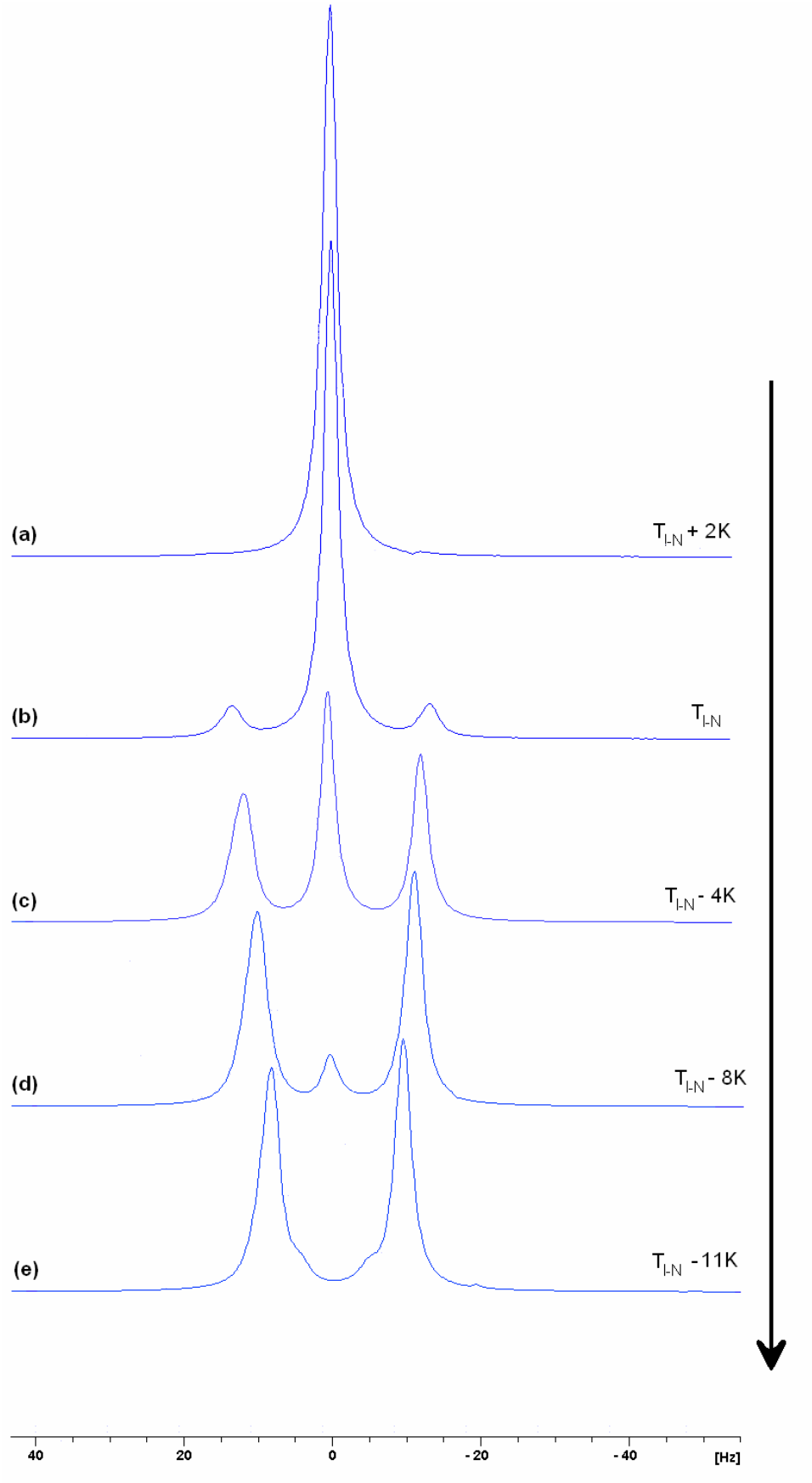

Figure 2.6: Control experiment of CTAB system under no shear in (a) isotropic, (b) - (d) isotropic and nematic, and (e) nematic phase.

The results from the control experiment showed a single peak in the NMR spectrum, indicating that the sample was in an isotropic state (figure 2.6 (a)), 2 K above the equilibrium Isotropic-Nematic transition state (T_{I-N} + 2 K). As the sample began to cool, both nematic ordering and an isotropic state (figure 2.6 (b) – (d)) were observed, characteristic of the bi-phasic region. The CTAB finally entered the pure nematic phase, indicated by the quadrupolar doublet (figure 2.6 (e)).

Once the isotropic-to-nematic transition was established, a shearing test was carried out to study the effects of an average shear rate of 120 s^{-1} on the CTAB system in an isotropic state at T_{I-N} + 1 K (figure 2.7).

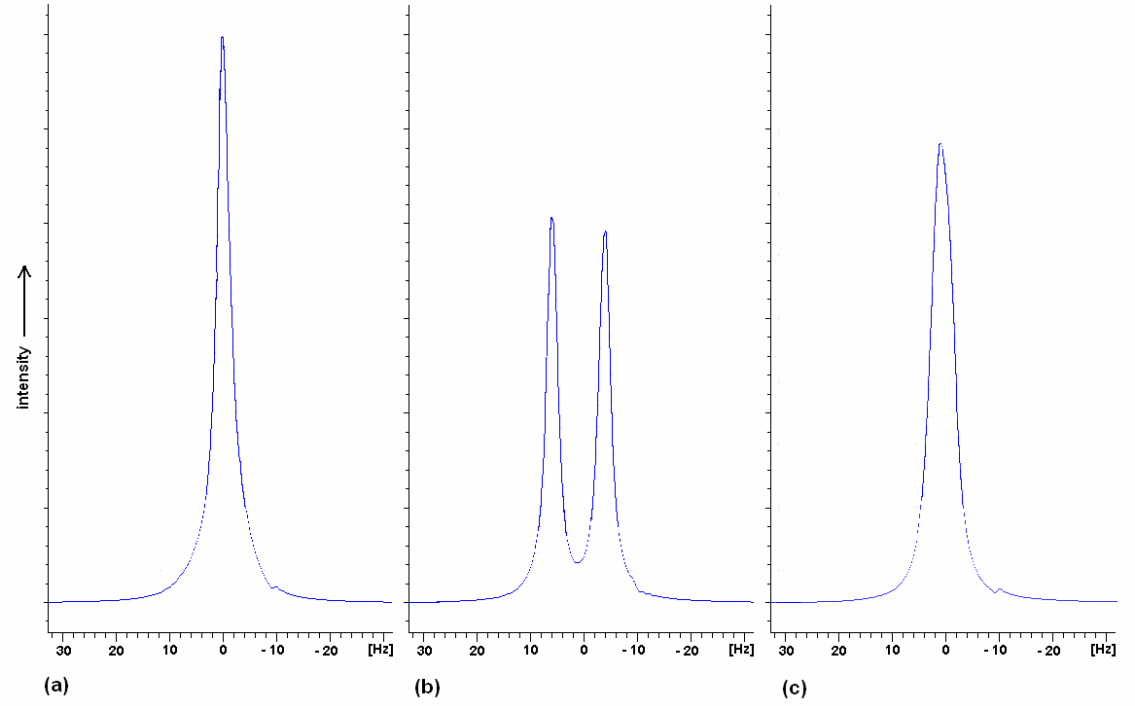

Figure 2.7: Shearing experiment for CTAB system at T_{I-N} + 1 K: (a) reference spectrum under no shear, (b) under 120 s^{-1} shear, and (c) 10 min after shear cessation.

Figure 2.7 (a), (b), and (c) showed the behaviour of CTAB under no shear, under a maintained average shear rate of 120 s^{-1}, and then the relaxed state following shear cessation. These results indicated that shearing CTAB in an isotropic state near the Isotropic-Nematic transition induces a phase transition to a nematic state. These results mirrored those obtained by Fischer and Callaghan, where the application of 105 s^{-1} shear to the CTAB system changed its shape from a singlet to a doublet peak while under shear, returning to a singlet peak 2 minutes after shear cessation [49].

2.2.4 Conclusion

Using ^2H NMR spectroscopy, nematic ordering was achieved by applying shear to a CTAB system in D_2O that was in an isotropic state. After shear cessation, the CTAB system relaxed back into an isotropic state, therefore demonstrating that CTAB behaviour under shear was consistent with corresponding results obtained by Fischer and Callaghan [49]. This demonstrated that the NMR couette shear cell was capable of producing shear flow.

2.3 Poly(gamma-benzyl-L-glutamate) (PBLG) in m-cresol

2.3.1 Introduction

Poly(gamma-benzyl-L-glutamate) (PBLG) is an amphiphilic molecule, and forms a lyotropic liquid crystal in certain organic solvents. The anisometric magnetic susceptibility of PBLG is such that the long axis of the PBLG molecule (and the liquid crystal director) tends to align parallel with the magnetic field (figure 2.8). If the PBLG director is tilted away from the magnetic field while in a nematic phase, then the characteristic doublet splitting $\Delta\nu$ of an oriented ^2H nucleus observed in NMR will be

given by:

$$\Delta\nu(\theta) = \frac{1}{2}\Delta\nu(0)\left(3\cos^2\theta - 1\right) \tag{2.2}$$

where θ is the angle (radians) made between the director and the magnetic field. In contrast to the experiments run on CTAB in section 2.2, which investigated the phase transition from isotropic to nematic phases under shear, here we looked at the orientation of the director in the nematic phase. Hence, in this experiment, if the application of shear tips the liquid crystal director away from the magnetic field direction, then we would expect to see ^{2}H NMR spectra consisting of doublets with reduced splitting compared to that of an un-sheared sample (refer to section 2.2.1 about ^{2}H NMR spectroscopy). For this experiment, deuterium signals were provided by the addition of a small amount of deuterated benzene, which becomes ordered in the liquid crystal environment, acting as a spy molecule. Some of the results from an experiment published by Leal et al. [52] were reproduced regarding the behaviour of PBLG director orientations in m-cresol during shear flow and after its sudden cessation, observed in ^{2}H NMR.

2.3.2 Experimental Setup

Two samples of PBLG (Sigma Aldrich) in m-cresol were prepared with weight fractions of 12.54% and 14.02%, with the addition of 1% deuterated benzene, C_6D_6, to provide a suitable probe for ^{2}H NMR. All samples were incubated in a waterbath at 323 K.

All shearing tests were carried out at 303 K on a Bruker 400 MHz NMR spectrometer, operating at 60 MHz, with a spectral width of 5.0 kHz. Samples were prepared in a NMR couette shear cell, using thin-walled inner and outer NMR tubes with 3 mm and 5 mm outer diameters respectively (figure 2.2). Each of the FIDs used 128 scans, with a

recycle delay of 0.1 s.

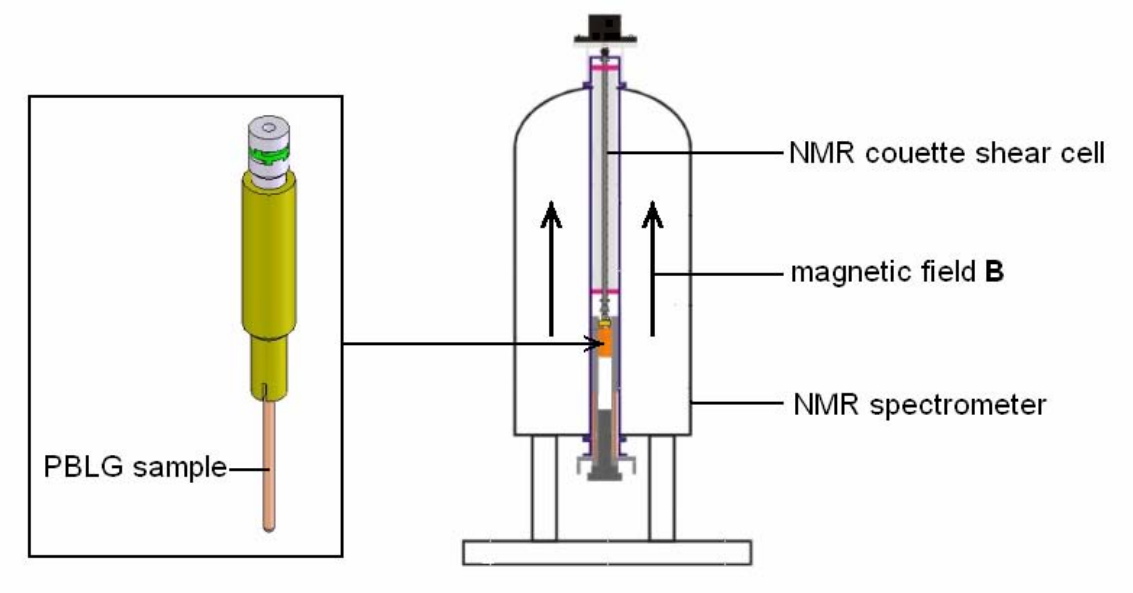

Figure 2.8: PBLG sample in NMR spectrometer, the PBLG director is in same direction as magnetic field *B*.

The experimental process involved recording a spectrum of the sample under no shear, under an average shear rate of 35 s^{-1}, then every minute for 10 minutes after shear cessation, to observe how the NMR line shape of PBLG relaxed.

2.3.3 Results and Discussion

Figure 2.9 shows the results from a shearing test on PBLG 14.02%:

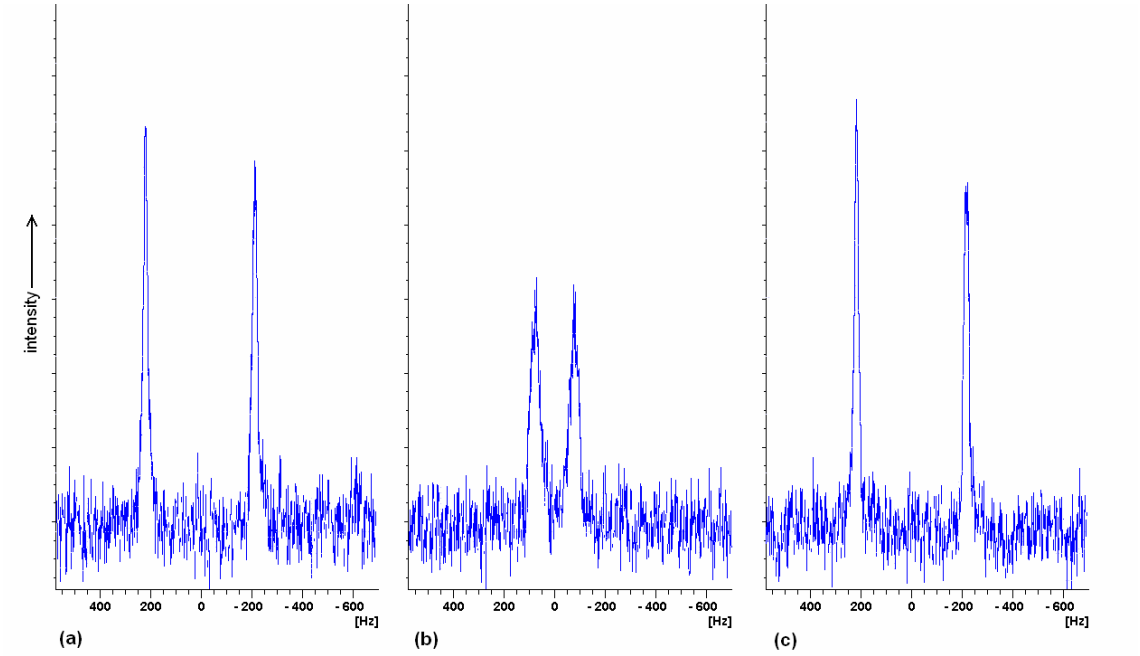

Figure 2.9: PBLG 14.02% shearing test: sample (a) under no shear, (b) under shear, and (c) after shear stopped for a few minutes.

The results from this test were consistent with those found by Leal et al. [52], starting with a quadrupolar doublet. The peak-to-peak separation of the doublet changed from 400 Hz to 160 Hz while under shear, relaxing back to a 400 Hz splitting following shear cessation, which was somewhat consistent with the corresponding results found by Leal et al., who suggests that the peak-to-peak separation decreases to half its original length [52]. Significant line broadening was observed in the PBLG system while under shear, most likely due to a spread in the orientational distribution about the director. A theoretical plot of the director behaviour $\left|\left(3\cos^2\theta - 1\right)\right|$ as the angle between the director and magnetic field vector changes is shown in figure 2.10.

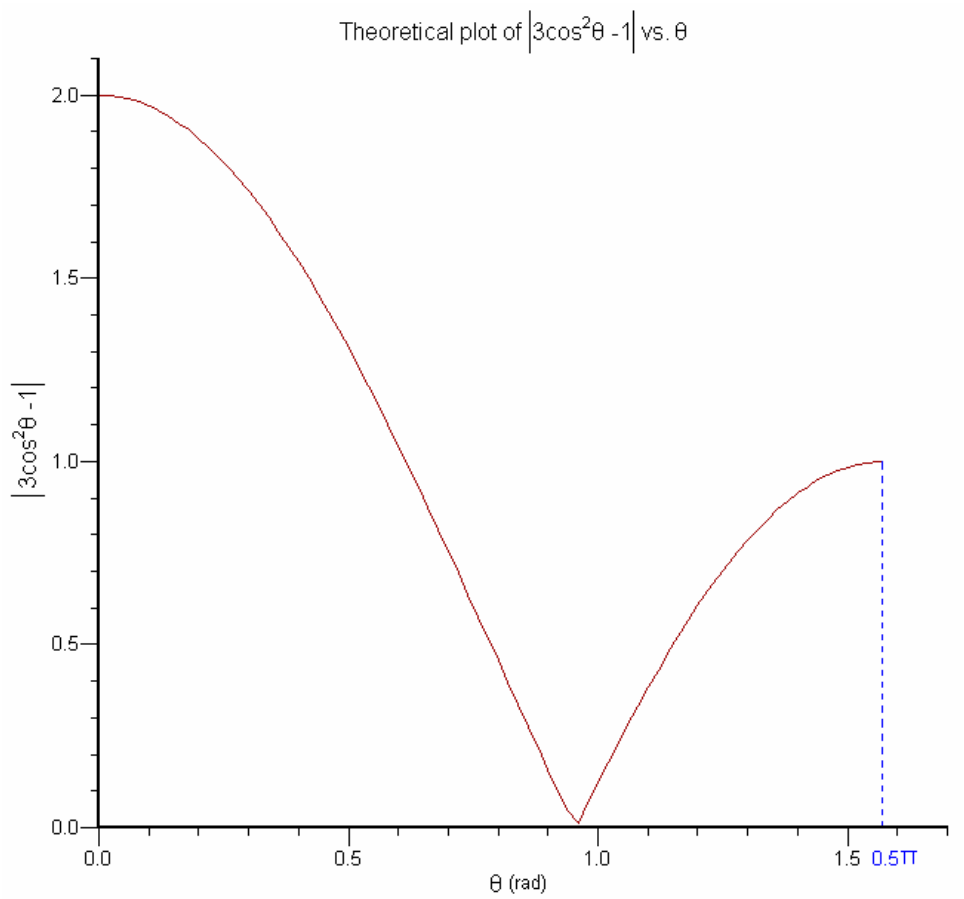

Figure 2.10: Theoretical plot of $\left|\left(3\cos^2\theta - 1\right)\right|$ vs. angle made between PBLG director and magnetic field in the NMR spectrometer.

In order to obtain a quadrupolar doublet splitting of exactly half its original value under shear requires the shear rate to be large enough to overcome the magnetic fields influence over the PBLG director (which makes it point parallel along *B*) and influence it to make a 90 degree angle (0.5π radians) with the magnetic field vector. Looking at figure 2.10, the result obtained from experimental data under shear, 160 Hz, corresponds to a ~85 degree angle between the PBLG director and the magnetic field, implying that the shear rate applied was not strong enough to completely rotate the director away from the magnetic field. This is consistent with the results found by Leal et al., where their doublet splitting decreases to less than half of the original value under shear rates of 10 and 40 s^{-1} [52].

The same shearing test was carried out on a PBLG 12.54% sample, yielding similar results (figure 2.11).

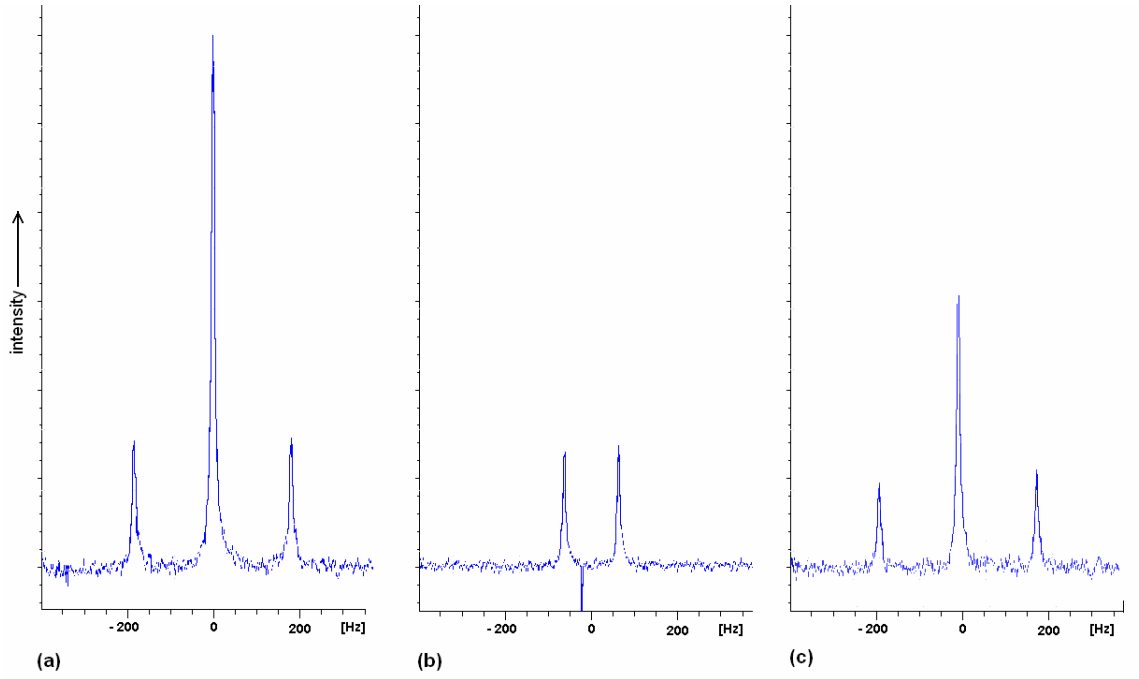

Figure 2.11: PBLG 12.54% shearing test: sample (a) under no shear, (b) under shear, and (c) after shear stopped for a few minutes.

The results from this test showed that the quadrupolar splitting changed from 360 Hz to 130 Hz under shear, relaxing back to 360 Hz after shear cessation. These results were consistent with those found by Leal et al. [52], and by the 14.02% PBLG sample. Line broadening was minimal compared with figure 2.9, and the splitting observed under shear is in roughly good agreement with corresponding results suggested by Leal et al. The reason for not obtaining an exact length of 180 Hz can be explained by the same reasons as discussed for PBLG 14.02%, where the shear rate applied was close to, but not enough to drive the PBLG director to make a 90 degree angle with the magnetic field vector, which would produce a doublet splitting of exactly half the original value. The large peak in the middle of the spectrum disappeared while the sample was sheared,

but re-appeared after relaxation. This signal was most likely due to a proportion of the benzene probe molecule being in the isotropic state (for which we expect a single peak).

2.3.4 Conclusion

By means of ^{2}H NMR spectroscopy, the results concerning PBLG behaviour under shear and following shear cessation were reproduced from a study by Leal et al. [52]. Shear flow was applied to the lyotropic liquid crystal, via a custom-built NMR couette shear cell. Results found that the peak-to-peak separation of the PBLG quadrupolar doublet decreased to roughly half of its original separation while under shear, relaxing back to its original length after shear cessation. Values changed from 400 to 160 Hz for the 14.02% sample, and 360 to 130 Hz for the 12.54% sample. These results were roughly consistent with those found by Leal et al., and showed that the shear cell was producing shear.

Chapter 3

3 Bovine β-lactoglobulin

3.1 Introduction

Bovine β-lactoglobulin (β-Lg) is a small (18.3 kDa, 162 amino acids), water soluble protein, and is the most abundant protein in the whey fraction of cow's milk. Its secondary structure is made up of 8 anti-parallel β-strands and an α-helix, and is mainly stabilized by weak forces (H-bonds) [53]. The tertiary and quaternary structures are also well established, forming a dimer at neutral pH, and being monomeric at pH 2 (although it retains its native-like tertiary structure). These structures have been confirmed by both X-ray [54] and NMR techniques [1, 55]. To date, β-Lg structure deformations have been studied by application of high pressures [56], shaking or stirring [57-59], aggregation as a result of denaturation by heating [60], and aggregation into amyloid fibrils by controlled shear [33]. In addition to this, there is also some anecdotal evidence that shear flow leads to changes in protein conformations, however detailed experimental data about this behaviour is scarce. Therefore, β-Lg appeared as a favourable candidate to test whether or not protein conformations could be altered by application of shear using our rheo-NMR cell.

3.2 Experimental Method

Bovine β-lactoglobulin containing A and B variants was obtained from Sigma-Aldrich. 7.0 mg/mL samples of β-Lg were prepared by dissolving β-Lg with a solvent mixture

containing 80% MilliQ water, 10% D_2O (99.9% deuteration degree for NMR spectroscopy, Merck), and adjusted to pH 2 using 1 M Hydrochloric acid (HCl). This β-Lg concentration was selected after results from preliminary experiments showed that 7.0 mg/mL gave a sufficient signal intensity to produce a 1D β-Lg proton (^1H) NMR spectrum with an adequate signal to noise ratio in a reasonably short time (~8 minutes). NMR was chosen as a probe for studying β-Lg as it is a well established method for determining conformation and solution properties of proteins [1]. Particularly in this experiment, where we sought to generate conformational changes, NMR provided high-resolution data capable of detecting chemical shift changes in backbone amide protons, which would imply changes in structural conformation. Another advantage of using NMR was that by continually recording NMR spectra over the period of an experiment, it could provide information about the rate at which any conformational changes were taking place and examine the possibility of transient species. D_2O primarily acted as a probe for the ^2H NMR lock system to avoid fluctuations in the magnetic field strength. pH 2 was selected as it enables the study of native β-Lg that is monomeric [61], but not denatured [62].

~300 µL of the sample was transferred into a thin-walled NMR tube with an outer diameter of 5 mm, with the addition of ring collars (figure 2.4) and a thin-walled NMR tube with a 3 mm outer diameter. The sample was then set up in a NMR couette shear cell (figure 2.1 (a)) and placed in the NMR spectrometer, followed by shear application (figure 2.1 (b)). Control experiments followed the same procedure, only without shear application.

All transferring of liquids was carried out using 100, 1000 µL eppendorf research pipettes, glass pipettes, and weighing was carried out using Mettler Toledo balances.

All 1D ^{1}H NMR spectra were recorded at 298 K, on a Bruker 500 MHz NMR spectrometer operating at 500.13 MHz, using a spectral width of 8.0 kHz. Water suppression was carried out using excitation sculpting [63]. Each of the FIDs used 256 scans, with a recycle delay of 1.0 s. Bruker's TopSpin software was used to process spectral data. 2D TOCSY spectra were recorded at 298 K, using excitation sculpting [63], and a spectral width of 6.5 kHz for frequency axes F_1 and F_2. Each of the FIDs used 16 scans, with a recycle delay of 1.5 s.

3.3 Results and Discussion

3.3.1 Initial NMR Spectra

A β-Lg spectrum with an adequate signal to noise ratio was observable and reproducible using the Bruker 500 MHz NMR spectrometer (figure 3.1) after an optimal sample concentration was established:

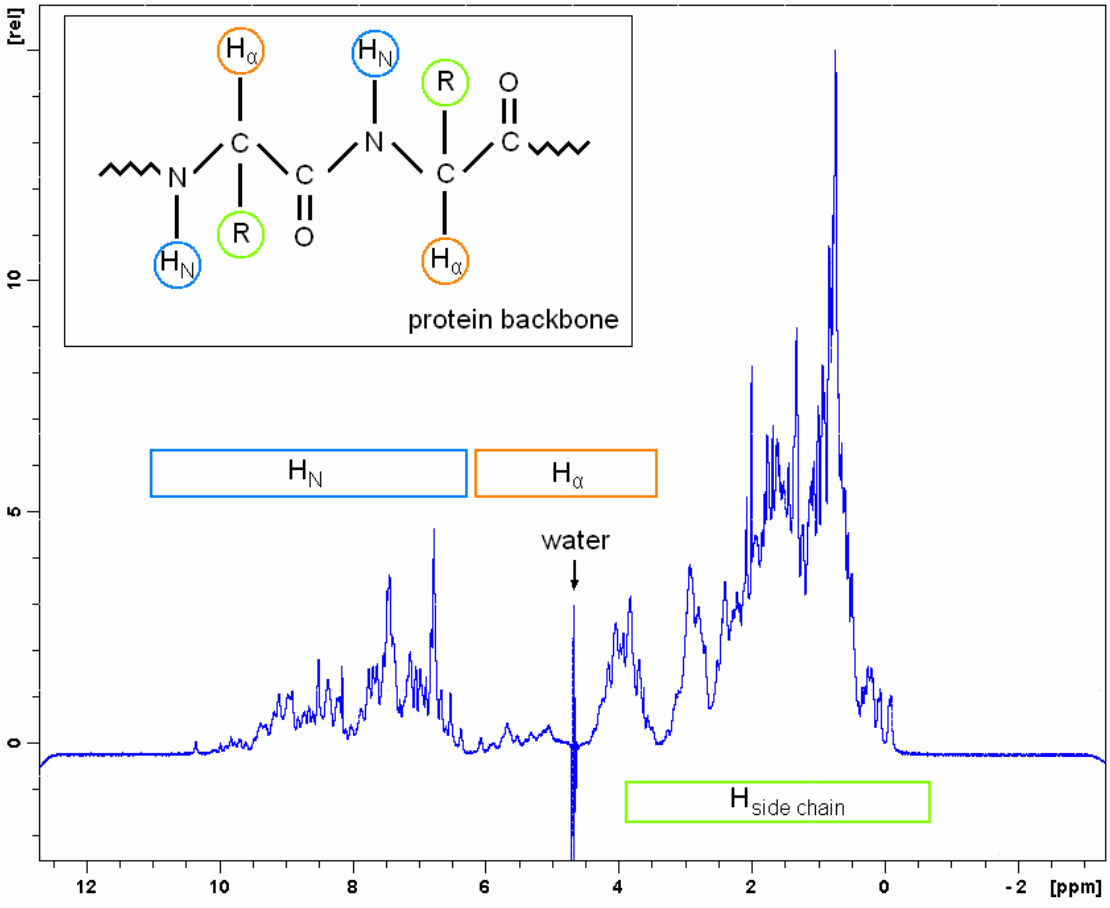

Figure 3.1: The β-Lg backbone structure, and a standard spectrum of β-Lg under no shear, recorded in a 500 MHz NMR spectrometer showing backbone amide protons, backbone α protons, and side chain protons $H_{side\ chain}$.

The protein signals to the left of the water peak in figure 3.1 include the signals from the backbone amino protons H_N (some aromatic sidechain protons H_{ar} have chemical shifts of ~7 ppm). It is expected that any conformational changes within the protein's folded structure would be detected in this area, because shear could affect the distances between amino acids on different structural elements of the protein, which would in turn affect the H_N chemical shifts. Throughout and between experiments, small changes in the phase of the residual water peak were observed from one scan to the next, affecting the intensity of nearby peaks from the H_αs in the final spectrum. Therefore, backbone H_α proton signals surrounding the water signal were not studied in detail as they would be inconsistently obscured by the water peak throughout each experiment.

3.3.2 Effect of Shear on Bovine β-lactoglobulin

3.3.2.1 1D ^{1}H NMR

Results from the initial shear experiments, where a shear rate of 120 s^{-1} was applied over a 15 hour period (overnight), showed a small change in the β-Lg spectrum (figure 3.2 (a)) around 8 ppm. This change was found to be irreversible after an identical spectrum was obtained from the same sample a day later. A control experiment without any shear application was carried out under otherwise identical conditions, and resulted in spectra that remained unchanged. This result confirmed that the small change was a consequence of shearing, and the focus turned to whether a shear rate applied over a longer time period could create a larger change in the β-Lg structure. Therefore, shear experiments were carried out under identical conditions as before, over periods of 2 days (figure 3.2b), and 4 days (figure 3.2c).

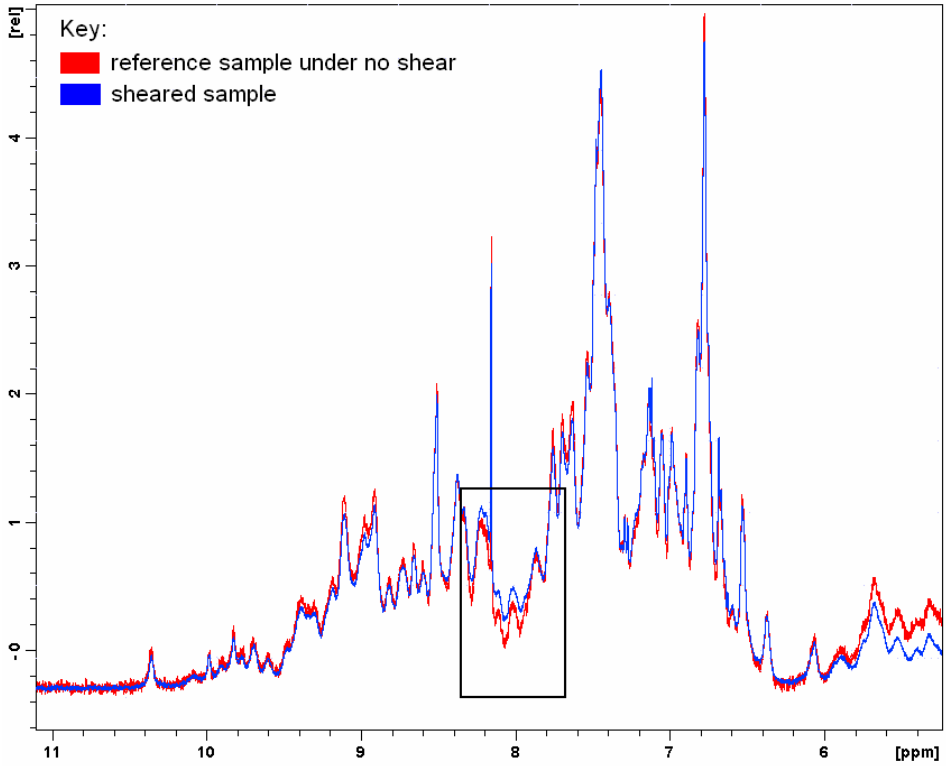

Figure 3.2 (a): Shearing experiment carried out on a β-Lg sample subjected to an average shear rate of 120 s^{-1} overnight, and compared with a spectrum of the sample prior to shear application.

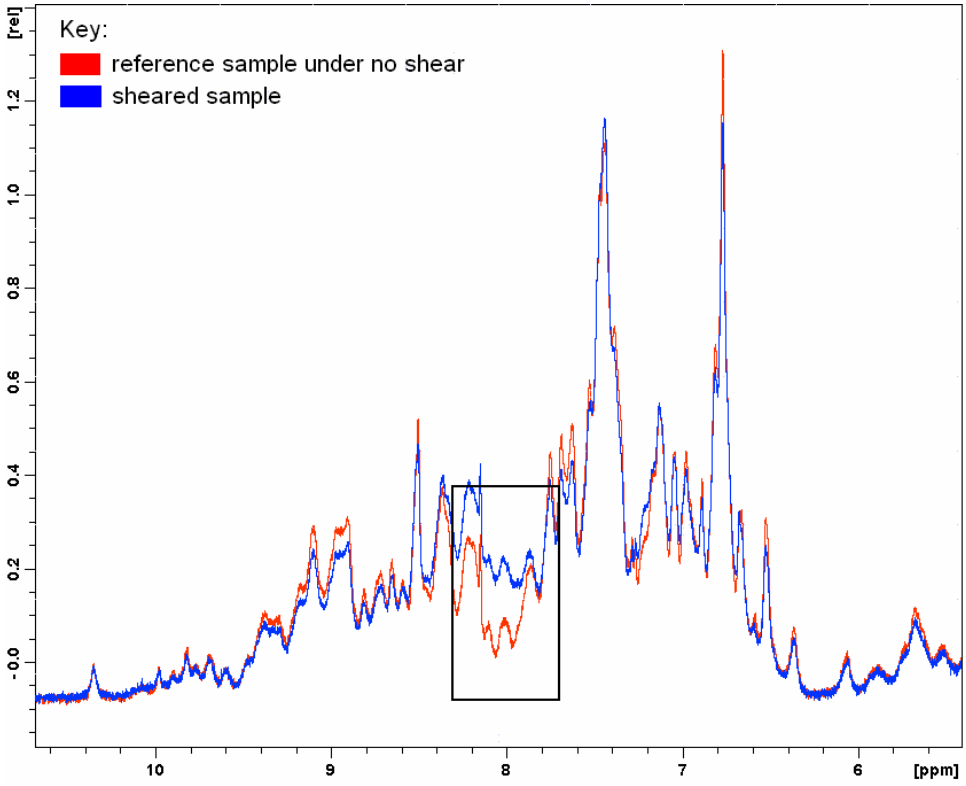

Figure 3.2 (b): Shearing experiment carried out on a β-Lg sample subjected to an average shear rate of 120 s^{-1} over 2 days, and compared with a spectrum of the sample prior to shear application.

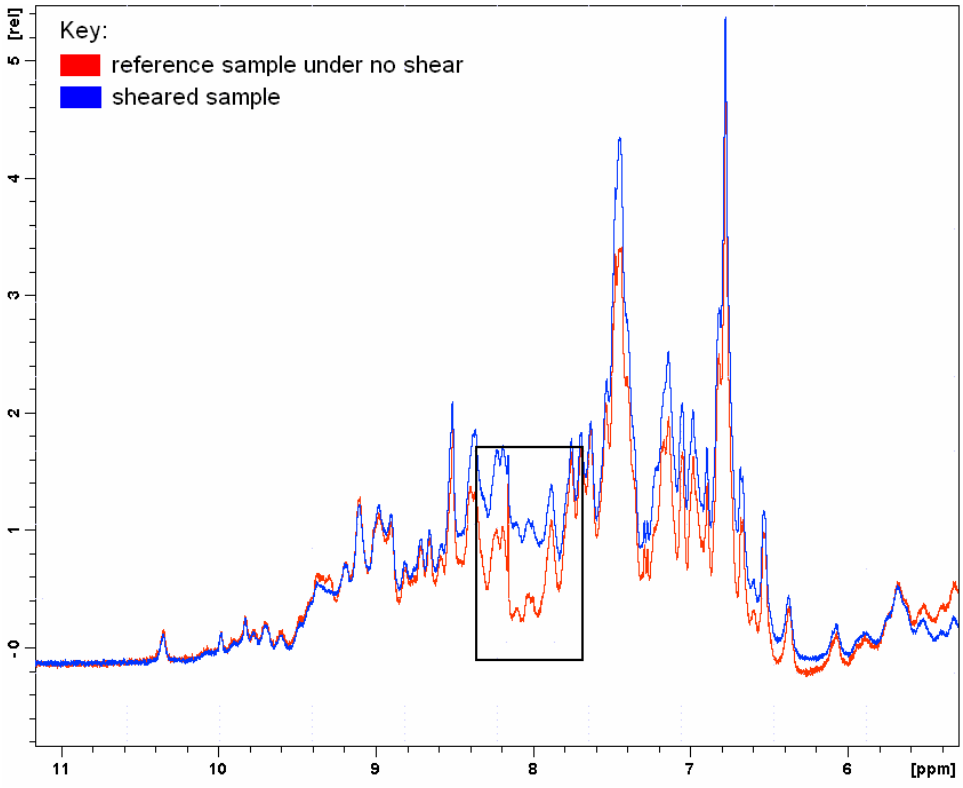

Figure 3.2 (c): Shearing experiment carried out on a β-Lg sample subjected to an average shear rate of 120 s^{-1} over 4 days, and compared with a spectrum of the sample prior to shear application.

The results obtained in figure 3.2 (b) and (c) demonstrated that a larger change could be generated by applying shear over longer periods of time, and were repeated several times with reasonable reproducibility. Figure 3.3 shows the rate of change in the signal area (integral) around 8 ppm (and others for comparison) by analyzing the area under the peaks from each recorded spectrum over an experiment. The results showed how the change was concentrated on one area in the NH region, and that the total area under the NH region (green trace in figure 3.3) and sidechain region (blue trace in figure 3.3) remained constant. This was expected, unless there was any significant aggregation and/or precipitation. The slight gradient of both traces probably reflect a slight change in spectrometer sensitivity or stability over the duration of the experiment.

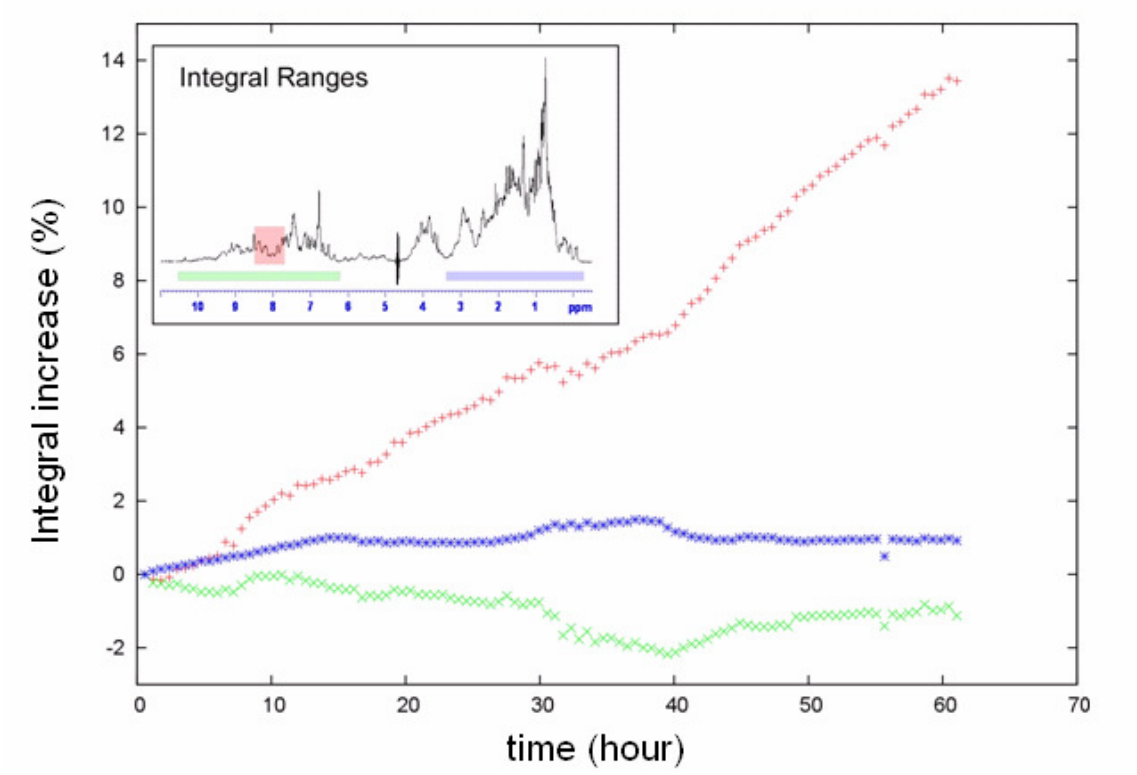

Figure 3.3: Rate of conformational change in a β-Lg shearing experiment.

After observing that small changes were generated subsequent to shear rates of 120 s^{-1}, this lead to the question concerning whether or not higher shear rates could generate larger changes. Therefore, an overnight shearing experiment was repeated under identical conditions as before, only this time, the thin-walled 5mm NMR tube was substituted with a medium-walled tube (figure 2.2), creating a smaller annular gap, which made it possible to reach a higher shear rate of 710 s^{-1} in the NMR couette shear cell. The results however, were consistent with those in figure 3.2 (a), implying that larger changes were not brought about by larger shear rates in this case.

After a benchtop couette shear cell was developed (refer to section 2.1.2), capable of generating average shear rates of up to 1570 s^{-1}, the experiment was repeated under identical conditions to those in figure 3.2, only that a shear rate of 1570 s^{-1} was applied overnight. The results mirrored those from the previous experiments, showing a small

change in the 8 ppm area, reinforcing the fact that larger changes were not brought about by larger shear rates.

3.3.2.2 2D NMR Experiments

Having observed a conformational change to protein structure by 1D ^{1}H NMR, it was now desirable to see if these changes in the NH region could be attributed to a particular amino acid(s), and thus, two-dimensional (2D) NMR experiments were carried out. Because β-Lg is a relatively large protein by NMR standards, in 1D NMR, it was not possible to identify individual amino acids due to spectral overlaps. 2D NMR alleviates this problem to a great extent, but at the cost of a significantly greater measurement time (several hours compared with a few minutes). By obtaining a 2D TOCSY spectrum of β-Lg (figure 3.4 (a)), the so called "fingerprint region" (figure 3.4 (b), 3.5) shows a single peak for each amino acid residue of a protein's sequence at coordinates that correspond to chemical shifts of the backbone H_Ns, and peptide C_α hydrogen atoms (H_αs). Refer to figure 3.4 (b) to see the NMR assignment of β-Lg H_N and H_α established by Uhrinova et al. [1], where each peak is associated with a particular amino acid. Any shear induced changes to the protein backbone structure might be expected to produce changes in the position of the peaks in the fingerprint region. Conditions were kept constant according to previous shearing experiments, and a shear rate of 120 s^{-1} was applied to the sample over 4 days. The results demonstrated that no significant shifts were observed for specific amino acids, implying that most of the β-Lg was still in a conformation similar to that of the native state. However, a small increase in intensity was observed around same part of the amide region as the changes observed in previous 1D NMR experiments (figure 3.2). An increase in this signal intensity in this chemical shift region may indicate the formation of a small amount of α-helical or random coil structure (figure 3.5).

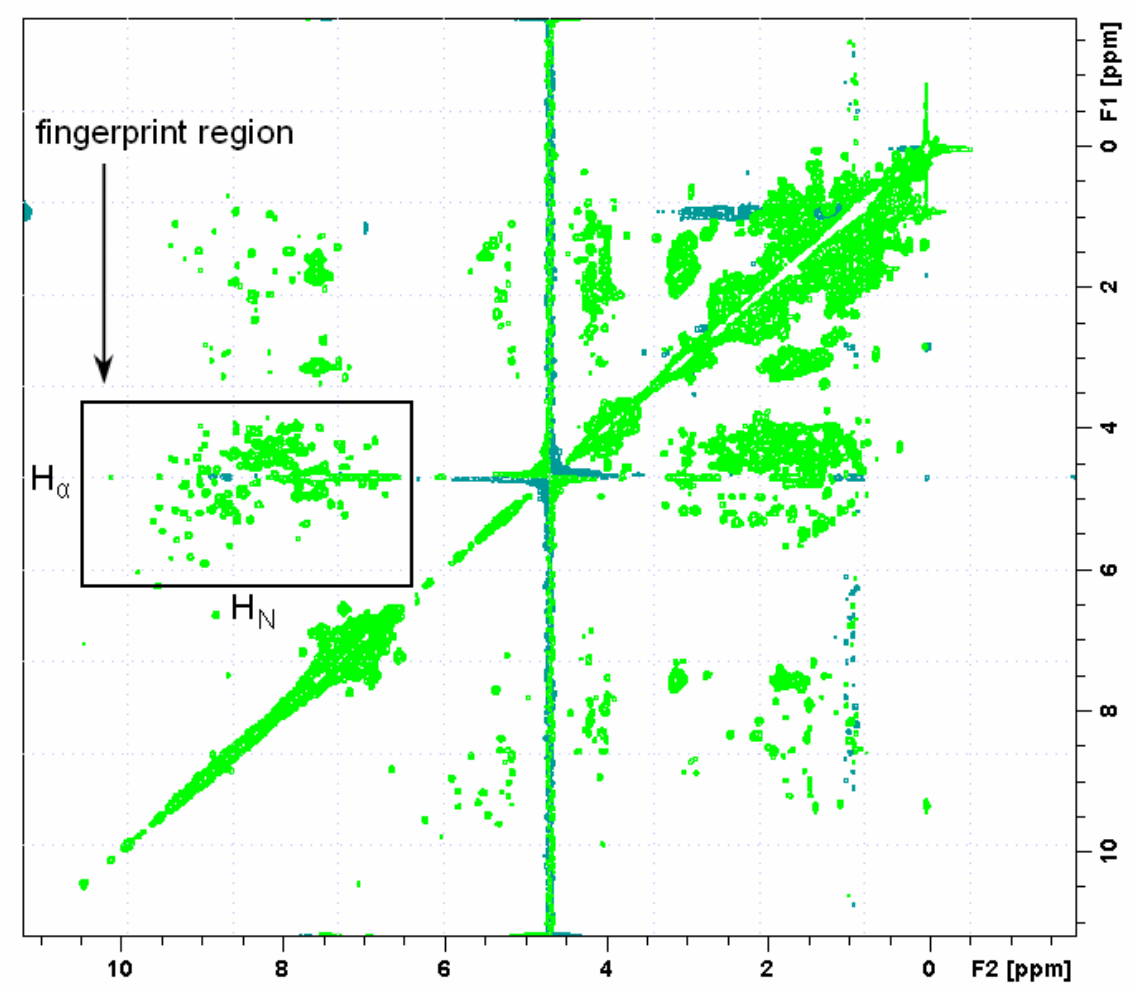

Figure 3.4 (a): 2D TOCSY spectrum of 6 mM/g β-Lg.

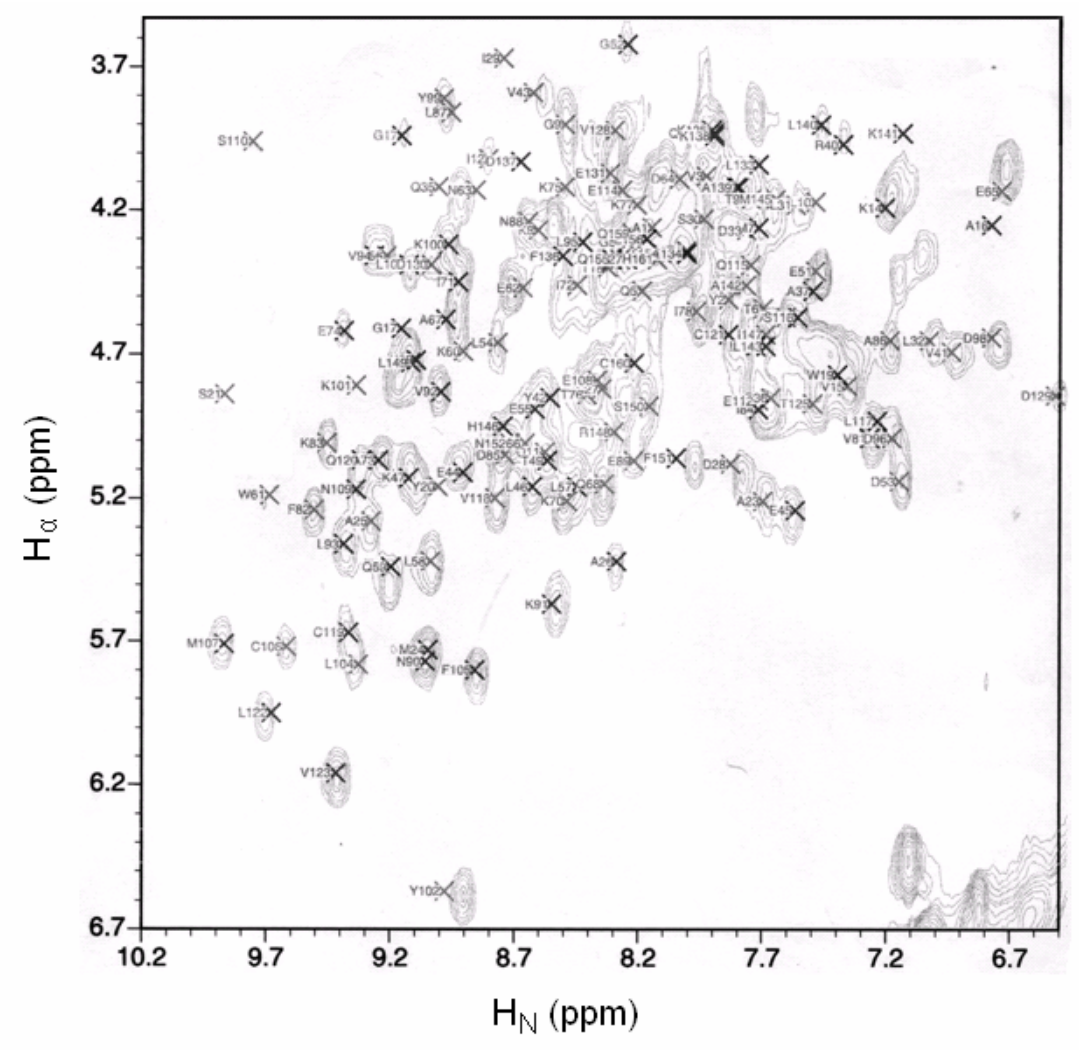

Figure 3.4 (b): TOCSY β-Lg structure assignment established by Uhrinova et al. [1].

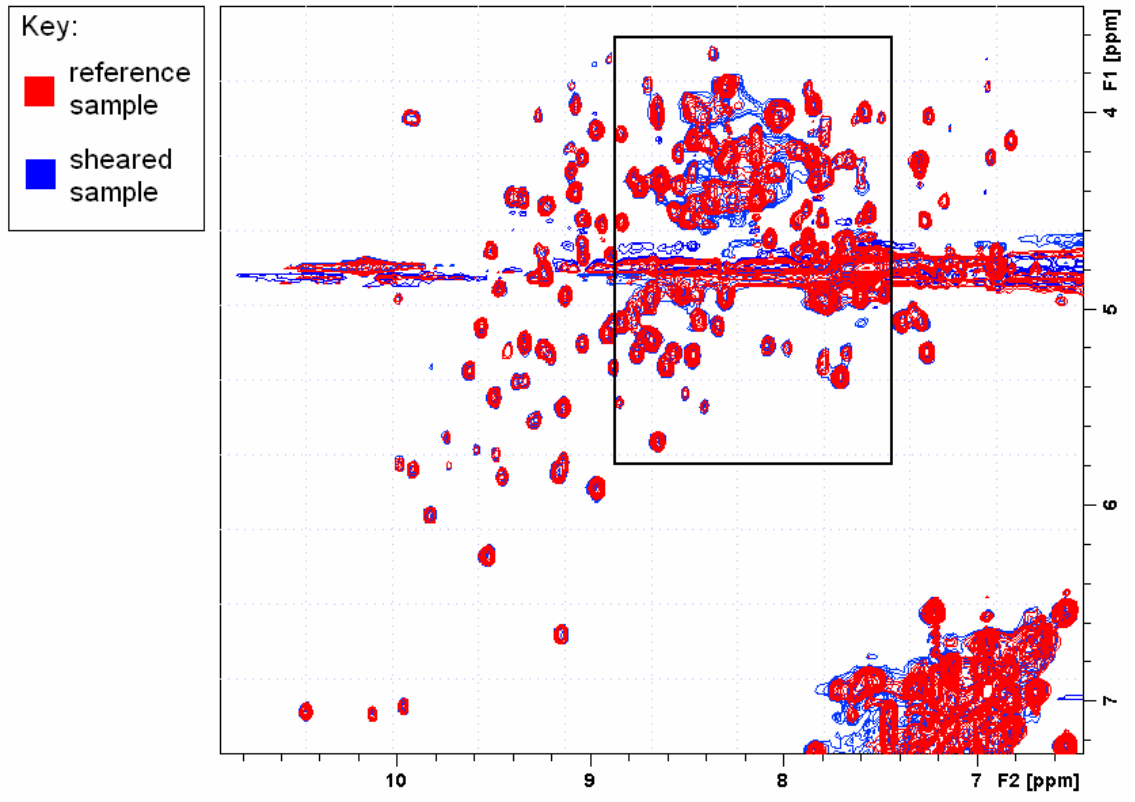

Figure 3.5: Fingerprint region overlay of 2D TOCSY spectra before and after shear application.

3.3.2.3 Light Scattering Tests

Light scattering tests were carried out to detect any presence of aggregates in a sheared β-Lg sample that showed conformational changes in 1D NMR tests (figure 3.2), and compared with a control β-Lg sample that showed no changes to protein structure. However, the results showed that only a minute difference between sheared and control samples could be detected. This suggested that although a conformational change was observable through 1D and 2D NMR, by means of an independent method, shear does not produce any significant aggregation under the conditions of our experiment. A recent study by Jaspe et al. [10], who used ultraviolet lasers to detect fluorescence changes in protein, found that globular proteins were not de-stabilized by high shear rates of 10^5 s^{-1} under well-defined flow conditions. Using their simple model based on the thermodynamic stability of the protein, their model calculations predicted that only

unusually high shear rates (>10^7 s^{-1}) would be enough to destabilize a small protein, and such shear rates are difficult to attain in laminar flow [10]. Although our results suggest that a small conformational change is detectable by means of NMR under our conditions, this does not appear to lead to the generation of aggregated states, and its molecular nature is elusive.

3.3.3 Effect of Shear on Destabilized β-Lg – Addition of Trifluoroethanol

After concluding that shear rates up to 1570 s^{-1} would generate a small conformational change to the β-Lg structure, experiments were carried out to investigate if the native conformation would be destabilized further by the addition of Trifluoroethanol (TFE). Studies in literature have established that TFE stabilizes the α-helical structure in proteins [64]. In the case of β-Lg, which is predominantly made up of β-sheets, TFE causes it to adopt a significant amount of α-helical structure, with a dramatic transformation at TFE concentrations between 10 – 20% [64]. Our intention was that the addition of a certain amount of TFE alone would result in a native-like, but destabilized β-Lg conformation close to the β-sheet-α-helical transition, and then the addition of shear could result in a significantly different β-Lg structure.

Figure 3.6 shows a series of 1D ^{1}H NMR spectra that were recorded using a β-Lg sample containing increasing amounts of TFE, under no shear and at 298 K. The predominantly β-sheet structure of β-Lg is characterized by its wide distribution of the chemical shifts in NMR, as confirmed by the experimental results from β-Lg samples containing 0 – 10% TFE (v/v). In contrast, α-helical secondary structure is characterized by a narrower chemical shift range for the H_N signals, usually centered at ~8 ppm, confirmed by spectra from β-Lg samples containing 15- 30% TFE (v/v). Based on the results of this experiment, β-Lg samples containing 10% TFE (v/v) were

prepared after observing that samples containing higher TFE concentrations resulted in spectra with predominantly α-helical protein structures. A shearing test on a β-Lg sample containing 10% TFE (v/v) was carried out, with a shear rate of 1570 s^{-1} applied over 2 days using a benchtop couette shear cell setup with thin-walled outer and inner NMR tubes with 5 mm and 3 mm outer diameters respectively (figure 3.7).

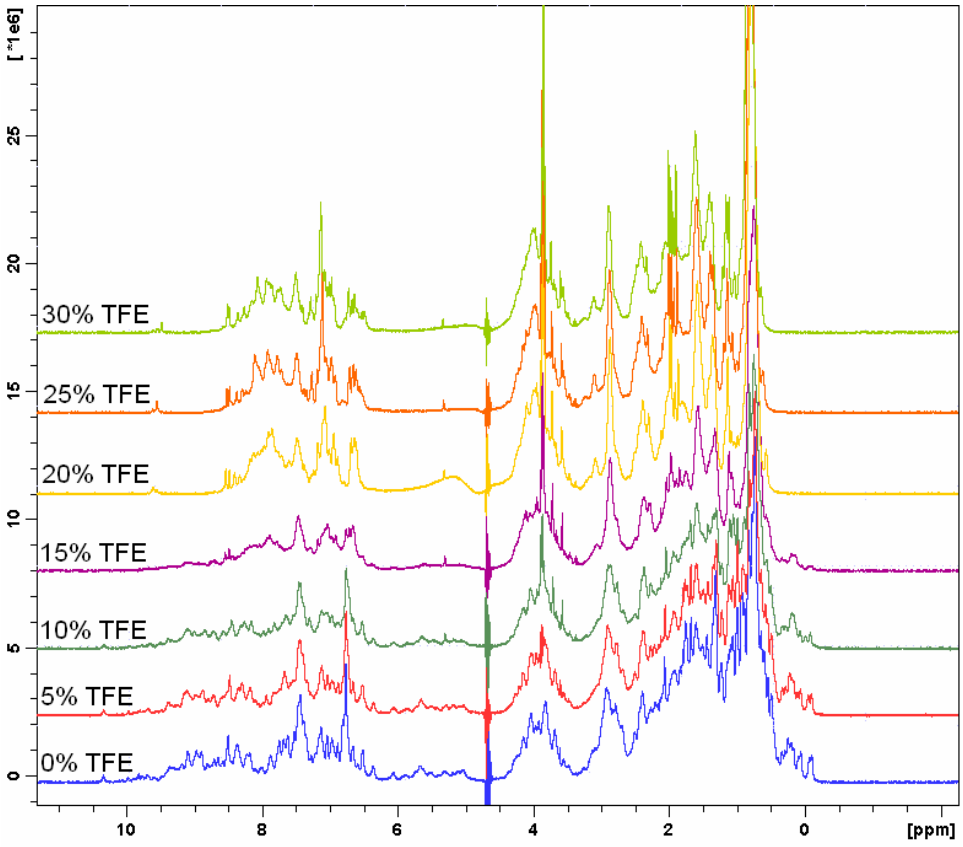

Figure 3.6: β-Lg containing various amounts of TFE (v/v), under no shear, at 298 K.

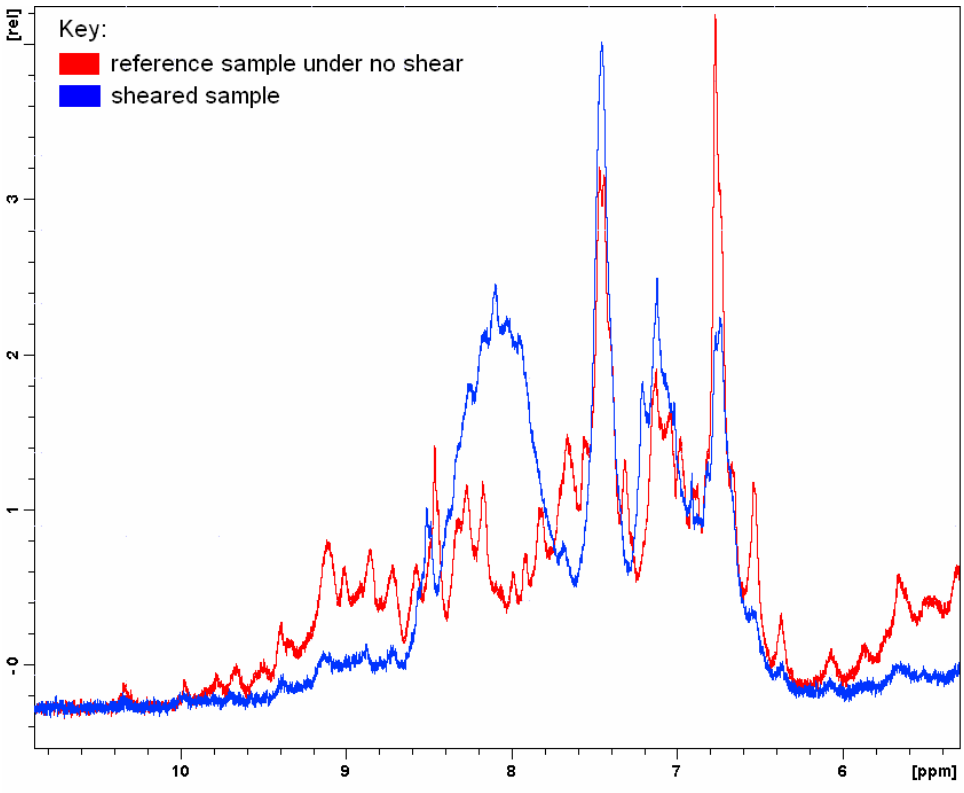

Figure 3.7: Shearing experiment on a β-Lg sample containing 10% TFE (v/v) under an average shear rate of 1570 s^{-1} over 2 days.

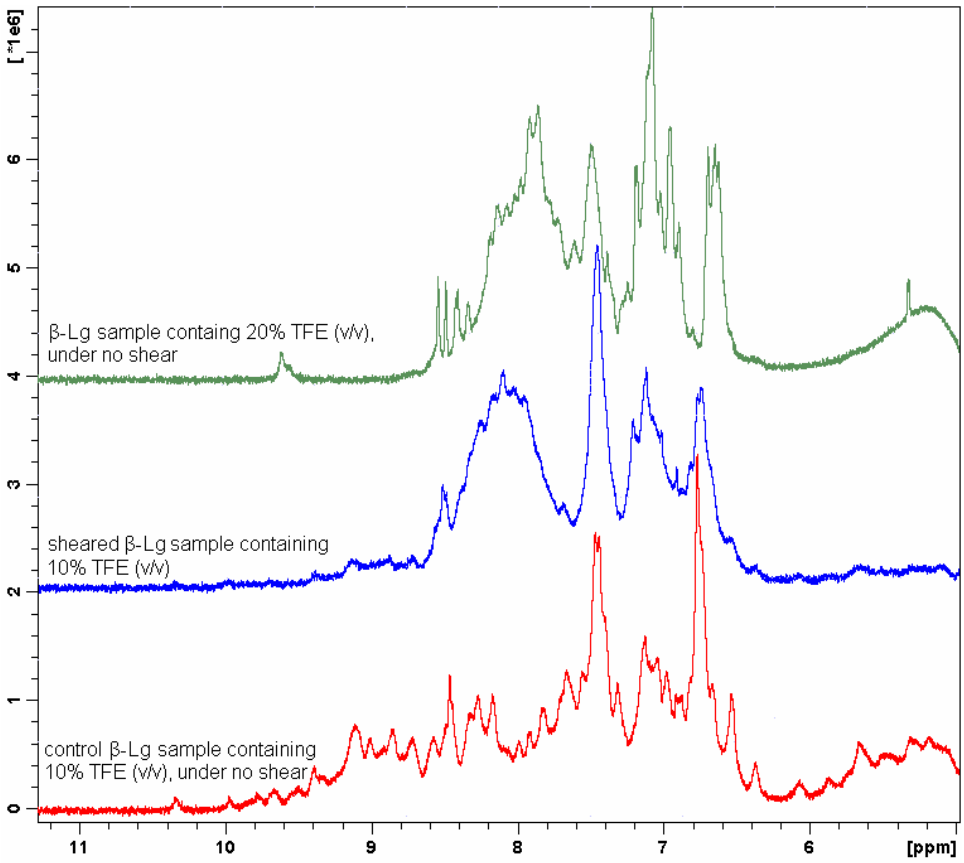

Figure 3.8 (a): Comparison of the sheared β-Lg sample (containing 10% TFE (v/v) and sheared at 1570 s^{-1} for 2 days) with a control sample (containing 10% TFE (v/v)), and a reference β-Lg sample containing 20% TFE.

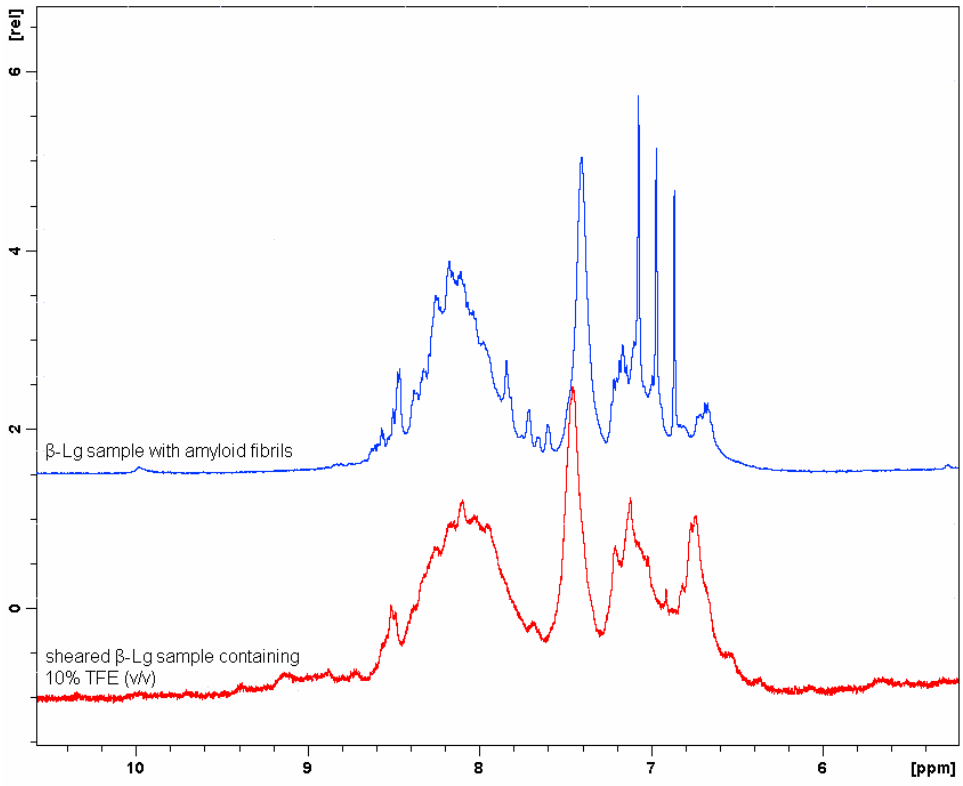

Figure 3.8 (b): Comparison of the sheared β-Lg sample (containing 10% TFE (v/v) and sheared at 1570 s^{-1} for 2 days) with a β-Lg sample known to contain amyloid fibrils.

The results observed in figure 3.7 produced a positive conformational change around 8 ppm, which was consistent with previous experimental results (figure 3.2, 3.5). From an NMR point of view, the β-Lg structure showed similarity with a β-Lg sample containing 20% TFE (figure 3.8 (a)), implying that shear could stabilize β-Lg into a α-helical dominating structure. This result was consistent with a theoretical model suggested by Jaspe et al., which suggests that partially unfolded proteins are more susceptible to strong shear; resulting in a larger degree of coil-stretch extension, rather than direct denaturation of a protein [10]. Interestingly, the β-Lg structure also showed good agreement with the NMR spectrum of a β-Lg sample known to contain amyloid fibrils (figure 3.8 (b)), which are largely made up of β-sheets. There are two scenarios that could explain why identical spectra are obtained for β-Lg samples largely made up

of α-helices or β-sheets: firstly, the NMR spectra of β-Lg made up of largely α-helices simply is similar to NMR spectra of β-Lg made up of largely β-sheets. Secondly, it is also possible that the β-Lg sample containing amyloid fibrils is such that the fibrils are too rigid that they are not detectable by means of NMR, leaving only the residual α-helical structures, which are detected and recorded in the NMR spectrum. A method into determining whether the sheared sample was made up of α-helices or β-sheets was not available at this time, but may be interesting to pursue in future work.

After running a buffer exchange on the sheared sample and the control sample containing 10% TFE (v/v), to remove the TFE, the sheared sample spectrum was unchanged, while the control sample reverted back into a spectrum of β-Lg containing no TFE, therefore concluding that the conformational change generated by shear was irreversible as opposed to that generated solely by TFE. However, repeats of this experiment gave negative results, showing no changes to the β-Lg structure, and no definite explanation could be reached that explained why this occurred. One possibility is simply that the probability of shear generating conformational changes to a β-Lg sample containing TFE is relatively low.

3.3.3.1 Gel Electrophoresis Test

Gel electrophoresis tests were carried out on this sheared sample under denaturing conditions (by mixing sodium dodecyl sulfate (SDS)) to see how the β-Lg had changed. However, the results showed little or no difference between the sheared sample and the control sample. This implied that whatever the changes were, they were a result of hydrophobic interactions since they disappeared in the presence of SDS.

3.4 Conclusions

The effect of shear flow on a biological macromolecule has been investigated using Bovine β-lactoglobulin, by means of an NMR couette shear cell and a benchtop couette shear cell setup. It has been demonstrated that shear generates a small, irreversible conformational change to the protein's backbone amino protons, detectable by 1D and 2D ^{1}H NMR, at shear rates ranging from 120 – 1570 s^{-1}. However, no measurable change is detected by light scattering, which suggests that although a conformational change was observed by means of NMR, by means of an independent method, shear does not produce any significant aggregation under our conditions. Investigations into the effects of shear flow on β-Lg containing 10% TFE (v/v) have also been carried out via a benchtop couette shear cell. It has been clearly shown by 1D NMR that a shear rate 1570 s^{-1} can under certain conditions, generate a large conformational change to the β-Lg structure. From an NMR point of view, this could imply that shear stabilizes a partially unfolded β-Lg structure into a α-helical dominating structure, and is consistent with a theoretical model suggested in literature [10], although reproducibility is difficult. The NMR spectrum of the sheared sample also shows some similarity to β-Lg containing β-sheet amyloid fibrils. The exact identity of the β-Lg structure was not able to be determined, but may be interesting to pursue in the future. Gel electrophoresis tests showed little or no change to this β-Lg sample under denaturing conditions, implying that the changes were a result of hydrophobic interactions.

Chapter Four

4 Enzyme Activity in Pectin

4.1 Introduction

The aim of these experiments was to study the effect of shear on inter-macromolecular interactions, by seeing if shear interfered with the de-esterification process performed by enzymes on the polysaccharide, pectin. Two types of enzymes were investigated: plant pectin methylesterase (pPME) and fungal pectin methylesterase (fPME). These two enzymes were selected as their degree of processivity varies, due to the fact that pPME and fPME function differently during pectin de-esterification.

4.1.1 Pectin

Pectin is a complex heterogeneous polysaccharide that plays an important role in controlling the mechanical strength and flexibility in the primary cell wall of most plants. The dominant structure of pectin is a linear chain of poly-α-(1-4)-linked D-galacturonic acid, which forms a homogalacturonan, the major component of the pectin backbone (figure 4.1). Pectin functionality varies significantly depending on its fine structure, which is largely controlled by the pattern and degree of methyl-esterification (DM) of the carboxyl groups on the pectin backbone [65]. Commercially, pectin has widespread use in both food and pharmaceutical industries as a gelling agent [66]. However, it should be noted that while commercially used pectins contain large amounts of homogalacturonan components, which can be easily methyl-esterified or manipulated to form pectins with desired properties, pectins found

in plant cell walls are a complex mixture of homogalacturonan and other polysaccharides such as rhamnogalacuturonan I and II, designed to meet specific needs within the plant. These components too, can easily vary between plants, and the precise arrangement of pectin macromolecules in the cell wall is still debatable. Today, the demand for pectins with varying ability to gel or stabilize fruits and acidified milk products has motivated research into developing pectin with controllable properties [38].

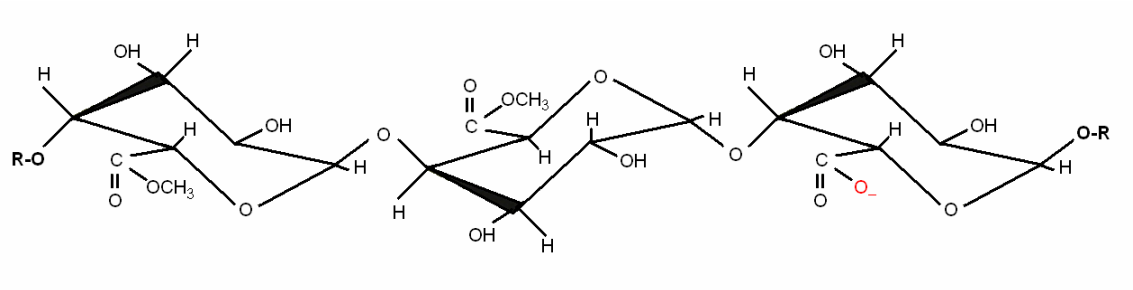

Figure 4.1: Linear chain of the smooth homogalacturonan region in pectin

4.1.2 Pectin Methylesterase (PME)

PME is an enzyme that is found in all plants, as well as some bacteria and fungi. Its main role in pathogens is to digest cell walls, while in plants it remodels mechanical properties by evoking changes to the pectin backbone. PME de-esterifies the highly methyl-esterified pectin backbone, and achieves this by catalyzing the de-esterification of methyl-esterified D-galacturonic acid components, liberating them as methanol (figure 4.2):

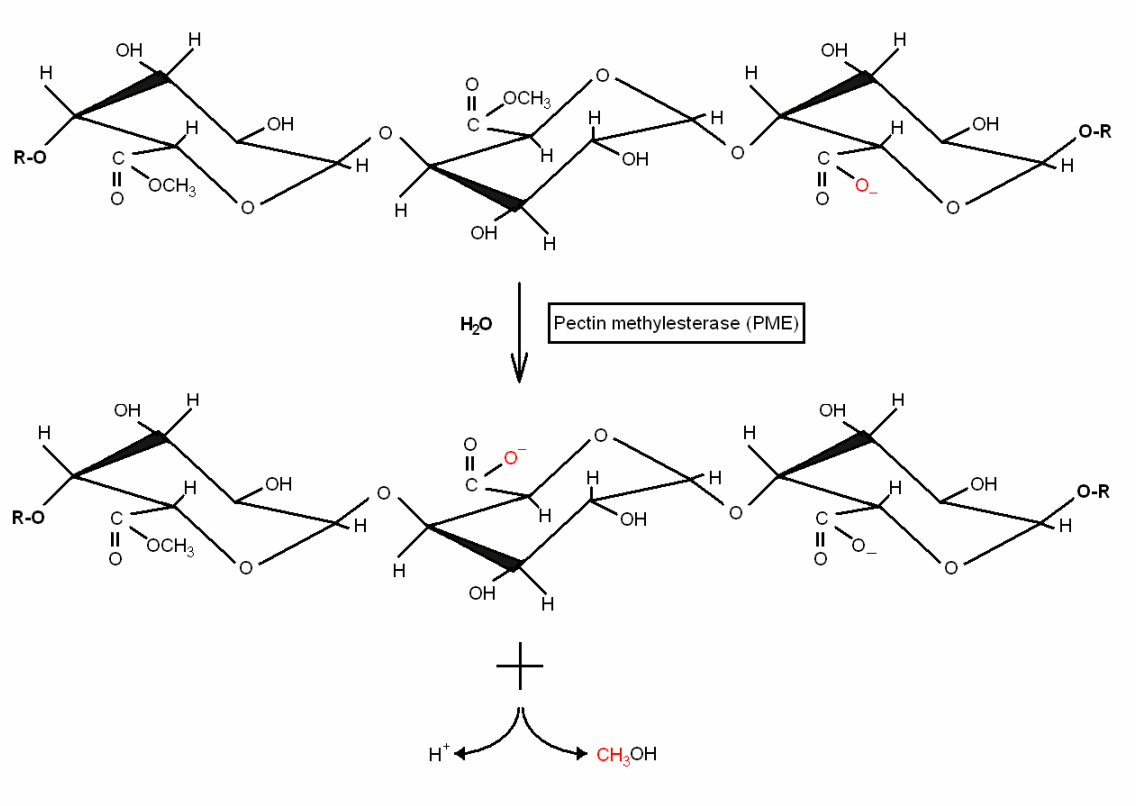

Figure 4.2: The de-esterification of pectin, catalyzed by pectin methylesterase.

PME kinetics generally follows a Michaelis-Menten model, but has been found to have isozymes with different pH optima and kinetic properties [65]. The Michaelis constant, K_m varies widely, depending on the type of substrate and on environmental conditions such as pH, temperature, ionic strength, or polarity, however, it generally lies between 10^{-1} – 10^{-7} M [67]. The optimal pH condition for PME activity is dependent on the PME origin. For example, plant PME shows optimal performance under plant conditions usually around pH 6.5 – 9.5, whereas fungal PME shows optimal performance under acidic conditions around pH 4.0 – 5.2 [65]. However, it should also be noted that enzyme activity is generally sensitive to cations, temperature, and purity of the enzyme [65]. Other characteristics of PME, concerning its functionality, suggest that PME does not act on a methyl-esterified component that is located between two de-esterified carboxyl groups, and that PME does not completely de-esterify pectin; stopping at a certain degree of esterification [68-72].

4.1.2.1 Plant Pectin Methylesterase (pPME)

Plant PME (pPME) initiates action on a methyl-esterified carboxyl group adjacent to a de-esterified carboxyl group, attracted by its charge, then removes the other methyl ester components on the pectin chain progressively [65] (figure 4.3). This can result in areas containing long stretches of de-esterified or esterified galacturonic acid components on pectin chains, forming blocky pectin. However, pPME action mechanism has been established as multiple attack, where the enzyme catalyses the transformation of a limited average number of residues (~10 residues) at a time on one pectin chain [39].

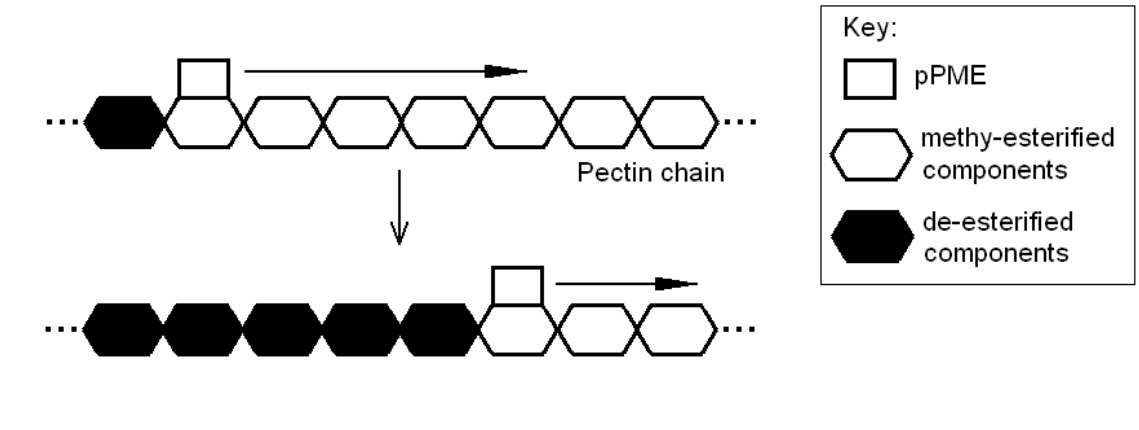

Figure 4.3: An example of pPME acting on a pectin chain over time.

4.1.2.2 Fungal Pectin Methylesterase (fPME)

Unlike pPME, fPME does not work progressively, but acts with a multiple chain mechanism. This means that the enzyme dissociates after each reaction, resulting in single residue attacks [39], leading to the random removal of methyl-ester groups [73] (figure 4.4). This results in pectin chains with only single components of galacturonic acid being esterified randomly.

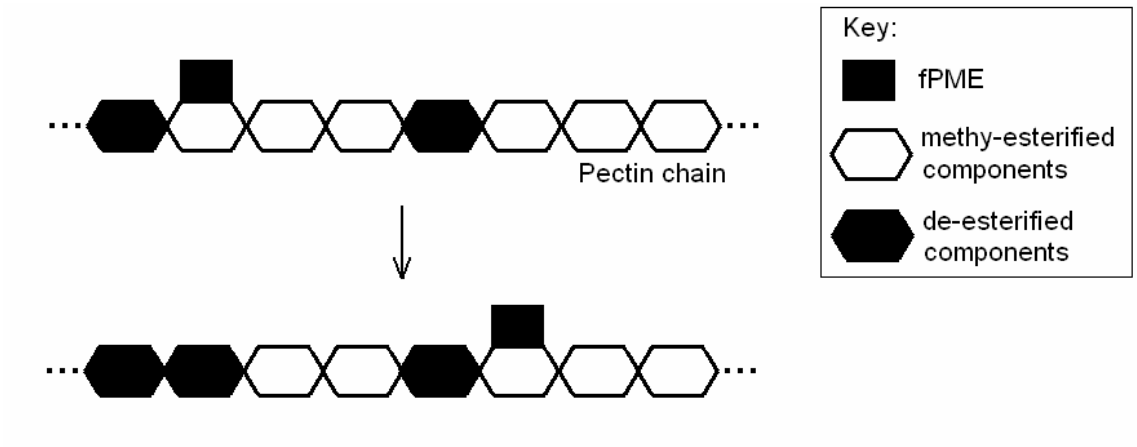

Figure 4.4: An example of fPME acting on a pectin chain over time.

4.2 Experimental Method

1% (w/w) samples of pectin from apples (Fluka Biochemika, with a DM value of ~78%), were prepared by dissolving 0.1 g of pectin in 9 mL of Phosphate buffer and 1 mL of 1 mM 3-(Trimethylsilyl)-propane sulphonic sodium salt (DSS) (Merck). This was all prepared in deuterium oxide (D_2O) (Merck, with 99.9% deuteration degree for NMR spectroscopy), although during preliminary experiments, samples were prepared in 90% MilliQ water and 10% D_2O.

A buffer was required in order to keep the pectin sample at constant pH throughout the de-esterification process. Preliminary experiments showed that without a buffer, the pH was reduced significantly during the first hour due to the de-esterification process, creating unfavourable conditions for the enzyme. Although the common procedure used in PME studies is to keep the pH constant by continually adding base to the pectin and PME sample (enabling the de-esterification process to be monitored by the amount of base required to keep the pH constant), this was not possible in NMR as it would require continuous assembling and dis-assembling of the couette shear cell.

Primarily, D_2O acted as an NMR lock system to avoid magnetic field strength fluctuations. However, another important reason why D_2O was used as the only solvent was to minimize interference by dissolved water and other impurities that could obscure regions within the ^1H NMR spectrum. Generally, water suppression schemes are used to reduce water proton signals, so that a high signal to noise ratio is achieved to produce clean pectin spectra (refer to section 1.5.1.6). After it was decided that control and shearing experiments were to be run simultaneously on two spectrometers, careful consideration of water suppression on both spectrometers was required. The results from preliminary control experiments, where samples were prepared in 90% MilliQ water and 10% D_2O, demonstrated that during time delays inherent in the suppression sequence, the signal decayed differently on separate spectrometers. This was because the spectrometers had different magnetic fields, and the fact that relaxation times T_1 (and T_2) are dependent on field strength [44]. Thus, the different relaxation times produced by separate spectrometers resulted in NMR spectra with observable variations, preventing any proper comparisons to be made between the samples. Based on this result, water suppression was carried out using presaturation in place of excitation sculpting, allowing low power (water suppression) RF pulses to be applied before high power RF pulses to prevent any interference with the relaxation processes within the macromolecular system that occur afterwards. Furthermore, the residual water was minimized by changing the solvent to ~99% D_2O. While on converting from a water solvent (with 10% D_2O) to a D_2O solvent, different PME kinetics could be observed. The aim of the experiment was to compare PME kinetics on pectin under shear and under no shear, so as long as these experiments were carried out using the same solvent, this was not a problem.

The de-esterification process was monitored by measuring the increase in the methanol

proton signal in each NMR spectrum recorded over the period of an experiment. The narrow shape and large intensity of the increasing signal made it favourable to analyse as opposed to the decreasing methyl group signals from groups still attached to the pectin, whose intensity decreased over time, making integration difficult. DSS was chosen as a reference sample to compare with the changing methanol peak. It was chosen for its narrow signal, located at a position where it would not interfere with the methylated sugar or methanol signals from the pectin. Because DSS was placed directly in the pectin and PME sample, acting as an internal reference, control tests were run to check if the direct presence of DSS affected the pectin and PME interactions. This was done by comparing previous results with ones where DSS was placed inside the 3 mm inner tube, acting as an external reference. Comparing the results obtained from using both setups found that there was little difference in enzyme kinetics, and therefore verified that the effects of DSS on the enzyme activity were insignificant. A 1 mM DSS concentration was chosen after preliminary tests using different concentrations of DSS in pectin samples showed that its NMR signal was not too small to integrate over, and not too large to obscure the pectin proton signals.

For experiments using pPME, 100 mM pD 7.4 phosphate buffer was prepared by mixing sodium dihydrogen phosphate (mono-sodium salt) with di-sodium hydrogen phosphate-2-hydrate (di-sodium salt) in D_2O. pD 7.4 was chosen for pPME as this enzyme is known to show optimal performance at a high pD. For work with fPME, 50 mM pD 4.75 phosphate buffer was prepared by mixing 1 M phosphoric acid (H_3PO_4) with 1 M dibasic potassium phosphate (K_2PO_4) in D_2O. For this enzyme, a lower pD was required in order to create optimal conditions for enzyme activity. All pD work reported here was carried out using a Mettler Toledo InLab423 pH probe, and adding a constant of 0.4 to the pH value, in order to obtain a pD value [74]. Mixtures were

allowed to stand on IKA magnetic stirrers for a few hours to enable the salts to dissolve completely.

After mixing pectin, phosphate buffer, and DSS together, the samples were transferred into a waterbath on an IKA magnetic stirrer with heating plate, and left to incubate at 323 K.

pPME stock aliquots were prepared by dissolving 0.01 g pPME (Sigma-Aldrich), in 20 g of MilliQ water. fPME stock aliquots were prepared by diluting 10 µL of fPME (originally prepared by dissolving 3.75 mg of fPME in 1 mL of 50 mM NaAc) in 990 µL of pD 4.75 phosphate buffer. It is important to note that for every experiment, a fresh aliquot of enzyme was taken from the freezer (where they are stored) shortly before an experiment, after preliminary experiments showed that different enzyme kinetics occurred after using aged PME samples (refer to section 4.3.2.2). For both control and shear experiments, 30.6 µL or 15 µL of pPME or fPME was added to the 1 mL samples of pectin respectively. These volumes were selected based on the results obtained from preliminary experiments, where various amounts of the pPME and fPME stock solution were added to pectin and their enzyme kinetics monitored by NMR. The results showed that 30.6 µL of pPME and 15 µL of fPME gave reaction times lasting over a few hours, which was long enough to observe the substantial reduction of ester groups under NMR, and easily repeatable. After the addition of the pPME, samples were then inverted several times to ensure that the enzyme was evenly mixed throughout the pectin sample, then centrifuged for 15 s at 13.4×10^3 rpm on an eppendorf Minispin centrifuge to remove any sample traces stuck on the eppendorf walls.

The amount of solution needed for a control sample and shear sample (~300 µL per sample) was then pipetted out, and transferred into thin-walled NMR tubes with a 5 mm outer diameter. The samples were then de-gassed under reduced pressure (using a syringe) by placing them in a sonicator for 1 min, to remove any dissolved oxygen within the sample that might interfere with NMR signals (figure 4.5). This process was necessary after results from previous experiments showed that any dissolved oxygen or air bubbles left in the sample would nucleate and grow within the sample. Because of the increased viscosity of the sample (caused by a tendency for aggregation of demethylesterified pectin), the air bubbles would remain in place, causing a change in the magnetic susceptibility of the solution, resulting in poor spectral resolution [43].

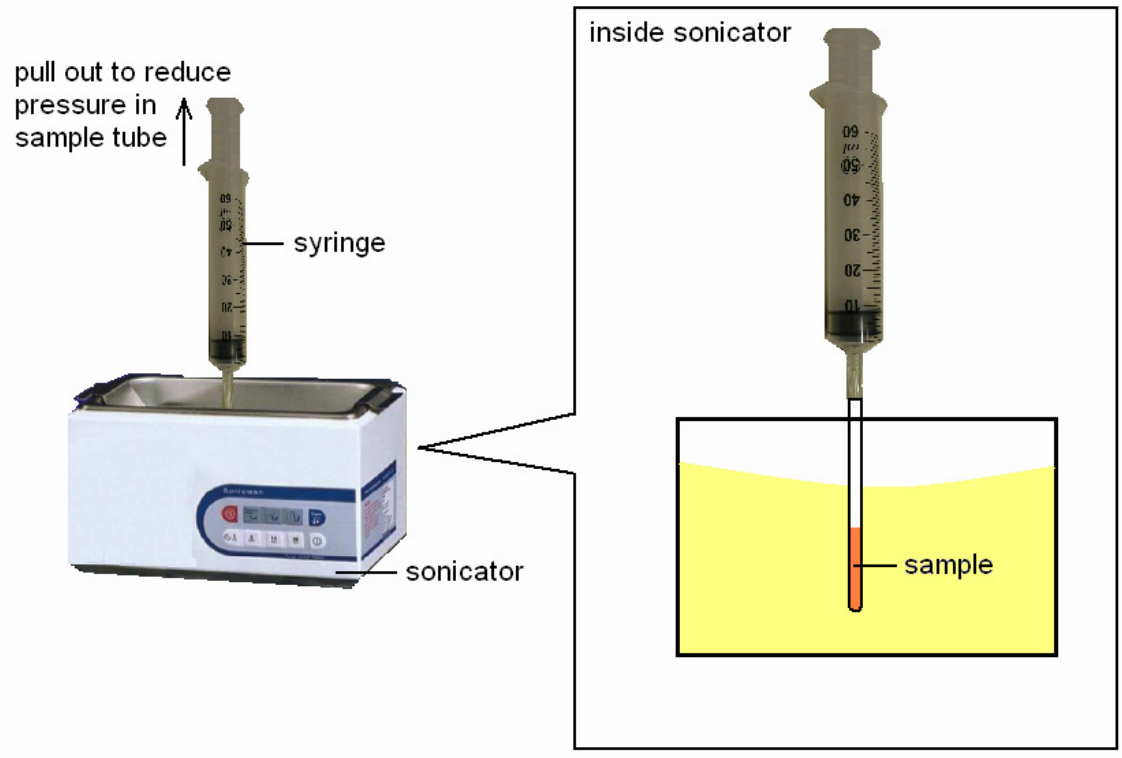

Figure 4.5: Setup of sample preparation: syringe used to de-gas NMR sample, and a sonicator used on a low sonicating setting for 1 min to remove air bubbles.

Following this, both samples had collars and thin-walled 3 mm NMR inner tubes added to them. The top of the control sample was wrapped in parafilm to keep the inner tube

in place and prevent any methanol produced during the experiment from evaporating off (figure 4.6). The other sample was set up in the NMR couette shear cell (figure 2.1), and parafilm was substituted with a top collar that was inserted at the top of the 5 mm tube to prevent methanol evaporation.

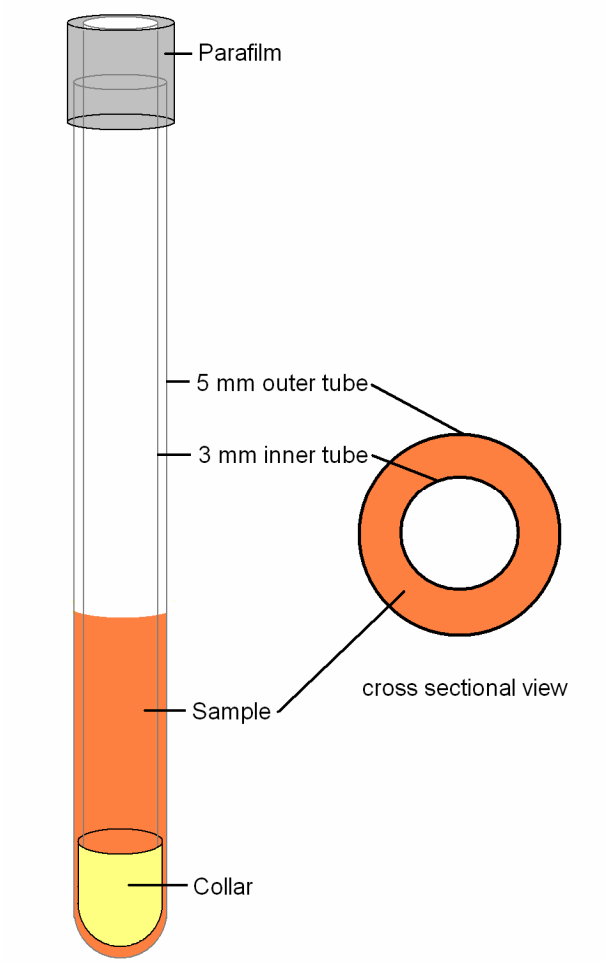

Figure 4.6: NMR tube set up of control sample.

All transferring of liquids were carried out using 10, 100, and 1000 µL eppendorf research pipettes, or glass pipettes, and weighing was carried out using Mettler Toledo balances.

All NMR work reported here using the NMR couette shear cell was carried out on a Bruker 500 MHz NMR spectrometer for the shear sample. A Bruker 700 MHz NMR

spectrometer was used to obtain data for the control sample. Both control and shear experiments were run simultaneously, where the FIDs used 2 scans, with a recycle delay of 88 s. Presaturation was used for water suppression (for traces of dissolved water or moisture absorbed during sample preparation). Bruker's TopSpin software was used to process spectra data.

The results from preliminary control experiments, where both samples sat in different spectrometers and had no shear applied, showed that the samples had different rates of enzyme activity despite both spectrometer temperatures being set to identical values (figure 4.11). This demonstrated that although spectrometer temperatures could be set to identical values using TopSpin, gas flow rates (used to vary and control temperature within the spectrometers), and the uncertainty within the thermocouples (which measures temperature from the gas flow in a spectrometer) varied between the two spectrometers. This caused the pectin samples to be exposed to temperatures that differed by several tenths of a degree. The results in figure 4.11 showed how temperature sensitive PME activity was, and reinforced the fact that an independent temperature calibration needed to be carried out between spectrometers if any proper sample comparison was to be made. This was carried out by an NMR methodology. It is well known that a sample of 80% Ethylene glycol, 20% Dimethyl sulfoxide (DMSO) has a highly temperature sensitive doublet peak-to-peak splitting distance (1.620 ppm at 303.2 K), which changes notably with temperature changes as small as 0.1 K. By altering the set spectrometer temperature until identical peak-to-peak splittings were obtained on both spectrometers before the experiment, this ensured that the real temperatures were identical. For the work reported here, all experiments were carried out at 303.2 K (as determined from the splitting value).

Before the mixing of the sample and enzyme, NMR spectrometer probes were tuned using dummy pectin samples to ensure that data could be obtained a short period after PME was added. This was important as preliminary tests showed that a large amount of methanol was liberated by PME in its first hour under our conditions, so it was important that as much of this data was obtained to observe enzyme kinetics at early stages of the reaction.

4.3 Results and Discussion

4.3.1 Initial NMR spectra

Enzyme activity in pectin was easily observable through NMR because it involves the enzyme liberating methanol, which can be observed as a narrow and large peak in the NMR spectrum. The methanol peak intensity increases as the amount of methanol being liberated increases over time, while at the same time, the large methylated sugar peak intensity decreases over time as it loses CH_3 components (figure 4.7).

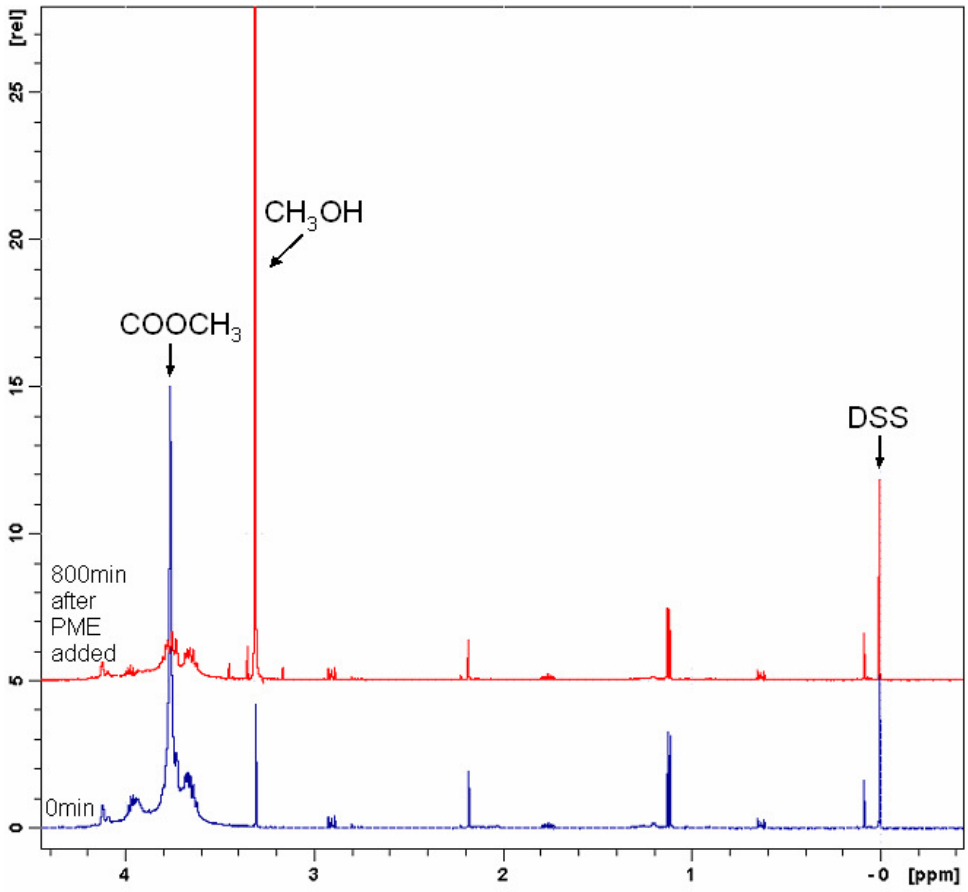

Figure 4.7: NMR spectrum showing peaks from the methyl ester group $COOCH_3$, methanol CH_3OH, and DSS, before and after pPME was added.

Because of the large size and narrow shape of the methanol peak, it was ideal to integrate over with good accuracy. The methanol peak integral was compared with the integral of a reference DSS peak, and these values were obtained from each spectrum over an experiment. This provided the information needed to calculate DM values and the rate of change of DM over time. To ensure that an accurate comparison could be made between control and shearing samples, integration and phasing of each NMR spectrum was taken over identical limits.

4.3.2 Control Experiments

The data collected during a control experiment, using only one sample that was set in the NMR couette shear cell with no shear applied, showed the rate at which methanol

was being liberated over time (figure 4.8 (a)). Figure 4.8 (b) shows the corresponding change in DM over time, which was calculated via the following derived formula and using the data from figure 4.8 (a):

Because there are 3 protons present in a methanol methyl peak, and 9 in the DSS peak chosen as a reference, then the ratio of the methanol integral over the DSS integral must be given by,

$$\frac{Integral(Methanol)}{Integral(DSS)} = \frac{3}{9}\left(\frac{Mol(Methanol)}{Mol(DSS)}\right) \tag{4.1}$$

By substituting the number of moles n, for molar concentration c, by means of $c = nV$, where the volume V of both methanol and DSS is equal since they are in the same sample, then equation 4.1 becomes:

$$c(Methanol) = \frac{Integral(Methanol)}{Integral(DSS)}\frac{9}{3}(c(DSS)) \tag{4.2}$$

In this case, we know that the DSS concentration is 1 mM, and so equation 4.2 simplifies to:

$$c(Methanol) = 3\frac{Integral(Methanol)}{Integral(DSS)} \tag{4.3}$$

Once the concentration of methanol, number of moles of methyl groups, and the initial GalA concentration were known, the DM was calculated to be:

$$DM(\%) = \left[0.73 - \left(\frac{c(Methanol)}{47.8}\right)\right] \times 100 \tag{4.4}$$

where 0.73 refers to the pectin DM at the beginning (~73%), and 47.8 mM is the initial concentration of GalA.

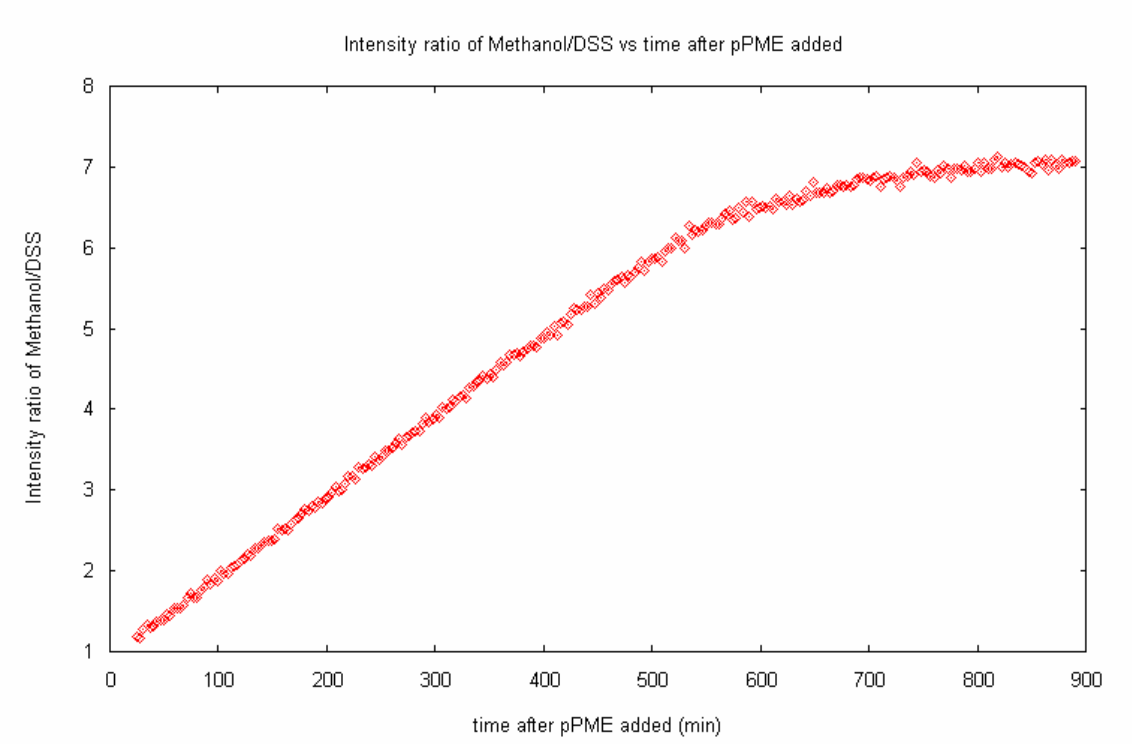

Figure 4.8 (a): Control experiment showing the rate of methanol liberated over time.

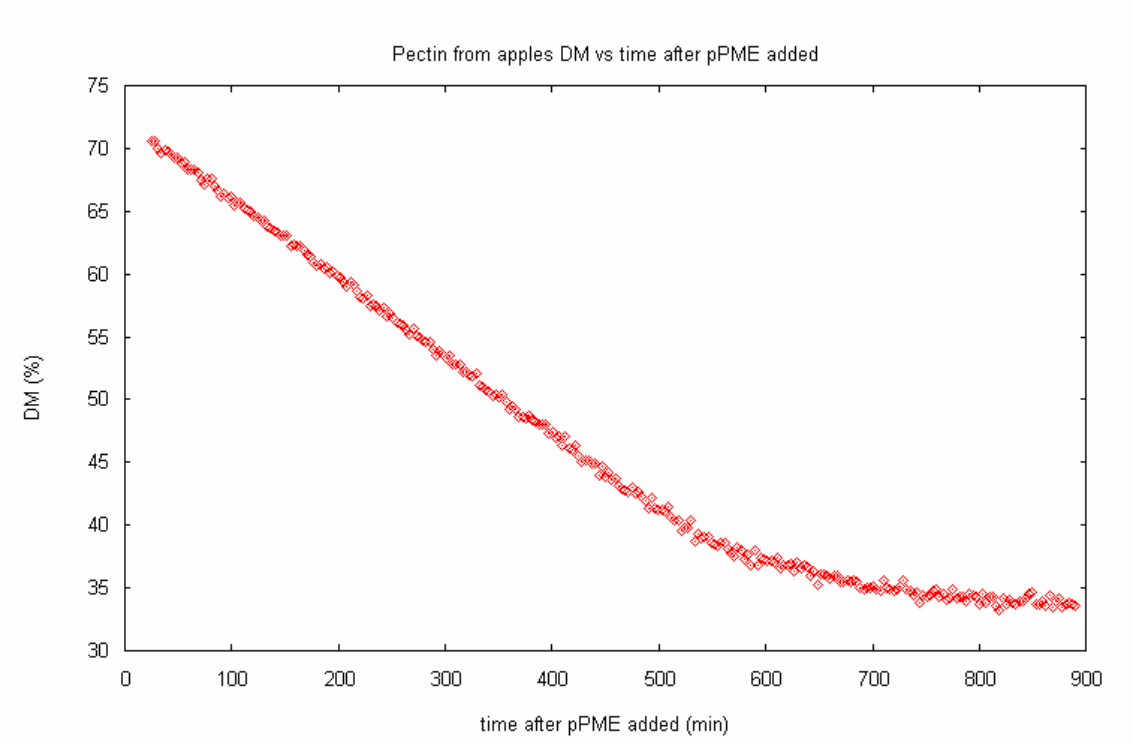

Figure 4.8 (b): Rate of de-esterification (DM) over time corresponding to figure 4.8 (a).

The results from the control experiment in figure 4.8 (a) initially showed a linear

relationship between the change in the methanol signal integral over time, which gradually slowed down to a limit and leveled off. This was expected as PME generally follows a Michaelis-Menten model [75].

4.3.2.1 Michaelis-Menten Model

Michaelis-Menten kinetics is a simple model that describes the reaction rate V of an enzyme as a function of the substrate concentration $[S]$. The reaction rate refers to the gradient of the linear phase of a product vs. time graph, or the amount of product (in this case, methanol) formed per unit of time. The Michaelis-Menten equation relates reaction rate to substrate concentration as [76]:

$$V = V_{\max} \frac{[S]}{[S] + K_m} \tag{4.5}$$

This equation provides important information about the maximum reaction rate V_{max}, and the Michaelis constant K_m, which reveals the substrate concentration at which the reaction rate is half its maximum value [76].

Several experiments were carried out at various pectin concentrations (1.5, 3, and 5%) to check if PME followed a Michaelis-Menten model (figure 4.9 (b)). For each experiment, the gradient was calculated for the linear region of the reaction, and a value for its reaction rate was obtained. It is well-established that by taking the reciprocals of equation 4.5, it can transform the equation into one that gives a straight line plot [76]:

$$\frac{1}{V} = \frac{1}{V_{\max}} + \frac{K_m}{V_{\max}} \cdot \frac{1}{[S]} \tag{4.6}$$

Therefore, a plot of $1/V$ vs. $1/[S]$ could be obtained, with a y-intercept of $1/V_{max}$ and gradient of K_m/V_{max} (figure 4.9 (a)).

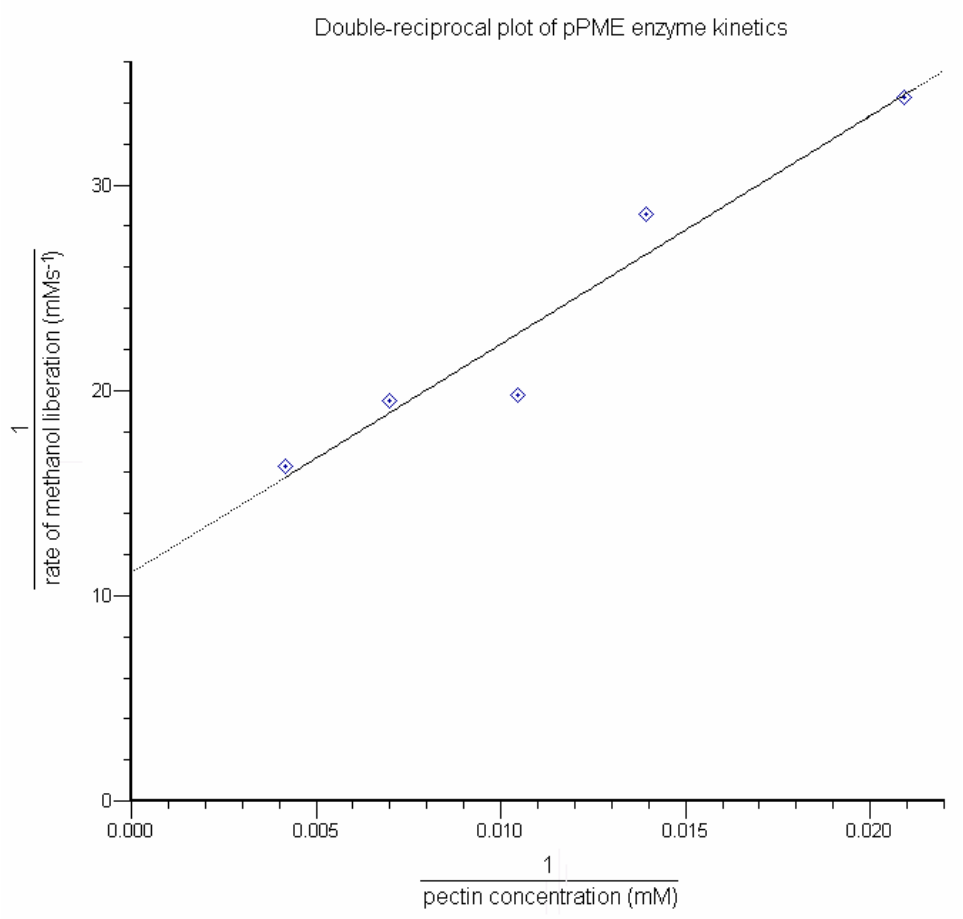

Figure 4.9 (a): 1/*V* vs. 1/*[S]* plot of experimental data of pPME acting on pectin.

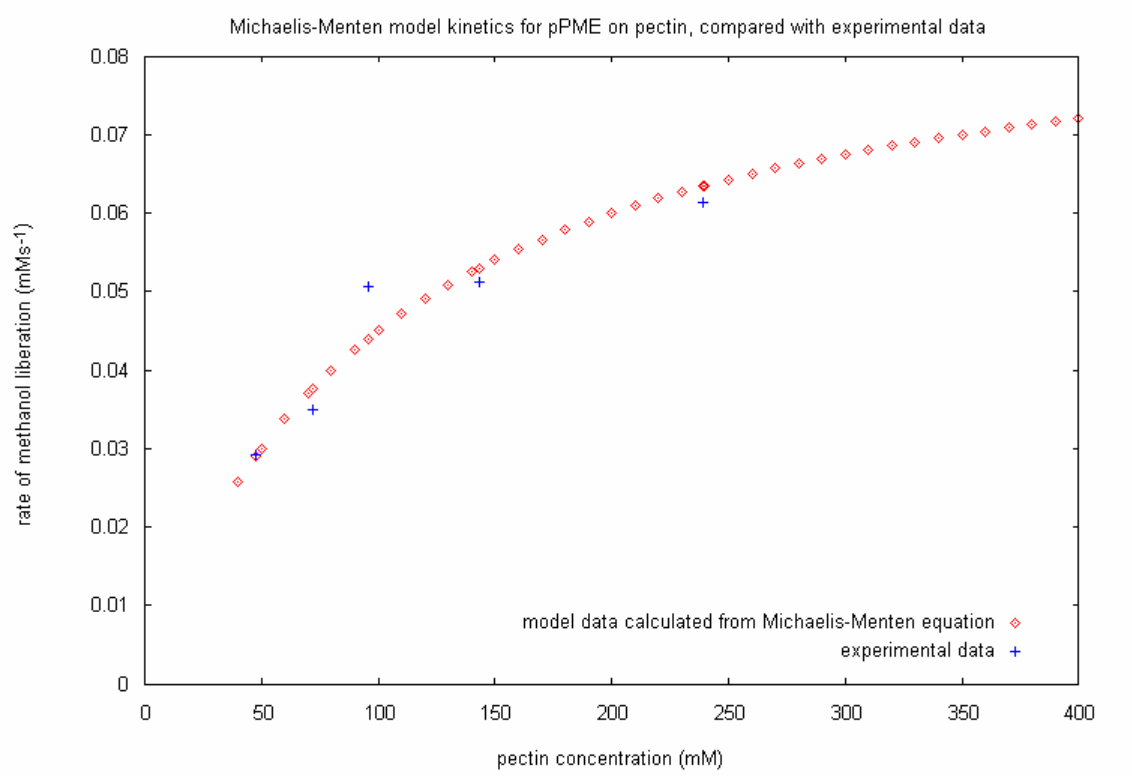

Figure 4.9 (b): Theoretical Michaelis-Menten model derived using K_m and V_{max} from figure 4.9 (a), compared with experimental data for pPME acting on pectin.

From figure 4.9 (a), values of K_m and V_{max} were deduced to be 100 ± 40 mM and 0.03 ± 0.07 mMs^{-1} respectively. Using this information, a theoretical Michaelis-Menten plot was obtained, and compared with the experimental data obtained, with good agreement (figure 4.9 (b)).

4.3.2.2 Simultaneous Control Experiments

It was deduced that control and shearing experiments would be carried out simultaneously using two NMR spectrometers after earlier experiments demonstrated that by carrying out control and shearing experiments using the same spectrometer on different days, using the same or different stock batches of PME could give different rates of enzyme activity (figure 4.10). Factors such as changes in bulk supplies of

PME, the time after PME had been taken out of the freezer, or room temperature during sample preparation were linked to this problem. These results were consistent with those found in literature that suggest that enzyme activity of purified PME is sensitive to temperature [65, 77].

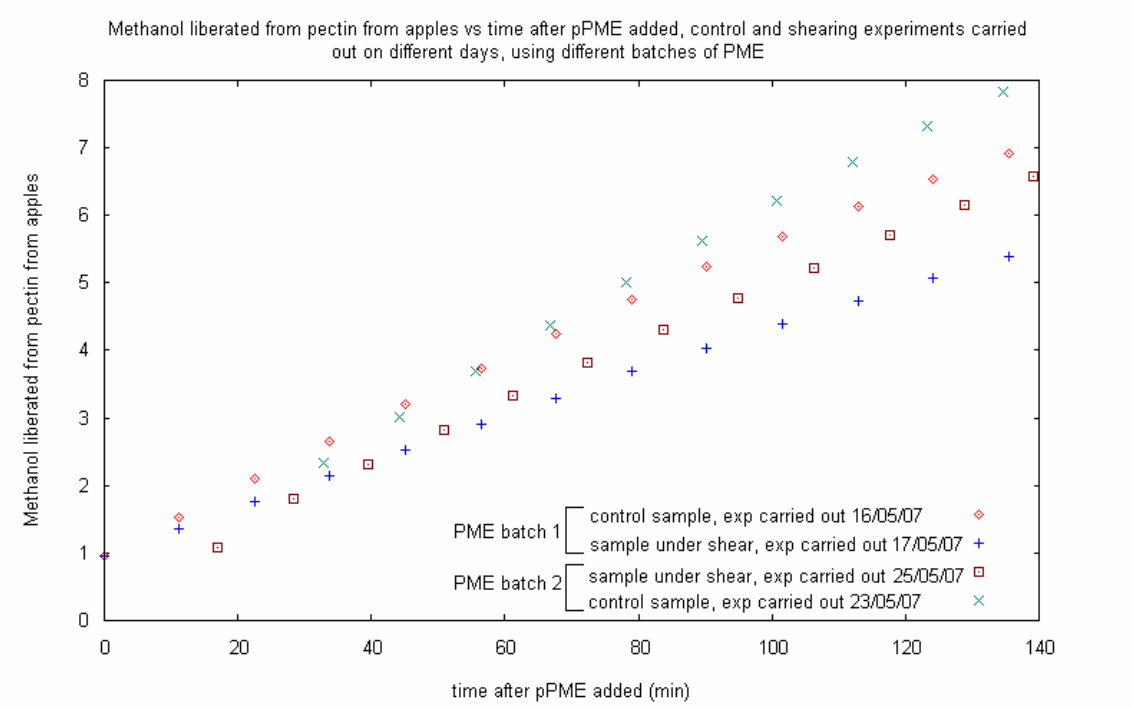

Figure 4.10: Amount of methanol liberated over time, with experiments conducted on different days.

Following this, it was necessary to carry out simultaneous control experiments, where one sample would be split into two, with one half of the sample wrapped in parafilm (figure 4.6) and set inside one spectrometer, while the remaining half of the sample was set in the NMR couette shear cell with no shear applied, and set inside another spectrometer. However, the results still showed different rates of enzyme activity despite both spectrometer temperatures being set to identical values (figure 4.11).

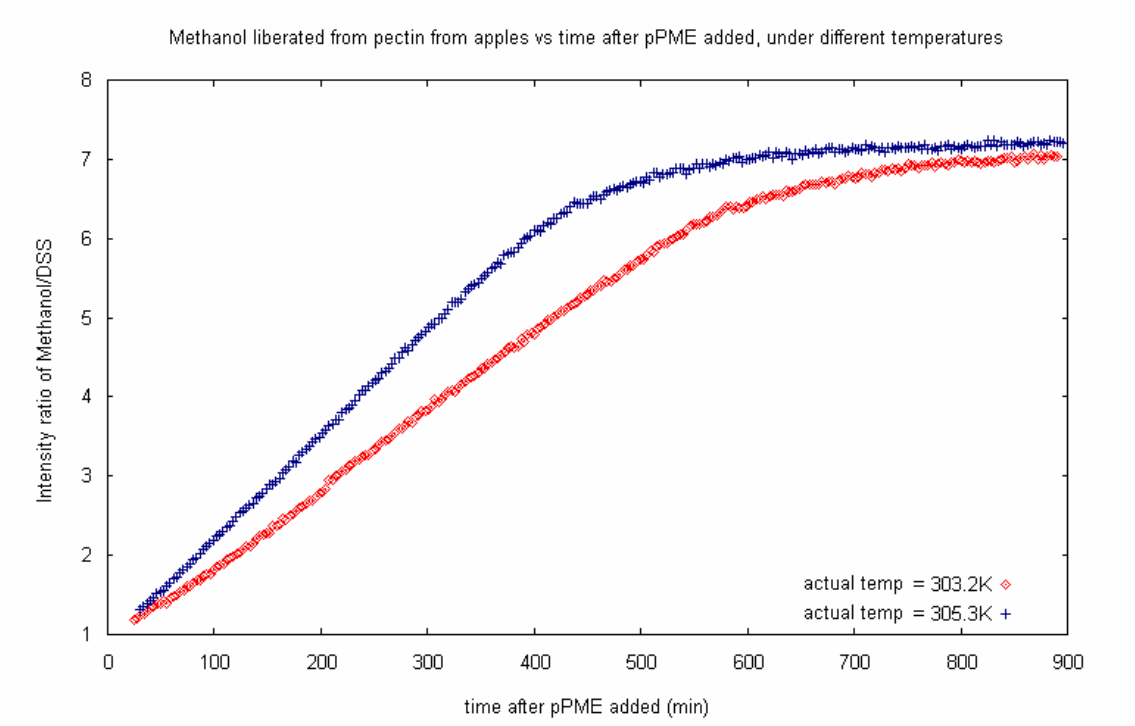

Figure 4.11: Control experiments showing the rate of methanol liberated over time, carried out at different temperatures: 303.2 K and 305.3 K.

This large difference was caused by the extremely temperature sensitive PME enzyme, where preliminary tests found that the actual temperature within each spectrometer was slightly different, but enough to change enzyme kinetics significantly. Temperature calibrations were carried out on both spectrometers using a sample of 80% Ethylene glycol and 20% DMSO, to ensure that the pectin samples would be subjected to identical temperatures (refer to section 4.2 for details).

Once challenges concerning temperature variations were overcome, several experiments were carried out to determine appropriate recycle delays in the NMR pulse sequence for both spectrometers. As quantification was important for this study, it was important to ensure that neither spectrometer was saturating the signal. However, as relaxation times are field dependent, T_1 was also required to be experimentally determined on both spectrometers. As explained in section 1.5.1.2, a number of nuclei in a lattice relax

exponentially from a higher energy state, back into a lower energy state, characterized by a decay constant, the spin-lattice relaxation time T_1. It was important to ensure that the excited nuclear spins in the system had relaxed back to create equilibrium spin populations, otherwise an RF pulse sent during a relaxation process would result in a disruption in the number of spin states in upper or lower states, leading to a false signal intensity recorded by NMR. Therefore, the recycle delay was extended to ~ $5T_1$ to ensure that spins had fully relaxed after a RF pulse, although at the cost of an extended experimental period.

4.3.3 The Effect of Shear on the Enzyme Activity of Plant PME (pPME) on Pectin

4.3.3.1 Shearing Experiments using the NMR Couette Shear Cell

Once all of the factors affecting enzyme kinetics were carefully considered and conditions optimized, a control experiment (figure 4.12 (a)) demonstrated that identical data could be recorded simultaneously on two separate spectrometers. The setup included one sample acting as a control (figure 4.6) and another sample in a NMR couette shear cell with no shear applied (figure 2.1), both using thin-walled 3 mm and 5 mm NMR tubes. The results ensured that conditions in both spectrometers were now identical, and shearing experiments could now be run.

When shearing experiments were carried out, an average shear rate of 240 s^{-1} was applied to the sample inside the NMR couette shear cell (figure 4.12 (b)), while the rest of the experiment was run under otherwise identical conditions to control experiments in figure 4.12 (a). The results however, showed no significant change in enzyme activity rate, implying that shear did not significantly change the conformation of the pectin chains or interfere with PME interactions on pectin. It was also clear that the

sheared sample data was scattered compared with the control data. This was attributed to the unstable shear conditions within the NMR couette shear cell caused by mechanical vibrations. This was caused by the difficulty of setting up the stepper motor on top of the cell shaft to rotate a 3 mm diameter tube located at the other end of the ~1 m shaft concentrically for 15 hours.

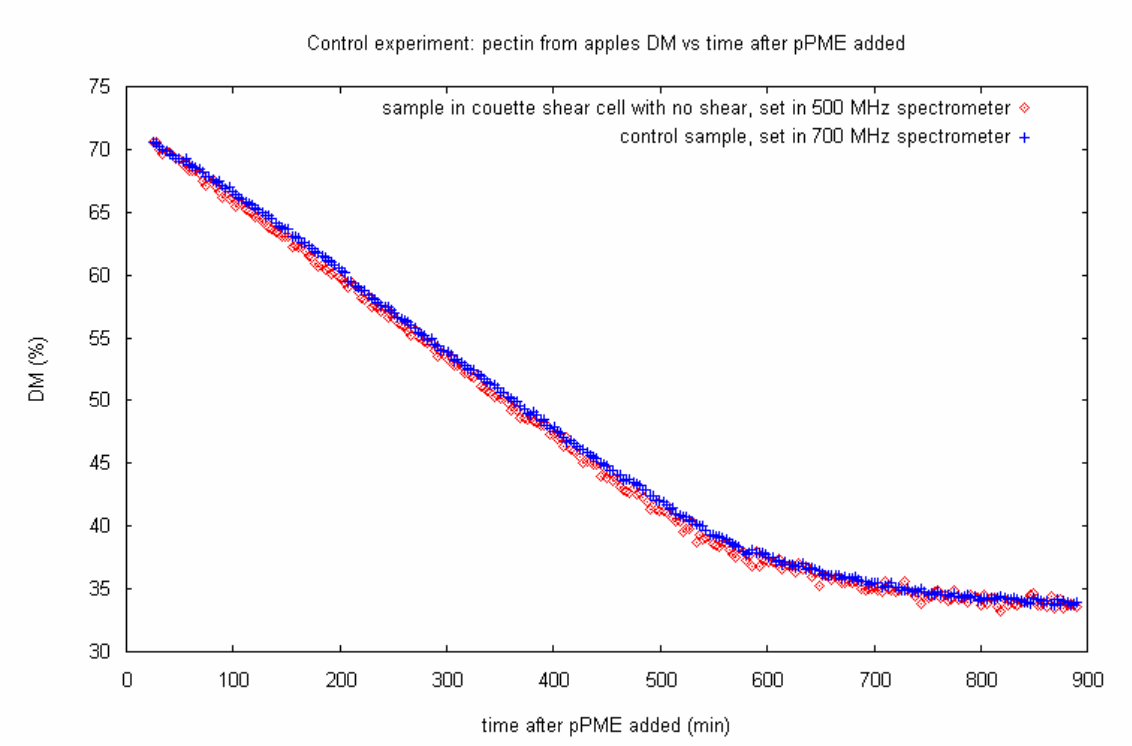

Figure 4.12 (a): Control experiment of pPME and pectin under optimized protocol, with a control sample, and a sample in the NMR couette shear cell with no shear applied.

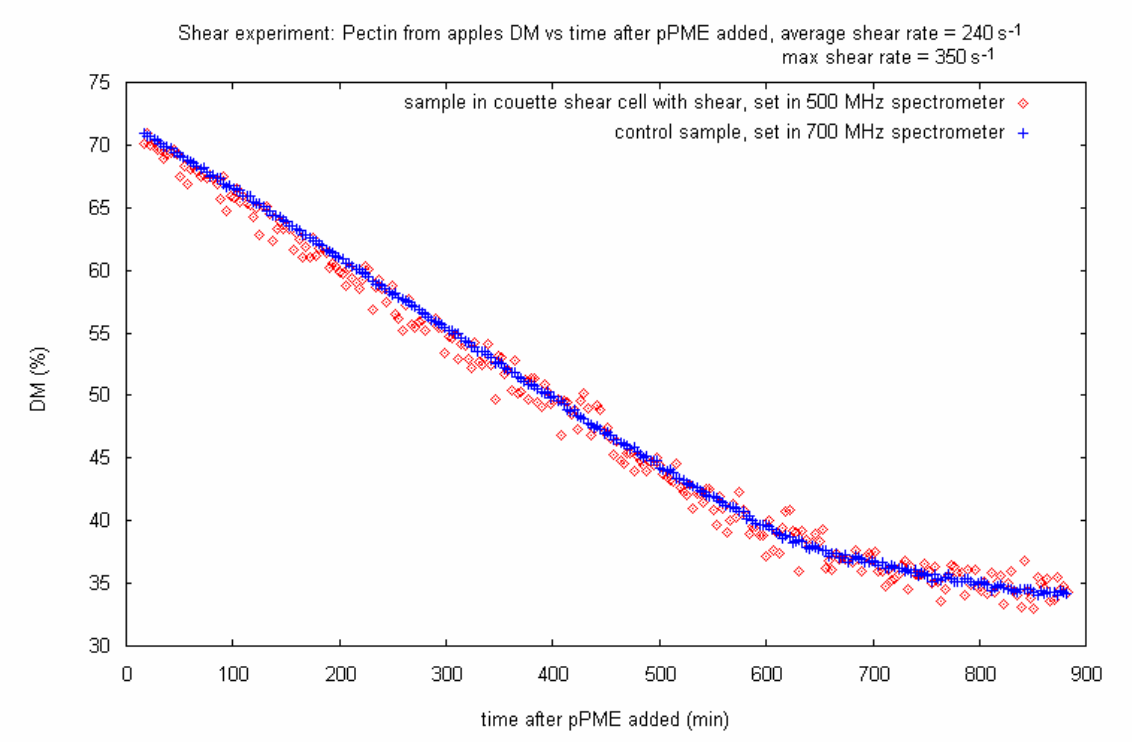

Figure 4.12 (b): Shearing experiment with pectin and pPME sample sheared at 240 s^{-1}, and compared with a control sample that showed no change in kinetics.

4.3.3.2 Shearing Experiments using the Benchtop Couette Shear Cell

After observing that no changes to enzyme activity were generated by shear rates of 240 s^{-1}, and by implication that no significant conformation changes had occurred, this raised the question about whether higher shear rates could interfere with the inter-macromolecular interactions. However, shear rates higher than 710 s^{-1} were not possible for the NMR couette shear cell due to difficulties with keeping the cell shaft, which was connected to the 3 mm inner tube, rotating concentrically at extreme shear rates. Therefore, this led to the development of a benchtop couette shear cell, consisting of a shorter cell shaft that enabled concentric rotation at high shear rates of up to 1570 s^{-1} using a thin-walled 3mm and 5mm NMR tube setup (figure 4.13 (a)).

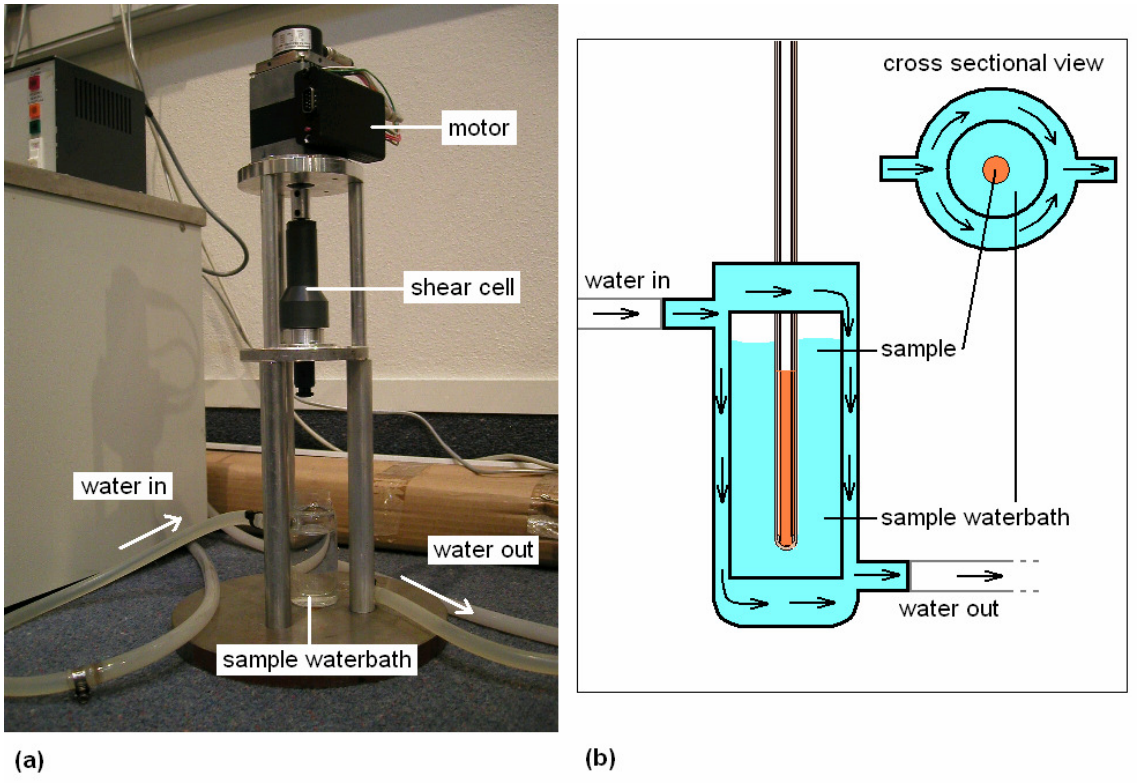

Figure 4.13: (a) Benchtop couette shear cell setup, and (b) close up of the sample waterbath being heated by water from a variable temperature waterbath.

The disadvantage of the benchtop setup was that real-time NMR spectra could not be recorded, and thus, data from the sample being sheared was only obtainable at the end of an experiment. This was because the shorter length of the shear cell made it incapable of fitting inside an NMR spectrometer. As well as this, stopping shear on the benchtop couette shear cell several times during the experiment to record data in a spectrometer meant that the sample would not be under constant shear for the entire experiment. The benchtop couette shear cell also required a variable temperature waterbath to ensure that the sample temperature could be controlled (figure 4.13 (b)). The challenge associated with this was that now temperature calibrations could not be run using a 80% Ethylene glycol, 20% DMSO sample since only the control sample was set in the 500 MHz NMR spectrometer. Therefore, a series of control experiments were carried out in order to find an identical temperature setting for both setups. This

process involved setting up a control sample in the spectrometer at 303 K and recording spectra, while another sample was set up in the benchtop couette shear cell and the waterbath set to various temperatures around a nominal 303 K under no shear. Both samples used thin-walled 3 mm and 5 mm outer diameter NMR tube setups. The samples (pectin and pPME) were left for 300 minutes in their respective setups, half the usual reaction period, before the benchtop shear cell sample in the waterbath was transferred to the spectrometer for analysis. This involved checking whether the data from the sample in the waterbath lay on the same data line as the control sample, i.e. whether both samples had the same enzyme kinetics and therefore identical temperatures. Obtaining spectra of this sample 300 minutes after pPME was added ensured that both samples were safely within the linear relationship region of the reaction (refer to figure 4.8 (a)). Any earlier and the samples may not have adapted to their respective temperatures, and any later, then the reaction rates may have begun to slow down. Once favourable conditions were achieved, and the separate setting on the waterbath corrected so that the same enzyme kinetics as the control sample in the spectrometer were measured, a shearing experiment was carried out under identical conditions as the control experiment. This time however, a shear rate of 1570 s^{-1} was applied to the sample in the benchtop couette shear cell (figure 4.14). However, despite the larger shear rate, the results showed no significant change in enzyme activity rate, again implying that shear flow did not create substantial conformational changes to the macromolecules, or interfere with the enzyme interactions over this period.

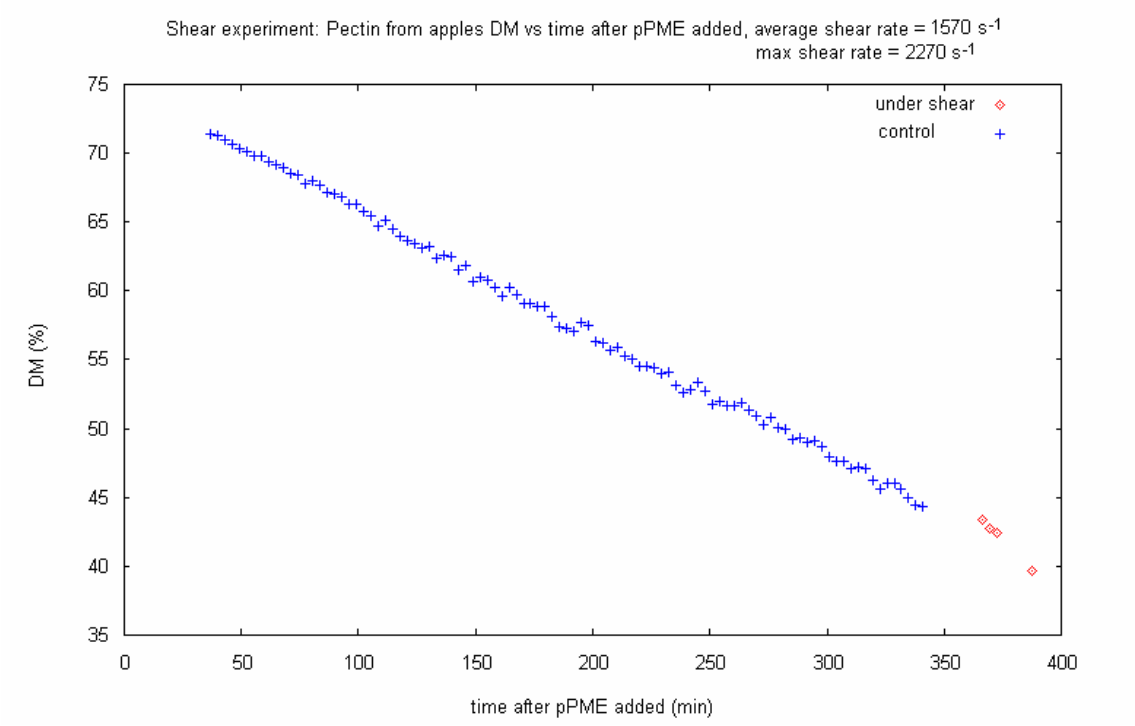

Figure 4.14: Shearing experiment with pectin and pPME sample sheared at 1570 s^{-1}, and compared with a control sample that showed no change in kinetics.

4.3.3.2.1 Shearing Experiments at Higher Concentrations

Furthermore, a shearing experiment was carried out on 5% pectin concentration, using the benchtop couette shear cell (figure 4.15). This was motivated by a study by Smith et al., who investigated conformational dynamics of individual polymer via simulations, considering the Weissenberg number W_i, which is the number that specifies the strength of an applied shear flow given as $W_i = \dot{\gamma}\tau$. This is the ratio of an applied shear rate $\dot{\gamma}$, to the polymer's natural relaxation $1/\tau$ [7]. Smith et al. found that at high viscosities, the amount of polymer chain extension increased, as shear and W_i increased due to an increase in the velocity gradient, and therefore the net hydrodynamic forces [7]. We wanted to see whether shearing could interfere with enzyme activity where the solution was more viscous, and had Non-Newtonian flow due to the formation of network structures caused by entangled pectin chains in the sample. A shearing test

was carried out under identical conditions as in figure 4.14, only now the pectin concentration was 5 times larger. Despite these efforts, this also gave results demonstrating that shear had no significant effect on enzyme activity in viscous pectin samples.

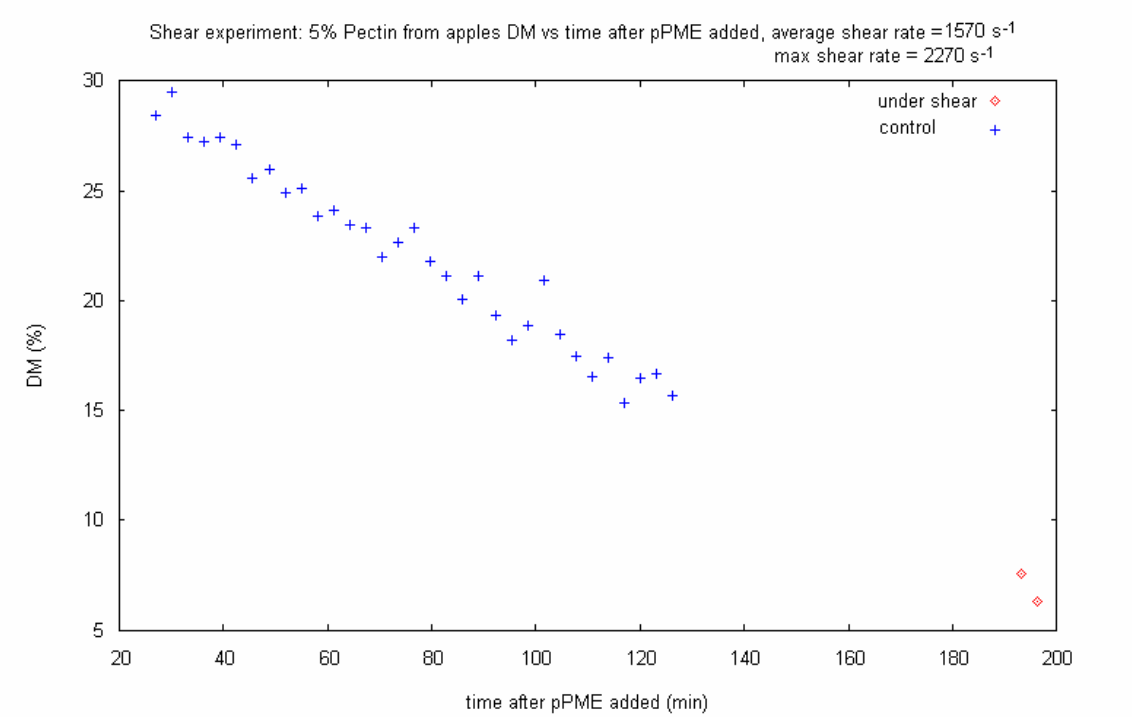

Figure 4.15: Shearing experiment on a 5% pectin sample (5 times usual concentration) with an average shear rate of 1540 s^{-1}, compared with control sample that showed no change in kinetics.

4.3.4 The Effect of Shear on the Enzyme Activity of Fungal PME (fPME) on Pectin

After the results obtained for pPME showed that shear had no effect on its enzyme activity at various shear rates and pectin concentrations, the experiment carried out in section 4.3.3.1 was repeated, substituting pPME for a randomly functioning enzyme, fPME. Different results might be anticipated because of the random nature of fPME, applying shear could interfere with more random binding and unbinding events, in contrast with pPME experiments. Shearing experiments on pectin and fPME samples

were run at an average shear rate of 240 s^{-1} (figure 4.16). The results however, showed no significant changes, further reinforcing the idea that shear does not create conformational changes to the macromolecules or interfere with the enzyme interactions under these conditions.

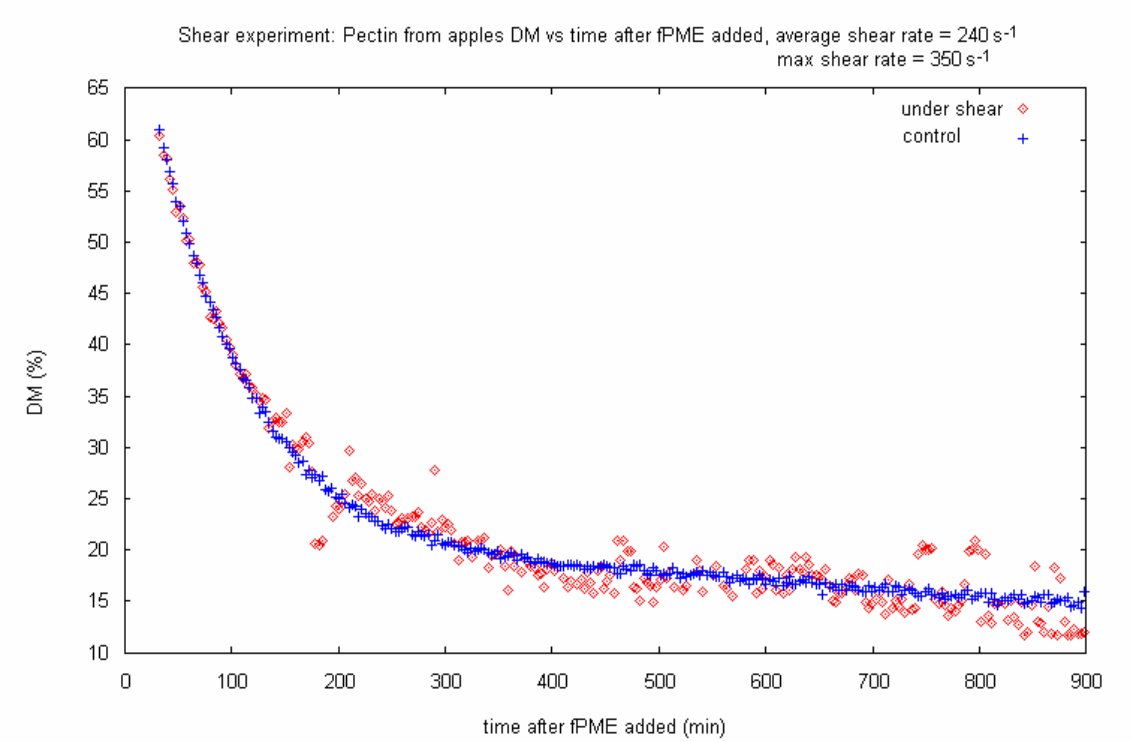

Figure 4.16: Shearing experiment with an average shear rate of 240 s^{-1} applied to a pectin and fPME sample, and compared with control sample that showed no change in kinetics.

The sheared sample data was scattered compared with the control data, consistent with the sheared data obtained when investigating pPME. This has been attributed to the same reasons as previously mentioned, where the unstable shear conditions within the NMR couette shear cell have been linked to the scattered data.

4.4 Conclusions

The effect of applying shear to an inter-macromolecular interaction has been investigated using the enzyme activity of PME on pectin by means of a NMR couette shear cell and a benchtop couette shear cell setup. New methods have been developed to study the effects of shear on pectin under optimal conditions. A formula was derived to find the degree of methylation (DM) in pectin using ^{1}H NMR spectroscopy data. It has been clearly shown that in the range investigated, shear does not interfere with the inter-macromolecular interactions between pectin and PME. Control and sheared experimental data show enzyme kinetics that are in good agreement with one another, and follow a Michaelis-Menten model. There is also good agreement between results obtained during experiments carried out at shear rates ranging from 240 - 1570 s^{-1} using both pPME and fPME, and experiments using higher pectin concentrations. This implies under these conditions that shear does not induce any conformational changes in the pectin structure or interfere with enzyme interactions under these conditions.

Chapter 5

Conclusions

5.1 Summary

In this thesis we investigated how Rheo-NMR could be used to obtain information about shear flow effects of macromolecular systems via a custom built NMR couette shear cell and Benchtop couette shear cell, both of which were developed in-house. The shear cells consisted of two cylindrical tubes of differing diameters, one inside another, where the inner tube rotates, creating shear across the annular gap where the sample sits.

Rheo-NMR is a combination of rheology and high resolution NMR, creating a technique to study polymer systems under shear. In this thesis, the NMR couette shear cell is placed inside a NMR spectrometer, allowing real-time observations of macromolecular systems under shear flow.

Firstly, it was important to establish whether or not the shear cells were producing a shear profile across the annular gap. By means of deuterium NMR spectroscopy, we reproduced results from two literature studies that report shear effects on liquid crystal systems: Cetyl Trimethyl Ammonium Bromide (CTAB) in deuterium oxide (D_2O), and Poly(gamma-benzyl-L-glutamate) (PBLG) in m-cresol. The results obtained were consistent with those found in literature, demonstrating that the shear cell was capable of producing shear flow.

After developing the Rheo-NMR device, we sought to investigate the possible conformational changes on proteins brought about by shear. By means of 1D and 2D ^{1}H NMR, we demonstrated that shear causes a small, irreversible conformational change to the protein structure of Bovine β-lactoglobulin (β-Lg) after applying shear rates ranging from 120 – 1570 s^{-1}, with reasonable reproducibility. The molecular nature of this change however, remains elusive. Repeating the experiment on β-Lg in a destabilized state, achieved by adding 10% Trifluoroethanol (TFE) (v/v), 1D NMR showed that shear creates a large conformational change to the β-Lg structure, although reproducibility is difficult. From an NMR point of view, the sheared state of the β-Lg structure was similar to β-Lg with an α-helical dominating structure, but also with β-Lg containing largely β-sheet amyloid fibrils. A method into determining whether the sheared sample was made up of α-helices or β-sheets was not available at this time, but may be interesting to pursue in future work.

Light scattering tests were carried out on β-Lg samples that showed small changes, however, no measurable changes were observed, suggesting that by means of an independent method, shear does not produce any significant aggregation under the conditions of our experiment. Gel electrophoresis tests were performed on a β-Lg sample that showed a large change, yielding results that showed little change under denaturing conditions, implying that the large changes were due to hydrophobic interactions.

A second Rheo-NMR investigation involved using an enzyme reaction (the de-esterification of pectin with pectin methylesterase) to study the effects of shear on this inter-macromolecular interaction. The de-esterification process was monitored by

measuring the increase in the methanol proton signal via NMR. Two types of enzymes were investigated: plant pectin methylesterase (pPME), which shows multiple attack mechanism, acting progressively on pectin chains; and fungal pectin methylesterase (fPME), which shows multiple chain mechanism, randomly removing methyl-ester groups on a pectin chain. Under no shear, the de-esterification process was in good agreement with a Michaelis-Menten model. Using NMR data, a formula was derived to find the degree of methylation (DM). An experimental method was developed to enable enzyme reaction studies under optimal conditions. Subjected to shear rates of 240 – 1570 s^{-1}, identical enzyme kinetics are displayed by quiescent and sheared samples using both pPME and fPME, showing that shear does not interfere with inter-macromolecular interactions of this system under these conditions.

5.2 Future Directions

Although rather insignificant conformational changes were found in the β-Lg structure subsequent to shear application, many questions can be raised from this experiment. Most obvious, is the fact that proteins are well known to be extremely sensitive to conditions such as pH, temperature, solvent, etc. so a different range of conditions could yield larger or different conformational changes that were not obtainable under our conditions.

Investigations into the rate of conformational change and its lack of reproducibility on β-Lg structures were attempted, but no conclusive explanations could be obtained. If this experiment were to be repeated, it may be interesting to prepare large sample sizes, applying various shear rates over various periods of time to investigate whether the

conformational changes undergo a certain type of kinetics, statistics of how many times the change did or did no occur, and what variables the changes may depend on.

Experiments investigating the effects of shear on β-Lg containing TFE yielded inconclusive explanations to explain the difficult reproducibility of obtaining a large conformational change to the protein structure subsequent to shear application. It may be interesting to find the precise experimental conditions required to reproduce this result, and to characterize the state of the problem where a large change was observed by means of techniques such as diffusion measurements.

The investigations that focused on studying the effects of shear on the inter-macromolecular interactions of PME on pectin were clearly conclusive. Nonetheless, the measurements made using our Rheo-NMR device have shown that accurate data can be obtained. Future work could be carried out to investigate the methylesterification patterns in order to see if any changes occur at a finer level of detail.

The systems investigated here highlight the diverse range of macromolecular systems that can be studied using our Rheo-NMR device and experimental methods, and its potential to collect high resolution data about macromolecular behaviour.

Appendix A

Shear rate in a couette cell

The cylindrical coordinate system (r, φ, z) was used to calculate the shear rate of a sample loaded in the annular gap created by two cylinders, where the inner cylinder rotates with angular velocity ω (figure A.1) [41].

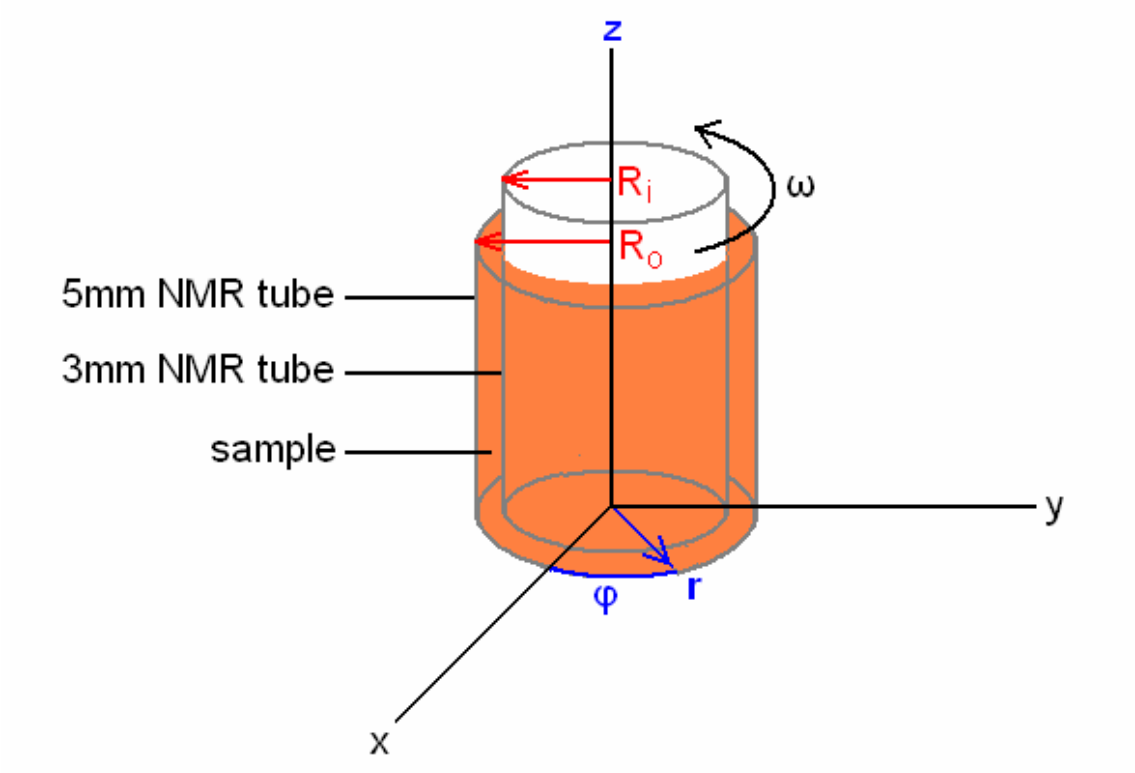

Figure A.1: Diagram of sample loaded in the annular gap between two cylinders, with the inner cylinder rotating with angular velocity ω.

The shear rate $\dot{\gamma}$ is defined as $\tau = -\mu\dot{\gamma}$, where τ is shear stress (generated as a result of the rotating inner cylinder), and μ is the solution's viscosity [48]. From figure A.1, it can be observed that only the r-φ component of the shear tensor is non-zero, and so

the shear stress is given by:

$$\tau_{r-\phi} = -\mu\left[r\frac{d}{dr}\left(\frac{v_\phi}{r}\right) + \frac{1}{r}\frac{d}{d\phi}v_r \right] \tag{A.1}$$

However, by assuming that the sample moves with a steady-state laminar flow around the inner cylinder, this implies that the radial velocity v_r (and axial velocity v_z) must be zero. Therefore, equation A.1 simplifies to:

$$\tau = -\mu\left(r\frac{d}{dr}\left(\frac{v_\phi}{r}\right)\right) \tag{A.2}$$

But we also know that $\tau = -\mu\dot{\gamma}$, so equation A.2 can be rewritten as:

$$\dot{\gamma} = \frac{\tau}{-\mu} = r\frac{d}{dr}\left(\frac{v_\phi}{r}\right) \tag{A.3}$$

In order to find v_φ as a function of radial coordinate r, the equation of motion for the φ-component is expressed in terms of the velocity gradient, and is found to be given as [41]:

$$v_\phi = \frac{C_1 r}{2} + \frac{C_2}{r} \tag{A.4}$$

$$\text{where} \quad C_1 = -\frac{2\omega\left(R_i/R_o\right)^2}{\left(1-\left(R_i/R_o\right)^2\right)} \tag{A.5}$$

$$\text{and} \quad C_2 = \frac{\omega r^2\left(r_i/r_o\right)^2}{\left(1-\left(r_i/r_o\right)^2\right)} \tag{A.6}$$

By substituting equation (A.4) into (A.3), we can obtain a formula for the average shear rate $\left\langle\dot{\gamma}\right\rangle$:

$$\left\langle \dot{\gamma} \right\rangle = r \frac{d}{dr} \left[\frac{\left(\frac{C_1 r}{2} + \frac{C_2}{r} \right)}{r} \right] \tag{A.7}$$

$$= -\frac{2C_2}{r^2} \tag{A.8}$$

Where C_2 can be expanded out and simplified to obtain:

$$\left\langle \dot{\gamma} \right\rangle = -\frac{2\omega}{\left(1 - \left(r_i / r_o \right)^2 \right)} \tag{A.9}$$

Bibliography

1. Uhrinova, S., Uhrin, D., Denton, H., Smith, M., Sawyer, L., and Barlow, P.N., *Journal of Biomolecular NMR*, **1998**, 12, 89.

2. Traub, O. and Berk, B.C., *Arteriosclerosis, Thrombosis, and Vascular Biology*, **1998**, 18, 677.

3. Abu-Jdayil, B., Al-Malah, K., and Asoud, H., *Food Hydrocolloids*, **2002**, 16, 55.

4. Altmann, N., Cooper-White, J.J., Dunstan, D.E., and Stokes, J.R., *Journal of Non-Newtonian Fluid Mechanics*, **2004**, 124(1-3), 129.

5. Khare, R., de Pablo, J.J., and Yethiraj, A., *Macromolecules*, **1996**, 29(24), 7910.

6. Xu, G. and Ding, J., *Journal of Chemical Physics*, **1997**, 107(10), 4070.

7. Smith, D.E., Babcook, H.P., and Chu, S., *Science*, **1999**, 283, 1724.

8. Schneider, S.W., Nuschele, S., Wixforth, A., Gorzelanny, C., Alexander-Katz, A., Netz, R.R., and Schneider, M.F., *PNAS*, **2007**, 104(19), 7899.

9. Minstry, N., Cranmer, S.L., Yuan, Y.P., Mangin, P., Dopheide, S.M., Harper, I., Guiliano, S., Dunstan, D.E., Lanza, F., Salem, H.H., and Jackson, S.P., *Blood*, **2000**, 96(10), 3480.

10. Jaspe, J. and Hagen, S.J., *Biophysical Journal*, **2006**, 91(9), 3415.

11. Charm, S.E. and Wong, B.L., *Biotechnology and Bioengineering*, **1970**, 12, 1103.

12. Tirrell, M. and Middleman, S., *Biotechnology and Bioengineering*, **1975**, 17, 299.

13. Tanner, R.I., *Engineering Rheology*. **1985**, New York: Oxford University Press.

14. Dadmun, M.D. and Han, C.C., *Macromolecules*, **1994**, 27(26), 7522.

15. Kalus, J., Neubauer, G., and Schmelzer, U., *Review of Scientific Instruments*, **1990**, 61(11), 3384.

16. Nakatani, A.I., Waldow, D.A., and Han, C.C., *Review of Scientific Instruments*,

1992, 63(7), 3590.

17. Plano, R.J., Safinya, C.R., Sirota, E.B., and Wenzel, L.J., *Review of Scientific Instruments*, **1993**, 64(5).

18. Gason, S.J., Smith, T.A., Boger, D.V., and Dunstan, D.E., *Polymer*, **2001**, 42(18), 7755.

19. Gason, S.J., Boger, D.V., and Dunstan, D.E., *Langmuir*, **1999**, 15(22), 7446.

20. Fuller, G.G., *Annual Review of Fluid Mechanics*, **1990**, 22, 387.

21. Fuller, G.G., *Optical Rheometry of Complex Fluids*. **1995**, Oxford: Clarendon Press.

22. Callaghan, P.T., *Reports on Progress in Physics*, **1999**, 62(4), 599.

23. Rofe, C.J., *Applications of Rheo-NMR Microscopy to Complex Fluids*, in *Physics*. **1997**: Massey University. p. 175.

24. Martins, A.F., Esnault, P., and Volino, F., *Physical Review Letters*, **1986**, 57(14), 1745.

25. Badiger, M.V., Rajamohanan, P.R., Suryavanshi, P.M., Ganapathy, S., and Mashelkar, R.A., *Macromolecules*, **2002**, 35.

26. Nakatani, A.I., Poliks, M.D., and Samulski, E.T., *Macromolecules*, **1990**, 23, 2686.

27. Xia, Y. and Callaghan, P.T., *Macromolecules*, **1991**, 24(17), 4777.

28. Strobl, G., *The Physics of Polymers: Concepts for Understanding Their Structures and Behaviour*. **2007**, Berlin: Springer-Verlag.

29. Pervaiz, S. and Brew, K., *Science*, **1985**, 228, 335.

30. Singh, H. and Bennett, R.J., *Dairy microbiology handbook*. 3rd ed, ed. Robinson, R.K. **2002**, Chichester: Wiley.

31. Eigel, W.N., Butler, J.E., Ernstrom, C.A., Farrell Jr., H.M., Harwalker, V.R., Jennes, R., and Whitney, R.M., *Journal of Dairy Science*, **1984**, 67, 1599.

32. Simmons, M.J.H., Jayaraman, P., and Fryer, P.J., *Journal of Food Engineering*, **2007**, 79, 517.

33. Hill, E.K., Krebs, B., Goodall, D.G., Howlett, G.J., and Dunstan, D.E., *Biomacromolecules*, **2006**, 7, 10.

34. Willats, W.G.T., Knox, J.P., and Mikkelsen, J.D., *Trends in Food Science & Technology*, **2006**, 17, 97.

35. Pilnik, W., ed. *Pectin - a many splendoured thing*. Gums and stabilizers for the food industry, ed. Phillips, G.O., Williams, P.A., and Wedlock, D.J. **1990**, Oxford: Oxford University Press. 313 - 326.

36. Savary, B., Hotchkiss, A.T., Fishman, M.L., Cameron, R.G., and Shatters, R.G., *Development of a Valencia orange pectin methyl esterase for generating novel pectin products*. Advances in pectin and pectinase research, ed. Voragen, F., Schols, H., and Visser, R. **2003**, The Netherlands: Kluswer Academic Publishers.

37. Braconnot, H., *Annales de chimie et de physique - Annals of Chemistry and Physics*, **1825**, 28(2), 173.

38. Rosenbohm, C., Lundt, I., Christensen, T.M.I.E., and Young, N., W.G., *Carbohydrate Research*, **2003**, 338, 637.

39. Denès, J.-M., Baron, A., Renard, C.M.G.C., Pean, C., and Drilleau, J.-F., *Carbohydrate Research*, **2000**, 327, 385.

40. Massey, B., *Mechanics of Fluids*. 8th ed, ed. Ward-Smith, J. **2006**, London: Taylor & Francis.

41. Maa, Y.-F. and Hsu, C.C., *Biotechnology and Bioengineering*, **1996**, 51, 458.

42. Hatada, K. and Kitayama, T., *NMR spectroscopy of polymers*. **2004**, Berlin: Springer.

43. Roberts, G.C.K., *NMR of macromolecules : a practical approach*, ed. Roberts, G.C.K. **1993**, Oxford ; New York: IRL Press at Oxford University.

44. Abraham, R.J., Fisher, J., and Loftus, P., *Introduction to NMR Spectroscopy*. **1988**, Chichester: John Wiley & Sons.

45. Hore, P.J., *Nuclear Magnetic Resonance*. **1995**, New York: Oxford University Press.

46. Freeman, R., *Spin Choreography*. **1997**, New York: Oxford University Press.

47. Frenkiel, T.A., *Instrumentation and pulse sequences*, in *NMR of Macromolecules : A Practical Approach*, Roberts, G.C.K., Editor. **1993**, IRL Press at Oxford University: Oxford; New York.

48. Krause, E., *Fluid Mechanics*. **2005**, Berlin: Springer-Verlag.

49. Fischer, E. and Callaghan, P.T., *Physical Review E*, **2001**, 64, 011501.

50. Rice, D.M., *Deuterium NMR of synthetic polymers*, in *NMR Spectroscopy of Polymers*, Ibbett, R.N., Editor. **1993**, Blackie Academic & Professional: London; New York.

51. Doane, J.W. and Crawford, G.P., *Polymer Dispersed Liquid Crystals*, in *Encyclopedia of polymer science and engineering*, Kroschwitz, J.I., Editor. **1987**, Wiley: New York. p. 3663 - 3668.

52. Leal, C.R., van der Klink, J., and Martins, A.F., *Molecular Crystals and Liquid Crystals*, **2004**, 420, 35.

53. Brownlow, S., Cabral, J.H.M., Cooper, R., Flower, D.R., Yewdall, S.J., Polikarpov, I., North, A.C.T., and Sawyer, L., *Structure*, **1997**, 5(4), 481.

54. Papiz, M.Z., Sawyer, L., Eliopoulos, E.E., North, A.C.T., Findlay, J.B.C., Sivaprasadarao, R., Jones, T.A., Newcomer, M.E., and Kraulis, P.J., *Nature (London)*, **1986**, 324, 383.

55. Kuwata, K., Hoshino, M., Forge, V., Era, S., Batt, C.A., and Goto, Y., *Protein Science*, **1999**, 8, 2541.

56. Belloque, J., Lopez-Fandino, R., and Smith, G.M., *Journal of Agricultural Food Chemistry*, **2000**, 48(9), 3906.

57. Collins, S.R., Douglass, A., Vale, R.D., and Weissman, J.S., *PLoS Biology*, **2004**, 2, 1582.

58. Liu, J.-J. and Lindquist, S.L., *Nature*, **1999**, 400, 573.

59. Serpell, L., Berriman, J., Jakes, R., Goedert, M., and Crowther, R.A., *Proceedings of the National Academy of Sciences of the United States of America*, **2000**, 97(9), 4897.

60. Qi, X.L., Holt, C., McNulty, D., Clarke, D.T., Brownlow, S., and Jones, G.R., *Biochemical Journal*, **1997**, 324, 341.

61. McKenzie, H.A. and Sawyer, W.H., *Nature (London)*, **1967**, 214, 1101.

62. Kella, N.K. and Kinsella, J.E., *Biochemical Journal*, **1988**, 255, 113.

63. Hwang, T.L. and Shaka, A.J., *Journal of Magnetic Resonance Series A*, **1995**, 112(2), 275.

64. Shiraki, K., Nishikawa, K., and Goto, Y., *Journal of Molecular Biology*, **1995**, 245, 180.

65. Sajjaanatakul, T. and Pitifer, L.A., *The Chemistry and Technology of Pectin*, ed. Walter, R.H. **1991**, New York: Academic Press.

66. Cros, S., Garnier, C., Axelos, M.A.V., Imberty, A., and Perez, S., *Biopolymers*, **1996**, 39, 339.

67. Marangoni, A.G., *Enzyme kinetics : a modern approach*. **2003**, Hoboken, N.J.: Wiley-Interscience.

68. Mills, G.B., *Biochemical Journal*, **1949**, 44, 302.

69. Evans, R. and McHale, D., *Phytochemistry*, **1978**, 17, 1073.

70. Kohn, R., Markovic, O., and Machova, E., *Coll. Czech. Chemistry Community*, **1983**, 48, 790.

71. King, K., Mitchell, J.R., Norton, G., and Caygill, J., *Journal of Food Agriculture*, **1986**, 37, 391.

72. Speirs, C.I., Blackwood, G.C., and Mitchell, J.R., *Journal of Agricultural Food Chemistry*, **1980**, 31, 1287.

73. Limberg, G., Korner, R., Buchholt, H.C., Christensen, T.M.I.E., Roepstorff, P., and Mikkelsen, J.D., *Carbohydrate Research*, **2000**, 327, 293.

74. Mikkelsen, K. and Nielson, S.O., *Journal of Physical Chemistry*, **1960**, 64, 632.

75. Versteeg, C., Rombouts, F.M., and Pilnik, W., *Lebensm. -Wiss. u. -Technol.*, **1978**, 11, 267.

76. Berg, J., Tymoczko, J., and Stryer, L., *Biochemistry*. 5th ed. **2001**, New York: W. H. Freeman and Co.

77. Pollard, A.D. and Kieser, M.E., *Journal of Science Food Agriculture*, **1951**, 2,

30.